Optimization of Infectious-Disease Mitigation Strategies with Economic or Equity Perspectives

Erin Stafford

A dissertation
submitted in partial fulfillment of the
requirements for the degree of

Doctor of Philosophy

University of Washington
2023

Reading Committee:
Mark Kot, Chair
Dobromir Dimitrov
Laura Matrajt

Program Authorized to Offer Degree:
Department of Applied Mathematics

University of Washington

Abstract

Optimization of Infectious-Disease Mitigation Strategies with Economic or Equity Perspectives

Erin Stafford

Chair of the Supervisory Committee:
Mark Kot
Department of Applied Mathematics

Infectious-disease outbreaks in human, livestock, and plant populations continue to be a problem that can affect our day-to-day lives and have broader societal implications. Therefore, the need to prevent the spread of infectious disease is of great importance. Which disease-mitigation strategies are best depends on which factors are most important to decision makers.

In this dissertation, I focus on the use of optimization with compartmental models to determine the best mitigation strategies for infectious-disease outbreaks. First, I describe the use of compartmental models to study infectious-disease dynamics. I also provide background on optimal control theory and give examples of how optimal control theory and other optimization methods are used to give insight into the effectiveness of different disease mitigation strategies.

Next, I use two optimal-control models to determine if contact-reducing disease-mitigation strategies can be economically advantageous when used to control the spread of *Staphylococcus aureus* in dairy cows. Both models use SIS models to describe the dynamics of *S.*

aureus transmission. Moreover, both models consider revenue from healthy cows producing saleable milk, a cost from sick cows, and a loss of revenue when implementing mitigation strategies. The second model, however, also takes into consideration mild infections of *S. aureus* where infected cows may still produce saleable milk of lesser quality. Using these models, I found that using costly mitigation strategies to reduce contacts between infective and susceptible cows is economically beneficial. The dynamics of the second optimal-control model, where severity is considered, are more interesting as multiple candidate solutions satisfying the necessary conditions of Pontryagin's maximum principle may coexist. The behaviors of these candidate solutions may be very different, but they may also produce similar economic outputs.

I then study the effects of a very different type of disease-mitigation strategy, vaccination, on COVID-19 outcomes. In this chapter, I find which vaccination strategies minimize either overall disease burden, inequity in disease outcomes between racial groups, or a combination of measures. I find that, when vaccine is limited, there is a trade-off between minimizing disease burden and minimizing inequity. Allocation strategies that minimize combinations of measures can similarly improve both disease burden and inequity, but not to the same extent as when minimizing either measure alone. By increasing the vaccine supply, however, the trade-off greatly lessens.

Contents

List of Figures

List of Tables

ACKNOWLEDGEMENTS

I am deeply thankful to my advisor, Professor Mark Kot, for his guidance. I enjoyed my work with him, and I have learned much from him about how to be a good researcher, not just in terms of mathematics, but also in terms of effectively communicating ideas. I would also like to thank Laura Matrajt and Dobromir Dimitrov for their mentorship. They enabled me grow in my career and opened doors for me to learn what it's like to do research outside of academia.

I would also like to thank the members of my committee, my fellow students, and the faculty and staff of the Department of Applied Mathematics that have supported me during this time. I am truly grateful for the wonderful experience I have had in this department and in Seattle, and this is largely due to the people I have met here.

Lastly, I would like to thank my family and friends for believing in me supporting me in my decision to pursue my PhD.

DEDICATION

To my parents for supporting me in all that I do.

Chapter 1

Introduction

1.1 Infectious disease models

Throughout history, pandemics have posed a great threat to human health. For example, plague, caused by *Yersinia pestis* bacteria and spread by fleas, is responsible for the plague of Justinian (541–543 CE) as well as the Black Death (1347–1351). These epidemics killed approximately 100 million people and a third of the European population, respectively [7, 8]. The influenza virus has also been around for centuries causing significant mortality. Typical seasonal influenza leads to as many as 500,000 deaths per season, globally [7]. The most severe influenza pandemic, the Spanish flu in 1918–1919, caused around 50 million deaths [7]. In recent years, the COVID-19 pandemic has killed approximately 7 million people [9] and greatly affected our day-to-day lives.

Communicable diseases also threaten both animal and plant populations, and epidemics within agricultural settings have the potential to decimate the agricultural industry and lead to famines or social upheaval. For example, an epidemic of wheat stem rust in the Soviet Union in 1932 caused a famine leading to the death of 5 million people [10]. Moreover, the potato blight epidemic in 1846 in England, Ireland, and Germany lead to a mass emigration [10] as well as over a million deaths [11]. Livestock disease have also taken a toll. For example,

outbreaks of foot and mouth disease [12], African swine fever [13], and avian influenza [14] have all had severe economic consequences.

Researchers have made much effort to study how these diseases spread and to determine effective mitigation strategies. Before the transmission of diseases was understood, researchers such as John Graunt (1620–1674), Daniel Bernoulli (1700–1782), and John Snow (1813–1858) were using mathematical reasoning to inform their study of infectious diseases [15–19].

The development of compartmental models of infectious disease started in the early 1900's. During this time, W.H. Hamer proposed that the spread of infectious diseases is dependent on the number of susceptibles and infectives in a population [15]. Making this assumption that a mass-action law governs the infection rate, public health physicians such as R.A. Ross, A.G. McKendrick, and W.O. Kermack were able to construct the first compartmental models of infectious diseases, which are still used today [15].

Compartmental models such at the Kermack–McKendrick [20] and Ross–Macdonald models [21] are used to study the dynamics of an infectious disease, determine which mitigation strategies may be effective, or even make predictions about the behavior of an outbreak. These models consist of differential equations representing disease classes within a population, such as the number of susceptible (S), infective (I), or recovered (R) individuals, as functions of time. To introduce the topic of compartmental models, I will go over several examples and describe how these examples can be expanded to incorporate more complex dynamics.

1.1.1 Example 1: The SI model

First, I will discuss the simple epidemic, or SI, model [22]. This model represents how individuals transition between the susceptible (S) and infective (I) classes. Once infected, individuals remain infected throughout the time interval under study. SI models often do a good job of describing the initial stages of many diseases [23]. These models are also

well-suited for diseases in which infected individuals are infectious for life. Examples of SI models, in practice, include models of feline infectious peritonitis and leukemia [24], herpes [25], and African swine fever [26].

The differential equations of this model are

$$\frac{dS}{dt} = -\beta SI, \tag{1.1}$$

$$\frac{dI}{dt} = \beta SI, \tag{1.2}$$

where $S + I = N$, and N is the total population size [23]. In this model, βI is the force of infection. The force of infection is the probability density of a susceptible contracting a disease in the next time step [23], so βSI is the rate of new infections [27]. This rate is based on the law of mass action and is considered mass action incidence, meaning that the rate of new infections is dependent on the numbers of susceptible and infective individuals in the population.

For simple models like SI models, we can solve the ordinary differential equations of the model. The assumption $S + I = N$ allows us to simplify the model to a single equation,

$$\frac{dI}{dt} = \beta(N - I)I. \tag{1.3}$$

We can solve this equation using the standard techniques for solving a Bernoulli differential equation. With the initial condition $I(0) = I_0$, the solution to this equation is

$$I(t) = \frac{I_0 N}{I_0 - (I_0 - N)\, e^{-\beta N t}}. \tag{1.4}$$

We can see that, for any $\beta, I_0 > 0$, the disease will spread through the population with this model. An example of the evaluation of this model is given in Figure 1.1.

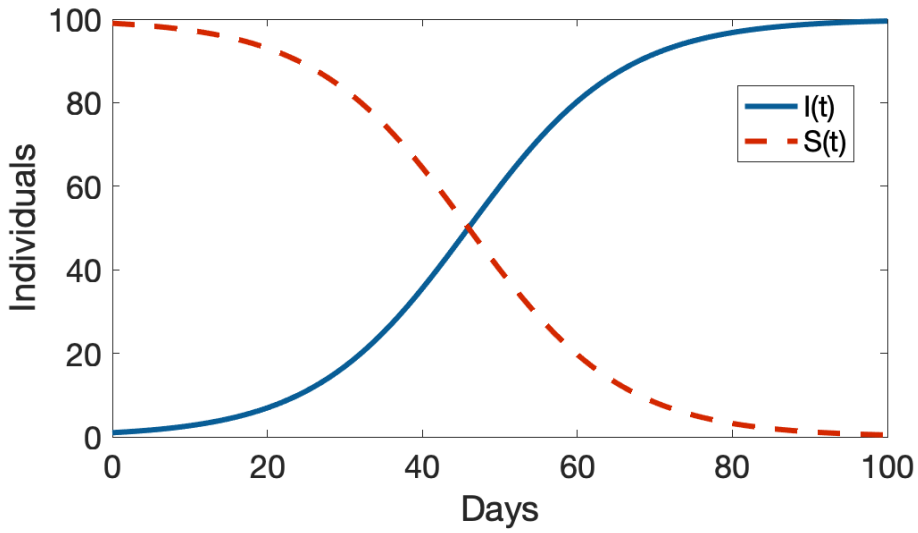

Figure 1.1: Example of a simple epidemic model. This figure shows an evaluation of the simple epidemic model with $(N, I_0, \beta) = (100, 1, 0.001)$. We can see that the number of infective individuals increases and the number of susceptible individuals decreases until the entire population is infected.

Again, the SI model assumes that, once infected, an infective individual will remain infected for the entire time interval. If we instead want to study a disease for which individuals may recover within a time frame, we would need to include an additional disease class.

1.1.2 Example 2: The SIR model

If infective individuals are able to recover and are unable to be reinfected within a given time frame, we include the recovered disease class (R). This gives us a susceptible–infective–recovered (SIR) model [20]. The recovered class may also be considered the removed class, which would also represent individuals that are permanently removed from the population due to death or isolation as well as immunity [23]. SIR models are useful for modeling epidemics, or outbreaks that run through a population in a relatively short time [28]. Examples of diseases that can be described by SIR models in practice include measles [29] and influenza [30].

The equations of this model are

$$\frac{dS}{dt} = -\beta SI, \tag{1.5}$$
$$\frac{dI}{dt} = \beta SI - \gamma I, \tag{1.6}$$
$$\frac{dR}{dt} = \gamma I, \tag{1.7}$$

where $I(0) = I_0$, $S(0) = S_0$, and $R(0) = 0$. In this model, susceptible individuals become infective at rate βI, and infective individuals recover at rate γ. Here, we are assuming that $S + I + R = N$, where N is the total population size. Therefore, this system reduces to

$$\frac{dS}{dt} = -\beta SI, \tag{1.8}$$
$$\frac{dI}{dt} = \beta SI - \gamma I. \tag{1.9}$$

Although we do not have a closed-form solution to this system of three nonlinear ODEs, we can extract much information about the system through analysing the basic reproductive number.

The basic reproductive number is the expected number of secondary infections caused by introducing a single infective individual into a wholly susceptible population [27]. The value of $\mathcal{R}_0$ determines whether or not an epidemic will occur. If $\mathcal{R}_0 > 1$, then $dI/dt > 0$ and an epidemic will occur, and if $\mathcal{R}_0 < 1$, then $dI/dt < 0$ and an epidemic will not occur. To find $\mathcal{R}_0$ for this example, we can simply determine where $dI/dt > 0$. Since we calculate $\mathcal{R}_0$ at the beginning of an outbreak, when $I_0 = 1$ and $S_0 \approx N$, this inequality reduces to

$$\frac{\beta N}{\gamma} > 1, \tag{1.10}$$

or

$$\frac{\text{(Rate that the infected individual makes infectious contacts)}}{\text{(Duration of infection)}} > 1. \tag{1.11}$$

Examples of evaluations of this model for $R_0 > 1$ and $R_0 < 1$ are given in Figure 1.2.

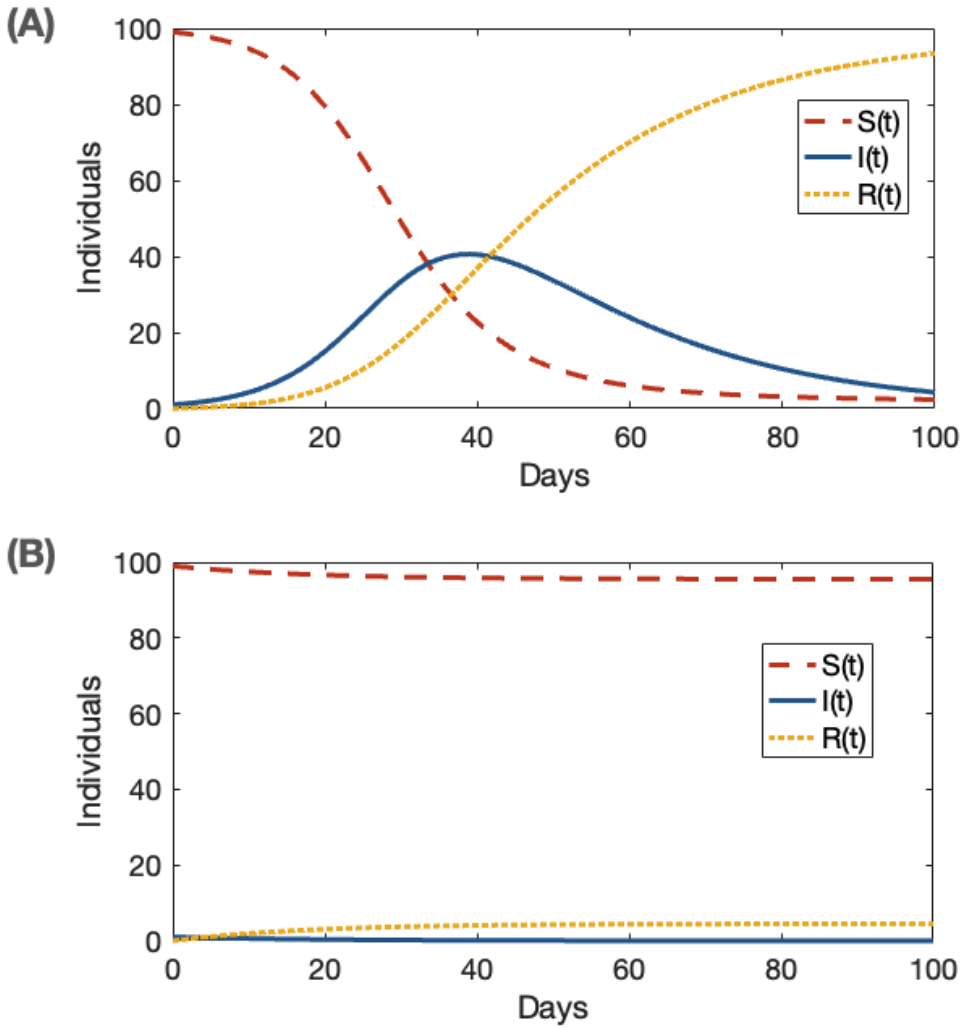

Figure 1.2: Example of an SIR model. Figure (A) shows an evaluation an SIR model with $(N, I_0, \beta, \gamma) = (100, 1, 0.002, 1/20)$. In this example, $\mathcal{R}_0 > 1$. Figure (B) shows an evaluation an SIR model with $(N, I_0, \beta, \gamma) = (100, 1, 0.002, 1/4)$. In this example, $\mathcal{R}_0 < 1$.

1.1.3 Example 3: The SIS model

If individuals do not gain immunity upon recovery, we can use an SIS model instead of an SIR model. SIS models, or susceptible-infectious-susceptible models, are used to study diseases like rotaviruses, sexually transmitted infections, and many bacterial infections [31]. They are are also appropriate for diseases that only confer variant-specific immunity [30].

The ordinary differential equations (ODEs) for the SIS model are

$$\frac{dS}{dt} = -\beta SI + \gamma I, \tag{1.12}$$

$$\frac{dI}{dt} = \beta SI - \gamma I, \tag{1.13}$$

where $I(0) = I_0$. In this model, susceptible individuals become infective at rate βI, and infective individuals recover and move back to the susceptible class at rate γ. Again, we are assuming that $S + I = N$, where N is the total population size. As with the SI model, this system reduces to a single ODE,

$$\frac{dI}{dt} = f(I) = \beta(N - I)I - \gamma I. \tag{1.14}$$

Also, like with the SI model, we can find a closed-form solution to this ODE by using the standard techniques for solving a Bernoulli differential equation. The solution to this ODE is

$$I(t) = \frac{(\beta N - \gamma)I_0 e^{t(\beta N - \gamma)}}{\beta I_0 e^{t(\beta N - \gamma)} + \beta(N - I_0) - \gamma}. \tag{1.15}$$

Although, we are able to find the closed for solution in this case, it is also helpful to determine $\mathcal{R}_0$ and analyze the equilibrium points of the dynamical system.

We determine $\mathcal{R}_0$ in the same way as in the previous example to get $\mathcal{R}_0 = \beta N/\gamma$. To find the equilibrium points, we set $I'(t) = 0$ and solve for $I(t)$. Doing this we get

$$I\left[\beta(N - I) - \gamma\right] = 0, \tag{1.16}$$

which can have two solutions. The first solution is $I = 0$, which means $S = N$. This solution is referred to as the disease-free equilibrium. The second solution is the endemic equilibrium. The endemic equilibrium is a constant solution where the disease persists in the population. In this case, the endemic equilibrium occurs when $\beta(N - I) - \gamma = 0$, or when

$$I = N - \frac{\gamma}{\beta} \quad \text{and} \quad S = \frac{\gamma}{\beta}. \tag{1.17}$$

To determine the Lyapunov stability of the equilibrium points, we plug them into the derivative of $f(I)$, from equation 1.14, with respect to I,

$$f'(I) = \beta(N - 2I) - \gamma. \tag{1.18}$$

The disease-free equilibrium yields

$$f'(I^*) = \beta N - \gamma. \tag{1.19}$$

This is asymptotically stable if $f'(I^*) < 0$ and unstable if $f'(I^*) > 0$. Therefore, the disease-free equilibrium is asymptotically stable when $\mathcal{R}_0 < 1$.

The endemic equilibrium yields

$$f'(I^*) = -\beta N + \gamma. \tag{1.20}$$

Again, this is asymptotically stable if $f'(I^*) < 0$ and unstable if $f'(I^*) > 0$. Therefore, the endemic equilibrium is asymptotically stable when $\mathcal{R}_0 > 1$.

An example of an evaluation of this model for $R_0 > 1$ is given in Figure 1.3.

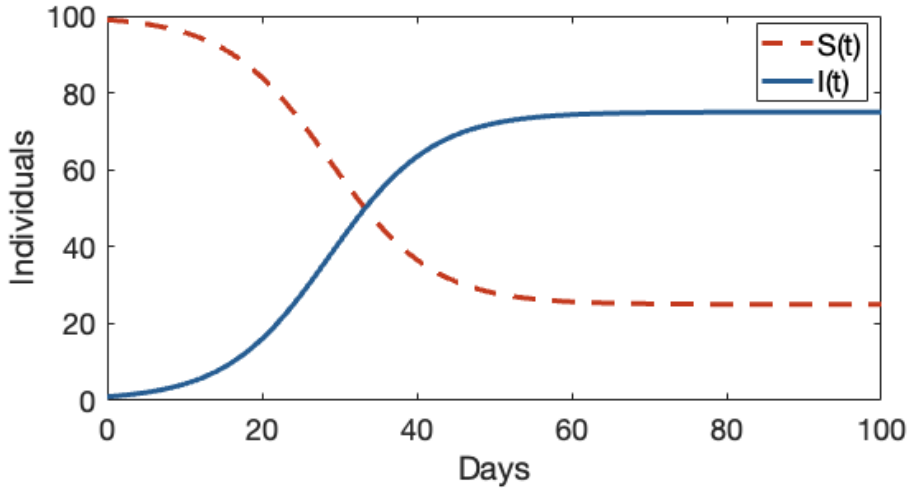

Figure 1.3: Example of an SIS model. This figure shows an evaluation an SIS model with $(N, I_0, \beta, \gamma) = (100, 1, 0.002, 1/20)$. In this example, $\mathcal{R}_0 > 1$, and we see that the endemic equilibrium is reached.

1.1.4 Incorporating complex disease dynamics

So far, we have only looked at examples of compartmental models with simple disease dynamics. When working with fatal diseases, diseases in populations with short life spans, and populations where new susceptibles may enter, birth and death rates or immigration or emigration rates should be included. Adding these rates into the model can affect the value of $\mathcal{R}_0$ as well as the stability of the equilibrium points. Moreover, depending on the dynamics of the disease or mitigation strategies under study, more compartments may be added. Also, the spread and progression of a disease and use of mitigation strategies may depend on the demographic features of individuals in the population, such as age or occupation. To capture these dynamics, age structure may need to be incorporated into a model.

Additional model compartments

We can add disease classes to a compartmental model to capture more complex disease dynamics. For example, if there is a latency period between infection and infectiousness, we add the exposed (E) compartment. Figure 1.4 shows a diagram of an SEIR model.

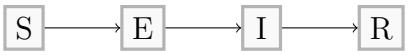

Figure 1.4: Diagram of an SEIR compartmental model

We can also add compartments to represent different species or disease strains to study disease transmission between populations as well as within populations. For example, models of vector-borne diseases include both human and vector populations with the possibility of transmission between them.

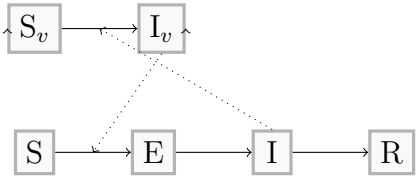

Figure 1.5: Diagram of a vector-borne disease model.

In Figure 1.5 above, the vector population is modeled by an SI model and has compartments S_v and I_v. The human population is modeled with an SEIR model. The dotted arrows show that infective humans infect susceptible vectors, and infective vectors infect susceptible humans.

If testing mitigation strategies like vaccination or quarantine, we can add compartments for vaccinated (V) or quarantined (Q).

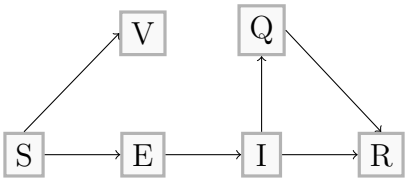

Figure 1.6: Diagram of a model with compartments for vaccination and quarantining.

In Figure 1.6 above, susceptible individuals may be vaccinated and move into compartment V, which confers perfect immunity in this case. Moreover, infective individuals may be quarantined and move into compartment Q before recovering. Quarantined individuals would not be able to infect susceptibles.

Age-structured models

In the example for a vector-borne disease in the previous section, we saw that we can use compartmental models to capture interactions between different populations. Similarly, we can also use compartmental models to capture interactions between subgroups within a population. A common example of this type of model is an age-structured model.

In age-structured models, the population is usually divided into age-classes such as children, young adults, adults, and the elderly [31]. In these models, individuals can transition between age classes as well as between disease states. Model parameters may also be dependent on age. For example, susceptibility, the rates of symptomatic infection, disease progression, recovery, and birth and death usually vary for different age-groups. Additionally, contact rates between different age groups often vary, which can greatly affect how a disease spreads.

As an example, a basic SIR model considering four age groups ($n = 1, 2, 3, 4$) consists of twelve ODEs with three ODEs per age group. The equations of this system for age-group a are

$$\frac{dS_a}{dt} = -S_a \sum_n \beta_{a,n} I_n, \tag{1.21}$$

$$\frac{dI_a}{dt} = S_a \sum_n \beta_{a,n} I_n - \gamma(a) I_a, \tag{1.22}$$

$$\frac{dR_a}{dt} = \gamma(a) I_a. \tag{1.23}$$

Here $\beta_{a,n}$ is an element of a transmission matrix describing the interactions between age-groups,

$$\beta = \begin{bmatrix} \beta_{1,1} & \beta_{1,2} & \beta_{1,3} & \beta_{1,4} \\ \beta_{2,1} & \beta_{2,2} & \beta_{2,3} & \beta_{2,4} \\ \beta_{3,1} & \beta_{3,2} & \beta_{3,3} & \beta_{3,4} \\ \beta_{4,1} & \beta_{4,2} & \beta_{4,3} & \beta_{4,4} \end{bmatrix}. \tag{1.24}$$

In this system, the per-capita recovery rate, γ, also depends on age.

Age-structured models can be used to test mitigation strategies that affect only certain age groups, such as school closures. Furthermore, determining which age groups to target for mitigation strategies like vaccination also requires age-structured models with age-dependent parameters.

1.2 Optimal control theory

Optimal control theory is a branch of mathematics in which we attempt to find a control that leads to a desired outcome for a dynamical system. In optimal control theory, state variables describe the behavior of the dynamical system. Controls act on the state variables in order to achieve a desired result, which is minimizing or maximizing an objective functional [32].

For state variable $x(t)$ and control $u(t)$, a basic optimal-control problem looks something like

$$\begin{aligned} \max_u \int_0^T f(t, x(t), u(t))dt, \\ \text{subject to} \quad \dot{x}(t) =& g(t, x(t), u(t)), \\ x(0) =& x_0, \\ x(T) =& \text{free}, \end{aligned} \tag{1.25}$$

where f and g are continuously differentiable functions, $u(t)$ is piecewise continuous, and $x(t)$ is piecewise differentiable. Moreover, $x(T)$ being free means that the value of $x(T)$ is unrestricted [32].

A solution to this problem satisfies the set of necessary conditions consisting of the optimality condition, the adjoint equation, and the transversality condition, which were developed by [33]. The optimality condition is that the Hamiltonian,

$$H(t, x, u, \lambda) = f(t, x, u) + \lambda g(t, x, u), \tag{1.26}$$

must be maximized with respect to the control such that, if $x^*(t)$,$u^*(t)$ are optimal for problem (1.25), then

$$H(t, x^*(t), u(t), \lambda(t)) \leq H(t, x^*(t), u^*(t), \lambda(t)). \tag{1.27}$$

In equations (1.26) and (1.27), λ is the adjoint variable. The adjoint equation, which must be satisfied, is

$$\dot{\lambda} = -\frac{\partial H}{\partial x} = -(f_x + \lambda g_x). \tag{1.28}$$

Lastly, the transversality condition is given by

$$\lambda(T) = 0. \tag{1.29}$$

1.2.1 Example

In this section, we will go over an example of how to solve a simple optimal-control problem using Pontryagin's maximum principle. The example we will solve is

$$\begin{aligned} &\max_u \int_0^T x(t) - u(t)^2 dt, \\ \text{subject to} \quad &\dot{x}(t) = u(t) + x(t), \\ &x(0) = 0, \\ &x(T) = \text{free}, \end{aligned} \tag{1.30}$$

We begin solving this by determining the control Hamiltonian as described in equation (1.26),

$$H = x - u^2 + \lambda(u + x). \tag{1.31}$$

The adjoint equation, is given by

$$\dot{\lambda} = -\frac{\partial H}{\partial x} = -(1 + \lambda). \tag{1.32}$$

This is a separable ODE and is easily solved to get

$$\lambda(t) = e^{T-t} - 1. \tag{1.33}$$

As the Hamiltonian is non-linear with respect to the control, we determine the control that maximizes the Hamiltonian by setting the derivative of 1.31 with respect to u equal to zero. This gives us

$$\frac{\partial H}{\partial u} = \lambda - 2u = 0. \tag{1.34}$$

At u^*, this implies that

$$u^* = \frac{1}{2}\lambda = \frac{1}{2}\left(e^{T-t} - 1\right). \tag{1.35}$$

Then, at x^*, $\dot{x}$ satisfies

$$\dot{x}(t) = \frac{1}{2}\left(e^{T-t} - 1\right) + x. \tag{1.36}$$

This can solved using an integrating factor to get

$$x^*(t) = \frac{1}{4}\left(1 - e^{-t}\right)\left(e^{T+t} + e^{T} - 2e^{t}\right). \tag{1.37}$$

Now, we have the solution to the state variable and control that maximizes the objective functional.

1.2.2 Numerical methods for solving optimal-control problems

It is often the case that we cannot solve optimal-control problems analytically and need to use numerical methods to determine solutions. A common approach for numerically solving optimal-control problems is forward-backward sweep (fbs), which finds a discrete-time approximation for the control variable [32, 34–36]. This method works by converting the optimal-control problem into a boundary value problem that can be solved numerically. We start this algorithm by making an initial guess for the control variable across the time interval. We then solve the state equation forward in time, starting with the initial condition, and the adjoint equation backward in time, starting from the transversality condition, $\lambda(T) = 0$. The final iterative step is to update the control variable using the updated values for the state

and adjoint variables. We continue this process iteratively until convergence is achieved.

Although the forward-backward sweep method is able to find a solution for many optimal-control problems, it does not always converge. Sometimes it is necessary to use more sophisticated optimal-control toolkits, such as the dsoa package [37]. This algorithm transforms the problem into a finite-dimensional parameter optimization problem, meaning the algorithm uses a direct method. This transformation is done by rewriting the Bolza type problem as a Mayer-type problem, parameterizing the control variable as piecewise constant, and discretizing the problem using a linearly implicit Runge-Kutta method. This results in a nonlinear programming problem that can be solved using sequential quadratic programming.

1.2.3 Use with epidemic models

Optimal-control problems can be used to study the effects of mitigation strategies, like vaccination or quarantine, on the transmission of infectious diseases. In this type of optimal-control problem, the state variables are governed by differential equations for the infectious disease compartments, like those described in Section 1.1. Moreover, the control variable can describe mitigation strategies like social distancing, quarantine or isolation, vaccination rates, or treatment with antibiotics. Optimal-control models in epidemiology take into account the resource constraints, such as economic constraints, involved with implementing mitigation strategies [38]. Therefore, they are often used to find the strategy that best reduces morbidity and mortality within the required constraints.

1.3 Other strategies for determining the best epidemic mitigation practices

In addition to optimal control, there are many other options for using optimization with epidemiological models. For example, cost-effectiveness analysis, linear and integer programming, and other optimization approaches combined with epidemic simulations have

been used to determine the best strategy for controlling an epidemic or the best way to distribute limited resources [39].

Each of these techniques has different formulations and limiting assumptions that determine their usefulness for solving various problems in epidemiology. Cost-effectiveness analysis is used for comparing the costs and health benefits of specific intervention strategies or finding the best way to allocate resources between given strategies [39, 40]. These analyses assume that any fraction of an intervention may be implemented, the health benefits from an intervention increase proportionally with increased implementation of that intervention, and interventions are independent of each other [40]. These assumptions do not hold for many epidemic-control problems.

Linear and integer programming formulations for resource allocation only make one of these assumptions, that interventions are independent of each other. This assumption means that the implementation of one mitigation strategy does not affect the cost-effectiveness of another, but this is again often not the case for epidemic control problems [40]. Both cost-effectiveness analysis and linear and integer programming approaches are not able to take the nonlinearities in cost-effectiveness due to the underlying epidemic dynamics into consideration [40].

Optimal-control models, like those discussed in Section 1.2.3 do not face the same limitations and are often used to determine the best vaccination, treatment, removal or culling, and isolation practices [41–47]. These models, however, are usually limited to studying a specific intervention in a specific population [40].

Similarly, optimization approaches combined with epidemic simulations have fewer limiting assumptions and can be used when testing the effects of disease mitigation strategies on realistic disease models [40]. Some examples of optimization approaches that have been used with compartmental models to find optimal disease-mitigation strategies include machine learning algorithms and evolutionary algorithms [48], particle swarm optimization [49], linear programming [50–52], dynamic programming [53] mathematical programming algorithms

[54], etc.

1.4 Overview

This work consists of three chapters. In the first chapter, I study an optimal-control problem that maximizes economic output during an infectious disease outbreak that obeys SIS disease dynamics [3]. In this model, revenue is due to healthy individuals and medical costs are associated with infective individuals. The control variable is the level of mixing in the population, which influences both revenue and the spread of the disease. Using Pontryagin's maximum principle, we find a closed-form solution for our problem. We explore an example of our problem with parameters for the transmission of *Staphylococcus aureus* in dairy cows and find that less mixing is preferable when the transmission rate is high, the per-capita recovery rate is low, or when the revenue parameter is much smaller than the cost parameter.

In the second chapter, I expand the optimal-control model from the previous chapter to consider the severity of the disease under study. In the new model, infective individuals can still be economically productive, and I continue the case study of *Staphylococcus aureus* in dairy cows. I also analyze candidate solutions to the new optimal-control problem that satisfy the first-order necessary conditions of Pontryagin's maximum principle. I find that multiple candidate solutions, exhibiting very different behavior, may coexist for some parameter sets. Moreover, the candidate solutions may have similar economic outputs and may trade optimality with small changes in parameter values. This result emphasizes that, in many situations, more factors need to be taken into consideration when making policy decisions.

The third chapter of this dissertation is on optimizing COVID-19 mitigation strategies, in this case vaccine distributions, when considering both equity and the burden of disease [55]. To provide a race-conscious framework to quantify and minimize inequity, I use an age-and-race-stratified mathematical model of SARS-CoV-2 transmission fitted to age-and-

race-stratified mortality data from 2020 in Oregon and analyze counterfactual vaccination strategies in early 2021. I consider two racial groups: non-Hispanic White persons and persons belonging to BIPOC groups (including non-Hispanic Black persons, non-Hispanic Asian persons, non-Hispanic American Indian or Alaska Native persons, and Hispanic or Latino persons). I allocate a limited amount of vaccine to minimize overall disease burden, inequity in disease outcomes between racial groups, or both. I find that, when allocating small amounts of vaccine (10% coverage), there is a trade-off between minimizing disease burden by prioritizing older age groups and minimizing inequity by prioritizing younger, BIPOC groups. The allocation strategies that minimize combinations of measures can produce middle-ground solutions that similarly improve both disease burden and inequity, but the trade-off can only be mitigated by increasing the vaccine supply. With enough resources to vaccinate 20% of the population the trade-off lessens, and with 30% coverage, I can optimize both equity and mortality.

Chapter 2

Optimal Reduced-Mixing for an SIS Infectious-Disease Model

Infectious-disease outbreaks are a growing problem. The rate at which diseases emerge or re-emerge is increasing [56–60] due to factors such as global travel, rural-to-urban migration, and climate change [56, 61–63]. Examples of recent disease outbreaks include foot and mouth disease [12], African swine fever [13], olive quick decline syndrome [64], tomato brown rugose fruit virus [65], tuberculosis [66], Zika [67], SARS [68], H1N1 [69], Ebola [70], and COVID-19 [68]. Many of these diseases have had severe economic consequences [12, 64, 71–73]. We clearly need to know how to respond to new outbreaks if and when they occur.

Ideally, we would like to minimize the duration of an outbreak, the cost of illness, or the cost of mitigation strategies. We may also wish to optimize some combination of these often-conflicting objectives. To achieve these goals, researchers often use optimal control theory to efficiently control dynamic disease systems [41–47]. In general, these systems consist of state variables, control variables, and state equations. The state variables often represent disease classes within a population, such as the number of susceptible (S), infective (I), or recovered (R) individuals, as functions of time. The control variables and the state equations govern the evolution of the state variables, and we want to choose the control variables so as to

maximize or minimize specified objective functionals [32].

An especially important topic in the study of emerging infectious diseases is the use of optimal control theory to control mixing. The goal here is to design strategies that limit the number of contacts between susceptible and infective individuals. For humans, strategies may include social-distancing measures such as limiting time spent in public spaces, isolating infectives, quarantining infected households, closing schools, and restricting large social gatherings [74–76]. For livestock, reduced-mixing strategies may include quarantining infected and exposed animals and shutting down facilities where animals are in close contact. For crops, reduced-mixing strategies may include using screenhouses, introducing barrier plants, or reducing planting density [77–79]. Many of these strategies do, however, have high economic costs [80–85].

To address these economic costs, many researchers have tried to balance economic output with the cost of infection, which can include death or the burden of disease on an individual or on medical and public health infrastructures. These researchers have frequently used complex multi-compartmental models, which they solve numerically, to minimize the size of an outbreak [86] or to minimize both the size and economic cost of an outbreak [39, 46, 87, 88].

In this paper, we instead focus on finding simple, analytic optimal-mixing strategies for SIS disease dynamics. In an SIS model, individuals are either susceptible or infectious, and individuals who recover may then be reinfected. This model is used to study diseases that do not confer immunity after recovery, such as rotaviruses, sexually transmitted infections, and many bacterial infections [31]. Also, as noted by [30], SIS models are often appropriate for diseases that confer variant-specific immunity, such as when many variants are circulating in a population. Examples of SIS models, in practice, include models of *Staphylococcus aureus* in dairy cows [1], typhoid fever in humans [89], trachoma in humans [90], trypanosomiasis in Indonesian buffaloes [30], and gonorrhea in humans [91, 92].

In Section 2.1, we introduce an optimal-control problem, with SIS disease dynamics, that will let us determine whether reduced mixing is economically beneficial. We assume

that economic profit, be it for a farm or a company, is the revenue generated by healthy susceptibles minus the cost of sick infectives over the given time interval. The control variable is the level of mixing in the population, which can range from little or no mixing to high or full mixing. In particular, the ability to reduce mixing may be limited by economic constraints or by a lack of willingness to comply with guidelines, and the ability to mix may be limited by fear of spreading disease or the need to gather resources to restart production.

In Section 2.2, we determine closed-form optimal solutions and find that reducing mixing can improve economic output. We also study under which conditions a longer period of reduced mixing is more profitable. We find that the optimal reduced-mixing strategy is bang-bang and has at most one switch from the lowest possible level of mixing to the highest possible level of mixing.

In Section 2.3, we use parameters for the transmission of *Staphylococcus aureus* in dairy cows and compare our analytical solutions with numerical simulations. Then, in Section 2.4, we explore the effects of varying key parameters such as the minimum and maximum mixing levels, the revenue generated per susceptible per day, the cost per infective per day, and the time horizon. We also look at the effects of varying the infectiousness, recovery time, and the initial number of infected individuals on the optimal length of the reduced-mixing period. Finally, in Section 2.5, we summarize our results and discuss the limitations and future directions of our research.

2.1 Optimizing reduced-mixing for an SIS model

We wish to maximize economic output during an infectious-disease outbreak. In this section, we assume that our outbreak obeys SIS dynamics. The SIS model describes a population transitioning from a susceptible state to an infectious state and back [93]. These models are commonly used for studying diseases that do not confer immunity upon recovery [31].

The ordinary differential equations (ODEs) for the SIS model are

$$\frac{dS}{dt} = -a(t)\beta SI + \gamma I, \tag{2.1}$$

$$\frac{dI}{dt} = a(t)\beta SI - \gamma I, \tag{2.2}$$

where $S(t)$ and $I(t)$ are state variables representing the number of susceptible and infectious individuals in the population. Some authors [28, 31] use S and I for the fractions of a population that are susceptible or infectious. We instead follow [93] and many other authors, e.g. [23, 27], in using these variables for the numbers of susceptibles and infectives.

In the above equations, the control variable $a(t)$ represents the level of mixing of the population at time t. The mixing level ranges between m, for the lowest possible level of mixing, and M, for the highest possible level of mixing. Both m and M can range between zero, for no mixing, and one, for full or normal levels of mixing. The parameter β is the transmission coefficient, or the rate of infection per susceptible per infective. The parameter γ represents the per-capita rate of recovery for infected individuals.

After adding equations (2.1) and (2.2), it quickly follows that $S + I = N$, where N is the total population size. We can, as a result, reduce equations (2.1) and (2.2) to a single state equation,

$$\frac{dI}{dt} = a(t)\beta(N - I)I - \gamma I, \tag{2.3}$$

with the initial condition $I(t) = I_0$, where $I_0 < N$. Our state equation and control variable in this case are like those in [94]. We focus, however, on reducing general mixing rather than on solely quarantining infectives.

The objective functional that we will maximize is

$$\max_{m \le a(t) \le M} \int_0^T ra(t)[N - I(t)] - cI(t)dt. \tag{2.4}$$

The first term in the objective functional is the revenue generated by the active susceptible population, while the second term represents the cost generated by infected individuals.

Higher activity increases revenue but also increases the spread of the disease.

The parameter r is the revenue generated per healthy susceptible per day, and the parameter c is the cost per sick infective per day. This cost is separate from (and in addition to) lost revenue or productivity. The parameter c typically includes medical or treatment costs. Both r and c are, by assumption, positive. T is the terminal time, also called the time horizon. It can be chosen based on factors such as vaccine development time or using economic or logistical criteria.

This formulation assumes that infective individuals do not contribute economically, but that they do interact with the population to the extent that the control variable, which limits mixing, permits. For humans, we assume, in other words, that infectives are too sick to work, but not too sick to interact with household members, health-care workers, and others. For livestock, we assume that sick animals cannot produce goods, but that they do still do interact with other animals. For crops, we assume that infected plants cannot be sold but do contribute to the spread of a disease.

2.2 Analytical solutions

We will determine the analytical solutions to the optimal-control problem described in Section 2.1 using Pontryagin's maximum principle [33]. First, we need to define the control Hamiltonian, H. The Hamiltonian is

$$\begin{aligned} H &= f(t, I, a) + \lambda g(t, I, a) \\ &= a(t)[N - I(t)][r + \lambda(t)\beta I(t)] - I(t)[c + \lambda(t)\gamma], \end{aligned} \tag{2.5}$$

where $f(t, I, a)$ is the integrand of objective functional (2.4) and $g(t, I, a)$ is the right-hand side of state equation (2.3).

For the problem given by equations (2.3) and (2.4), the maximum principle tells us that, for the optimal trajectories $I^*(t)$ and $a^*(t)$, there exists a piecewise-differentiable adjoint variable, $\lambda(t)$, obeying the differential equation

$$\begin{aligned}\dot{\lambda}(t) &= -\frac{\partial H(t, I^*(t), a(t), \lambda(t))}{\partial I} \\ &= a\left[r - \lambda\beta\left(N - 2I\right)\right] + c + \gamma\lambda\end{aligned} \tag{2.6}$$

and the transversality condition $\lambda(T) = 0$. The maximum principle also tells us that

$$H(t, I^*(t), a(t), \lambda(t)) \leq H(t, I^*(t), a^*(t), \lambda(t)) \tag{2.7}$$

for all possible a at time t [32, 95].

Before we find the analytical solution, it is helpful to note that we have defined an optimization problem with three variables: the state variable, $I(t)$, the control variable, $a(t)$, and the adjoint variable, $\lambda(t)$. In addition to maximization condition (2.7), the problem is subject to two ODEs that describe the dynamics of the state and adjoint variables. We also have an initial condition for the state equation and a terminal condition for the adjoint equation. Therefore, the ODEs form a two-point boundary value problem. In general, we want to solve the state equation forwards in time and the adjoint equation backwards in time.

Now, we can begin to solve the problem. First, we observe that the Hamiltonian is linear in the control variable,

$$H = a\phi(t) - (c + \lambda\gamma)I, \tag{2.8}$$

where

$$\phi = (N - I)\left(r + \lambda\beta I\right) \tag{2.9}$$

is known as the switching function.

The above linearity implies that the form of the optimal control that maximizes the Hamiltonian is bang-bang, meaning the control must be at either its maximum or minimum possible value at any time. If the switching function is either positive or negative, the optimal

control is

$$a(t) = \begin{cases} m, & \phi(t) < 0, \\ M, & \phi(t) > 0. \end{cases} \tag{2.10}$$

A switch occurs when $\phi = 0$ or when

$$\lambda = -\frac{r}{\beta I} \tag{2.11}$$

In addition, cases may arise where the optimal-control model has a singular solution. This occurs if $\phi(t) = 0$ over an entire interval. To determine if a singular solution exists for our problem, we set the derivative of λ, obtained from the switching condition (2.11), equal to equation (2.6) at the time of the switch. From this, we find that a singular solution is only possible for $c = 0$. Since c is positive, this precludes the possibility of a singular solution for our problem.

The next step is to solve the state and adjoint equations using what we have learned about the control. To do this, we will assume that at most one switch occurs, which we will demonstrate later. Also, the transversality condition for the adjoint equation tells us that $\lambda(T) = 0$, so that $\phi(T) = r(N - I)$ is positive, in light of equation (2.3) and our assumption that $I_0 < N$. We now know, from equation (2.10), that $a(T) = M$. In other words, the solution to the optimal-control problem must be at the highest level of mixing at the final time. This implies that if a switch occurs, the switch will be from the lowest level of mixing, $a = m$, to the highest level of mixing, $a = M$. If no switch occurs, the population is always at the highest level of mixing.

If we assume that at most one switch occurs, we can find an analytical solution to the generalized optimal-control model. Before the switch occurs at $t = t_1$, we know that $a = m$. Using this and the initial condition, $I(0) = I_0$, we solve the state equation for times $t \leq t_1$ to get

$$I(t) = \frac{\delta_m I_0}{m\beta I_0 + (\delta_m - m\beta I_0)e^{-\delta_m t}}, \tag{2.12}$$

where $\delta_m = mN\beta - \gamma$.

Similarly, we can solve the state equation at times $t \geq t_1$ using the conditions $I(t_1) = I_1$ and $a = M$ for $t \geq t_1$. The solution to the state equation after the switch is

$$I(t) = \frac{\delta_M I_1}{M\beta I_1 + (\delta_M - M\beta I_1)e^{-\delta_M (t-t_1)}}, \tag{2.13}$$

where $\delta_M = MN\beta - \gamma$. By evaluating equation (2.12) at time t_1, we find I_1, which is used in equation (2.13).

To solve the adjoint equation, we again find the solution in two parts. Since we have the transversality condition, $\lambda(T) = 0$, we will solve the adjoint equation backwards in time. First, we will determine the solution to the adjoint equation after the switch. When $t > t_1$, we know that $a = M$, and the adjoint equation is

$$\dot{\lambda}(t) + [\delta_M - 2M\beta I]\,\lambda(t) = Mr + c. \tag{2.14}$$

Using an integrating factor and the transversality condition, we find that the solution after the switch is

$$\lambda(t) = \frac{(Mr + c)\left[1 - e^{\delta_M (T-t)}\right] u(t)}{\delta_M u(T)}, \tag{2.15}$$

where

$$u(t) = (\delta_M - M\beta I_1) + M\beta I_1 e^{\delta_M (t-t_1)}. \tag{2.16}$$

Before the switch, we know that $t < t_1$ and $a = m$. With this information, we can solve the adjoint equation before the switch. Using an integrating factor, and the condition that the solution must equal equation (2.15) at time t_1, we find that the solution to the adjoint equation before the switch is

$$\lambda(t) = \frac{e^{-\delta_m t} v(t)}{m\beta I_0 \delta_m} \left[\frac{cv(t)}{v(t_1)} - (mr + c) \right], \tag{2.17}$$

where

$$v(t) = (\delta_m - m\beta I_0) + m\beta I_0 e^{\delta_m t}. \tag{2.18}$$

By setting equation (2.15) for the adjoint variable equal to switching condition (2.11), we find the ratio of the revenue and cost parameters as a function of the switching time,

$$\frac{r}{c} = \frac{\delta_m I_0 \beta \left[e^{\delta_M (T - t_1)} - 1 \right]}{\delta_M \left[m\beta I_0 + (\delta_m - m\beta I_0) e^{-\delta_m t_1} \right]}, \tag{2.19}$$

This allows us to numerically solve for the switching time. The effect of the ratio of the revenue and cost parameters on the switching time will be explored numerically in Section 2.4.1.

To prove that at most one switch occurs, we show that a second switch cannot occur before t_1. This means that we must have

$$\lambda(t) < -\frac{r}{\beta I(t)} \tag{2.20}$$

for all $t < t_1$. Plugging in solutions (2.17) and (2.12) for the adjoint and state equations before the switch at $t = t_1$, equation (2.20) becomes

$$\frac{e^{-\delta_m t} v(t)}{m\beta I_0 \delta_m} \left[\frac{cv(t)}{v(t_1)} - (mr + c) \right] < -\frac{re^{-\delta_m t} v(t)}{\beta \delta_m I_0}, \tag{2.21}$$

which reduces to $v(t) < v(t_1)$, where $v(t)$ is defined in equation (2.18). Since for $0 < t < t_1$ equation $v(t) < v(t_1)$ is true, we know that we can have at most one switch.

Figure 2.1 shows a typical (I,λ) phase portrait, on both sides of the switching function. This figure provides further evidence that, for various terminal times, only one switch is possible.

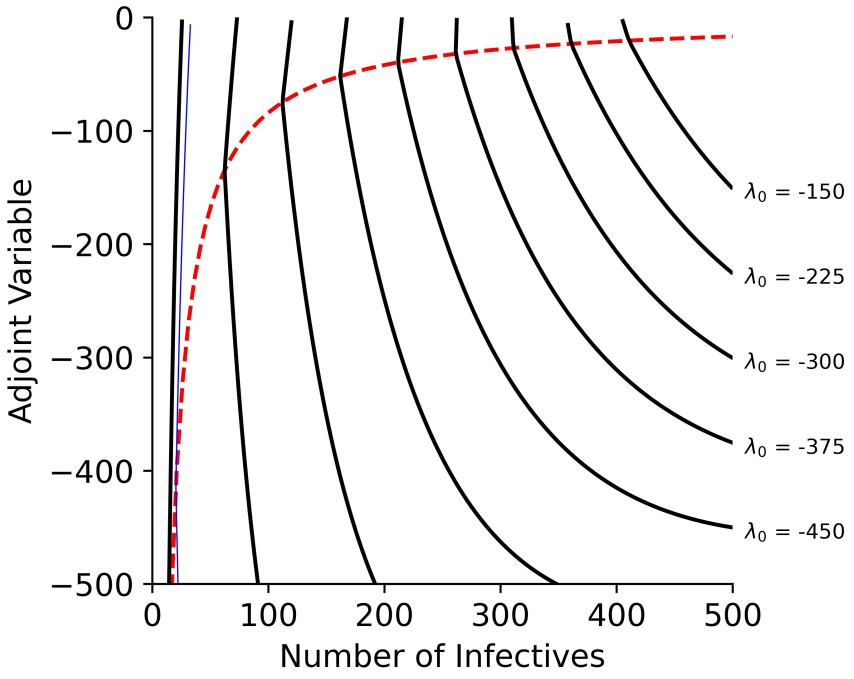

Figure 2.1: Phase portrait of optimal-control problem. The parameters used in this example are given in Table 2.1 with the exception of I_0, which we set to 499 individuals. In this figure, we see the behavior of λ, the adjoint variable (solid curves) and the value of the switching function (dashed curve) versus I, the number of infective individuals. Each of the solid lines is from an evaluation of the optimal-control model for a different terminal time. In this figure, we can see that the adjoint variable crosses the switching function at most once for each simulation. The thin solid line shows the phase portrait of the case study in Section 2.3.

A special case of the above SIS system occurs when $\gamma = 0$. Now, infected individuals do not recover. In this case, our outbreak obeys a simple epidemic, or SI, model [22]. This model is frequently used to describe highly-infectious diseases that are not serious [22, 96] or to study the initial (pre-recovery) stages of many other diseases [23]. The solution to the optimal-control problem for the SI case can be found by letting $\gamma = 0$ in the above solutions. For example, the ratio of the revenue and the cost parameters as a function of the switching time for the SI system is now just

$$\frac{r}{c} = \frac{\left[e^{MN\beta(T-t_1)} - 1\right] I_0}{M\left[(N - I_0)\, e^{-mN\beta t_1} + I_0\right]}. \tag{2.22}$$

2.3 Case study: bovine mastitis

As an example, we consider the transmission of *Staphylococcus aureus* genotype B (GTB) in Swiss communal dairy herds [1]. *S. aureus* GTB is a contagious pathogen that commonly causes mastitis in dairy cows. Mastitis, an inflammation of the mammary gland, leads to economic loss in the dairy industry due to reduced yield and poor milk quality. Mastitis can be categorized as clinical or subclinical. In cases of clinical mastitis, abnormalities are visible and can include watery milk with flakes or clots, a red and swollen udder, or fever. In cases of subclinical mastitis, which is more prevalent, abnormalities are not visually detectable and therefore, cases of subclinical mastitis are often undetected.

Both classes of mastitis decrease milk production during and after infection, but subclinical mastitis accounts for more financial loss than clinical mastitis due to its prevalence. This financial loss is, however, difficult to quantify [97, 98]. We will, therefore, use the economics associated with clinical mastitis to determine revenue and cost parameters, while keeping in mind that clinical mastitis is more costly (than subclinical mastitis) on a per-case basis.

In this example, revenue comes from milk produced by the dairy cows, and cost includes the cost of veterinary care, diagnostics, labor, therapeutics, future production loss, and future reproductive loss. These parameters were estimated from [98]. It is important to note that if infected cows are treated with antibiotics during the lactation period, the milk produced is discarded due to contamination. The treatment of subclinical mastitis with antibiotics is not generally cost effective. For highly contagious pathogens like *S. aureus*, however, treatment is still recommended [99]. Reduced-mixing strategies are also useful for preventing the spread of *S. aureus* and include quarantining cows with mastitis and milking cows with mastitis on separate machines or after uninfected cows [100].

As subclinical mastitis cases often go undetected, it may be beneficial to treat cows that are more likely to have subclinical mastitis, such as those with higher somatic cell counts (SCC, an indicator of milk quality), as infected. Thus, when the level of mixing is low, more cows are quarantined or milked separately. We also assume that they are treated with

antibiotics. Treatment costs and costs due to future production loss are only applied to infectives as we are assuming a higher cost of treatment associated with clinical mastitis, and only infectives will have future production losses.

We use a time horizon of 90 days because the communal pasture-based dairy operations, in our example, occur in the 2 to 3 months of the summer when cows are brought together at higher altitudes where they share pastures, milking equipment and housing facilities. As the mean duration for intramammary infections is 110 days, an outbreak during this time can be significant [1]. We adapted the transmission coefficient and the per-capita recovery rate for our simulation of mastitis from [1]. In their model, the transmission coefficient is estimated as $\beta N = 0.0232$ per day, so to adapt their parameter to our model, we divide by N. In [1], transmission is assumed to be cow-to-cow. Also, S represents susceptible cows, and I represents infected cows.

The parameters used to model the dynamics of *S. aureus* GTB transmission are in Table 2.1. The values of the parameters m and M are unknown, so we assume the values $m = 0.2$ and $M = 0.9$. We assume $m = 0.2$ as the minimum mixing level as it is unlikely that mixing between dairy cows can be completely eliminated due to spatial limitations at housing facilities and human error in milking practices that may lead to exposure to pathogens. We assume $M = 0.9$ as recommended milking practices will reduce mixing to some extent. We will see how different choices for m and M affect the results of our problem in Section 2.4.1.

To numerically solve our optimal-control problem we chose to explore freely available, optimal-control toolkits, including the dsoa package [37]. From the available options, we found dsoa to be the easiest to implement, and it was able to converge for all tested cases. This package transforms the optimal-control problem into a nonlinear programming problem that can be solved using sequential quadratic programming.

Figure 2.2 shows that with the parameter values for *S. aureus* GTB transmission given in Table 2.1 and the SIS state equations, the results from using dsoa and the analytical solutions are the same. In this case, the optimal solution is to switch to a higher level of

Table 2.1. Parameters used for numerical verification.

Parameter	Value	Meaning
β	$\frac{0.0232}{N}$ (indiv·day)$^{-1}$	Transmission coefficient
γ	$\frac{1}{110}$ day^{-1}	Per-capita recovery rate
T	90 days	Time horizon
r	0.39 $\frac{\text{US\$}}{\text{indiv} \cdot \text{day}}$	Revenue per susceptible per day
c	6.83 $\frac{\text{US\$}}{\text{indiv} \cdot \text{day}}$	Cost per infective per day
m	0.2	Minimum mixing level
M	0.9	Maximum mixing level
I_0	0.05N individuals	Initial number of infectives
N	500 individuals	Total population size

Sources: Disease parameters are estimated from [1]. Revenue and cost parameters are estimated from [98].

mixing about halfway through the simulation. At the time of the switch, which is after 44 days, about 4% of the population is infected, and, at the terminal time, about 6% of the population is infected. These dynamics are resonable, because subclinical mastitis is a mild infection. Thus, when low levels of infection are present, the cost of care and loss of productivity are not too high.

Figure 2.3 shows that the switching time determined in this solution maximized the economic output relative to other possible switching times.

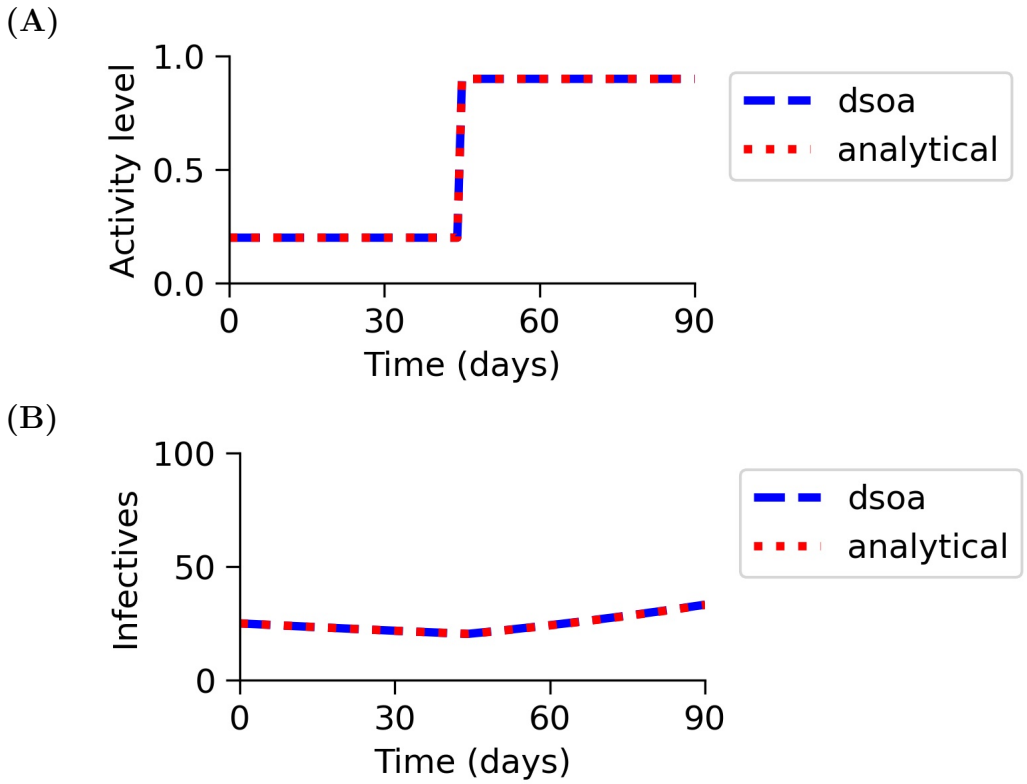

Figure 2.2: Analytical results and numerical results for the general SIS model. This figure shows that for the parameters given in Table 2.1, the results from using dsoa and the analytical solutions are the same. Figure (A) shows that the activity level, a, switches after about 44 days. Figure (B) shows that the infective population, I, decreases before the switch, and then increases after the switch.

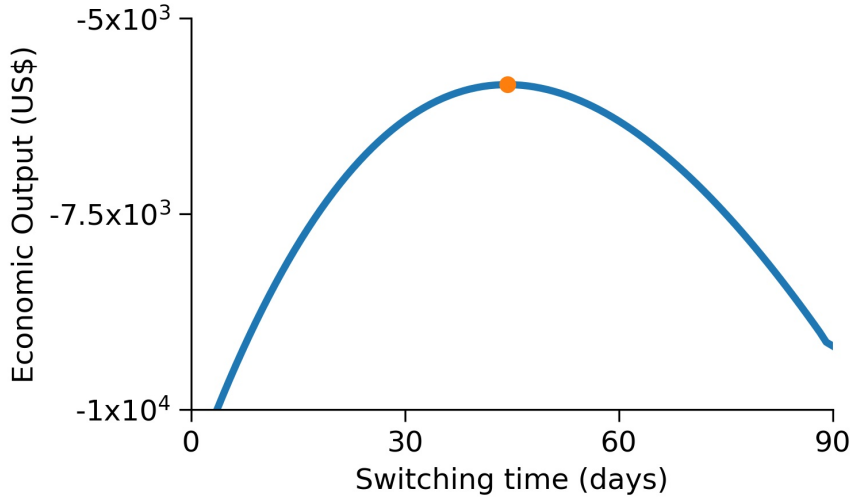

Figure 2.3: Verification of results for the optimal switching time. For the parameters given in Table 2.1, we vary t_1 from 0 days to T days and calculate the value of the objective functional. The solution for optimal switching time is shown as the dot. For the general SIS model, the maximum economic output is achieved at the solution for the optimal switching time, at about 44 days.

2.4 Sensitivity of results to model parameters

In Section 2.4.1, we will determine how changes in the ratio of the revenue and cost parameters change the switching time from that of the baseline simulations. We will see that, for the SIS model, reducing mixing is economically beneficial in many cases. In Section 2.4.1, we will vary the minimum and maximum mixing levels for the population and find that increasing either increases the switching time. In Section 2.4.1, we will vary the terminal time, T, and find that the switching time increases with the time horizon. In Section 2.4.2, we will vary the transmission coefficient as well as the per-capita recovery rate to see how the implementation of mitigation strategies affects the switching time. We also vary I_0 to determine how the initial number of infectives affects the optimal switching time. In all of Section 2.4, we use analytic formula (2.19) for the ratio of the revenue and cost parameters from the SIS model to determine how switching times vary with model parameters. In Figure 2.4, we verify these results numerically using dsoa.

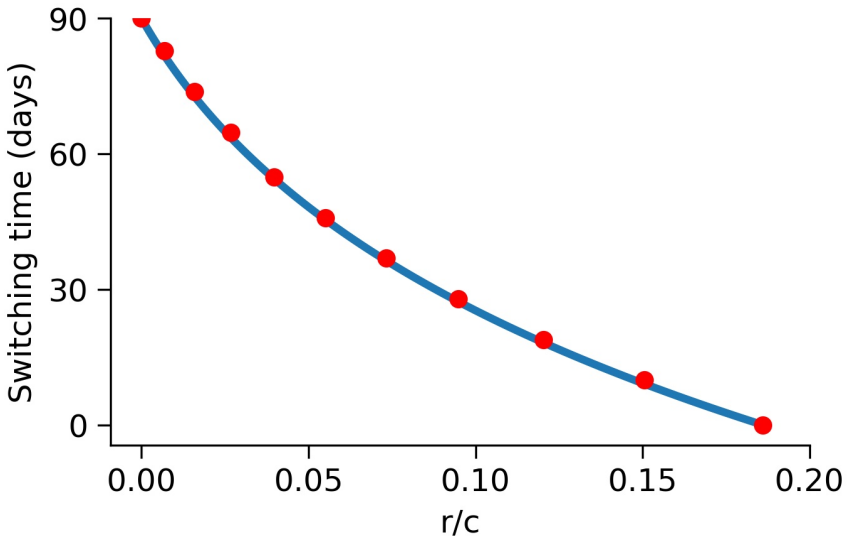

Figure 2.4: Switching time as a function of the ratio of the revenue and cost parameters. In this figure, we see that the switching time decreases as the revenue parameter increases relative to the cost parameter. This plot is for the SIS model with the parameters given in Table 2.1. In this example, the optimal mixing strategy greatly depends on the value of the revenue parameter. The solid curve corresponds to equation (2.19) while the circles are points where the switching time was computed numerically, using dsoa.

2.4.1 Sensitivity with respect to optimal-control parameters

First, we would like to see how changes in optimal-control parameter values affect the optimal switching time. If these changes are significant, it indicates that correctly estimating the revenue and cost parameters, minimum and maximum mixing levels, and the time horizon not only adds to our understanding of the disease but is also important for determining the best reduced-mixing strategy.

Effects of varying the revenue and cost parameters

One of the most important components of our models is the switching time, or when the population should change from a lower mixing level to a higher mixing level. Since we want to explore the optimal switching time from an economic perspective, we first look at how the ratio of the revenue and cost parameters affects the switch.

The effect of the ratio of the revenue and cost parameters on the switching time when the SIS model is used can be seen in Figure 2.4. We can see that as the revenue parameter, r, increases relative to the cost parameter, c, the switching time decreases. When r is much smaller than c, the switch happens later. When r is approximately 0.2 times c, a switch does not occur and the population remains at the higher mixing level the entire time. This tells us that, for a mild illness like in our example, mixing should be reduced only if the cost associated with a sick infective is significantly greater than the potential revenue.

Effects of varying M and m

For the SIS model, we defined m to be the minimum mixing level and M to be the maximum mixing level. The values of these parameters limit the intensity of the reduced-mixing strategy. Figure 2.5 shows us that increasing M in the SIS case causes an increase in the switching time. This increase is about 10 days. We also see that increasing m increases the switching time. In this example, there is a greater difference of about 15 days as m increases. Therefore, changes in the lowest and highest possible levels of mixing could result

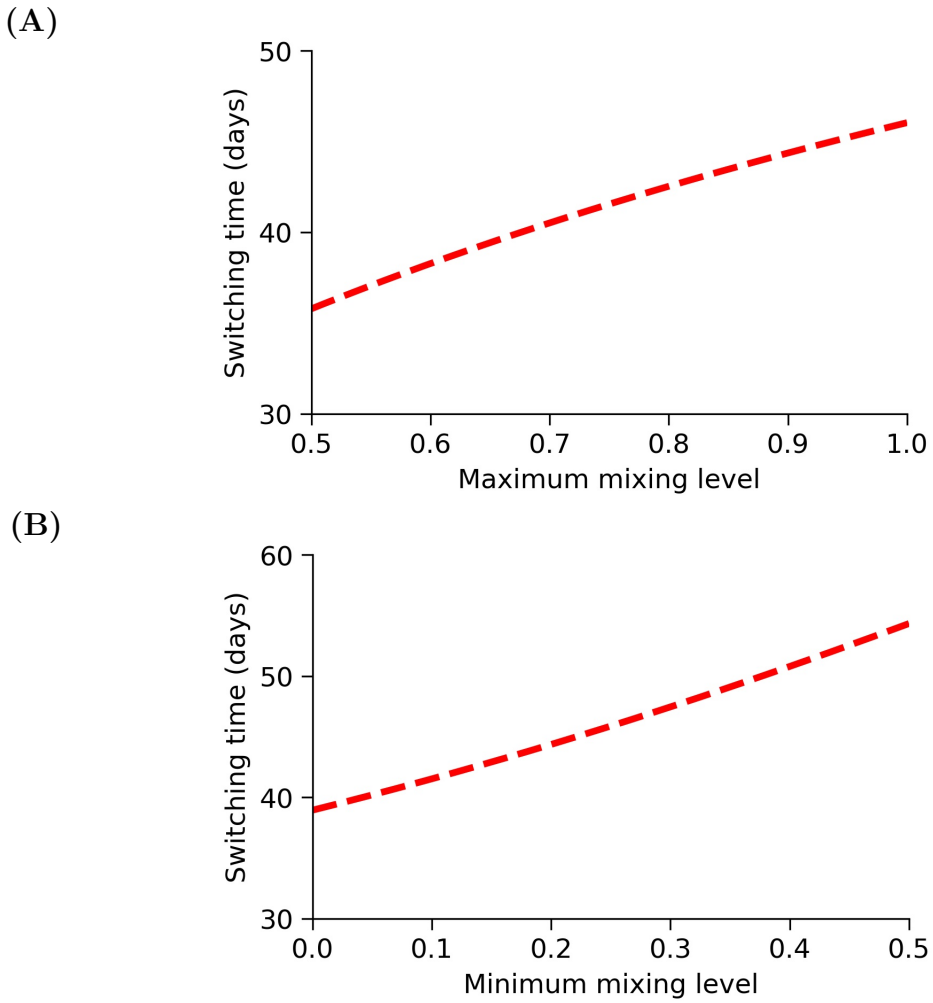

Figure 2.5: Changes in switching time, t_1, due to changes in activity levels. In **A**, we increase the maximum mixing level, M, from 0.5 to 1 while holding $m = 0.2$ constant, and in **B**, we increase the minimum mixing level, m, from 0.01 to 0.5 while holding $M = 0.9$ constant. In both cases, we see that the switching time increases as the highest or lowest possible level of mixing increases.

in a significant difference in amount of time spent at the lowest level of mixing.

Effects of varying T

The last optimal-control parameter we vary is T, the time horizon of the simulation. This parameter is an important component of the model and can represent the time for a vaccine to be developed, the time for an infectious disease to run through the population, or a fiscal quarter or year. For our example, T was determined by the amount of time that communal pasture-based dairy operations are typically used. We can see in Figure 2.6, the switching

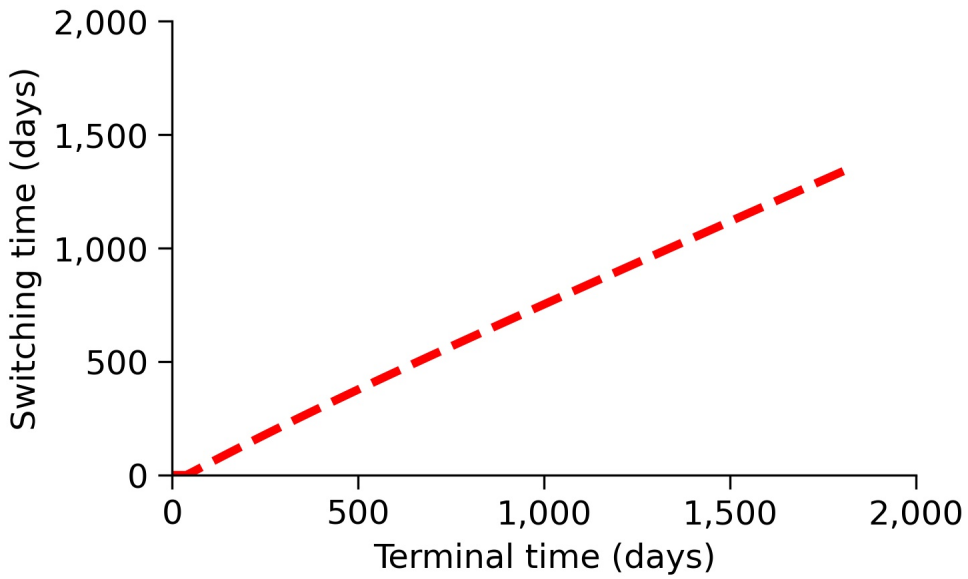

Figure 2.6: Changes in switching time, t_1, due to changes in the time horizon. This figure shows how the switching time changes depending on the terminal time of the simulation, T. We see that as the terminal time increases, the switching time also increases.

time increases monotonically with the terminal time.

In Figure 2.7, we see that the proportion of time spent at the maximum mixing level initially increases as the terminal time T increases, but levels off. For larger T, about 70% of the time frame is spent at the most active mixing level.

2.4.2 Sensitivity with respect to disease parameters

Next, we would like to see how changes in parameter values relating to the disease under study affect the optimal switching time for the mixing level. If these changes are significant, it may indicate that promoting mitigation strategies other than reduced mixing could be economically beneficial.

Effects of varying β

The first parameter we will look at is β, the transmission coefficient. In Figure 2.8, we vary β and find that decreasing the transmission coefficient means that mixing levels can be raised sooner, as expected. Since the value of β estimated from [1] is around $0.463 \times 10^{-4}(\text{indiv} \cdot$

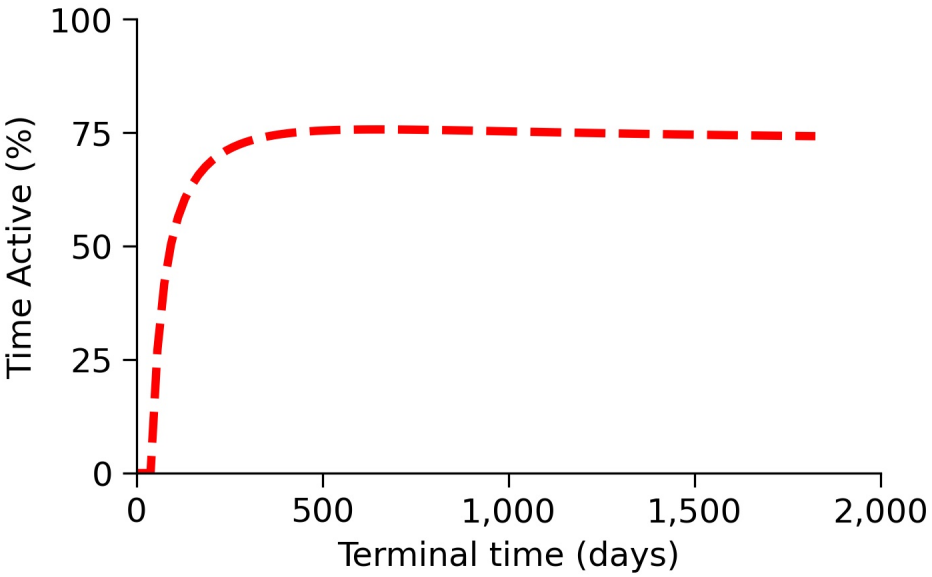

Figure 2.7: Changes in the proportion of time spent at the maximum mixing level due to changes in the time horizon. This figure shows that proportion of time spent at the maximum mixing level initially increases as the terminal time, T, increases, but starts to level off for $T > 350$ days.

day)$^{-1}$, using mitigation strategies that further reduce transmission may be effective.

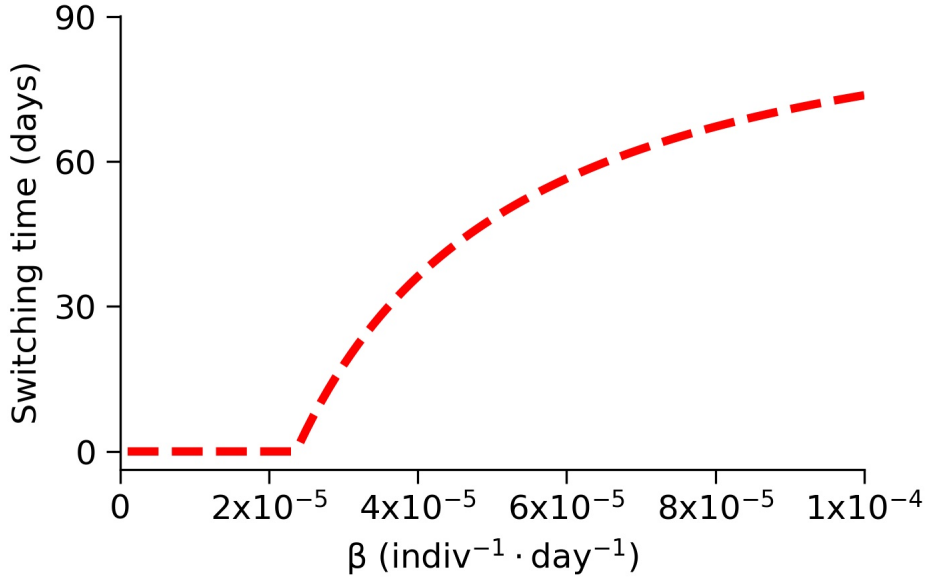

Figure 2.8: Changes in switching time, t_1, due to changes in β. We see that the switching time decreases quickly when we decrease the transmission coefficient, β, from the baseline value.

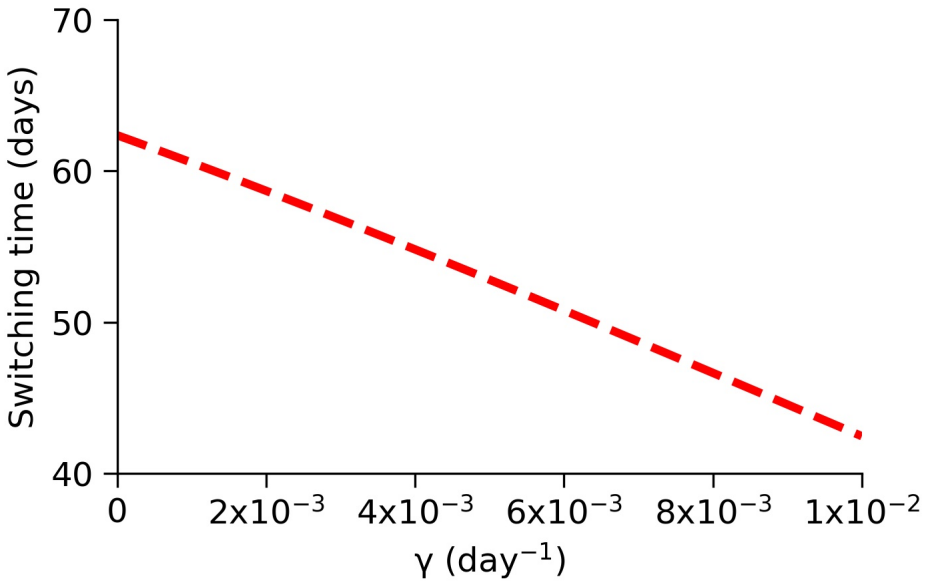

Figure 2.9: Changes in switching time, t_1, due to changes in γ. We see that as the per-capita recovery rate, γ, increases from 1.0×10^{-6} days^{-1} to 1.0×10^{-2} days^{-1}, the optimal switching time decreases from about 62 days to 42 days.

Effects of varying γ

Another parameter that affects the spread of a disease is γ, the per-capita rate of recovery. As we increase γ, infected individuals recover sooner and reenter the susceptible pool faster. Figure 2.9 shows that, as we increase γ, the optimal switching time decreases. Therefore, decreasing the time to recover by developing effective treatment strategies is a beneficial mitigation strategy.

Effects of varying I_0

Lastly, it is common for a disease to spread through a significant proportion of a population before mitigation strategies are implemented. Therefore, we determine how varying the initial number of infected individuals changes the optimal switching time. Figure 2.10 shows that if a greater proportion of the population is infected before reduced mixing strategies are implemented, mixing levels should be reduced for longer.

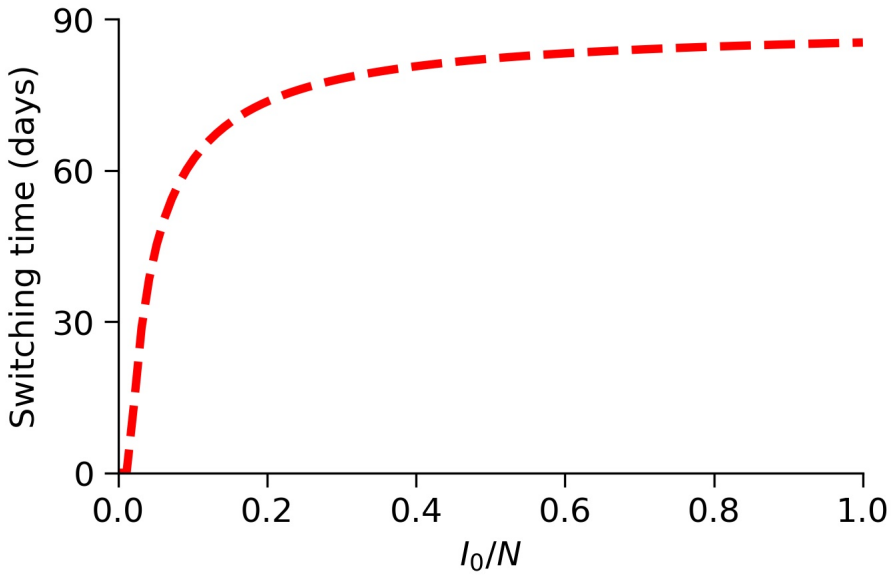

Figure 2.10: Changes in switching time, t_1, due to changes in I_0. We see that as the initial number of infectives, I_0, increases from $0.001N$ individuals to $1.0N$ individuals, the optimal switching time increases quickly from 0 days (always active) to 85 days.

2.4.3 Sensitivity of the objective functional

Although the switching time is our key output and thus, the focus of our analysis, we also explore the effects of changes in parameter values on the objective functional. In general, the changes in the objective functional with respect to the disease parameters are as expected, which can be seen in Figure 2.11. Changes in the optimal control parameters can cause payoff to both increase and decrease, which can be seen in Figure 2.12.

2.5 Discussion

In this study, we formulated an optimal-control problem for maximizing economic output during an infectious-disease outbreak. We studied a problem that obeys SIS dynamics, and we allowed the level of mixing in the population to range from the lowest possible level of mixing to the highest possible level of mixing.

We determined that the optimal solution used bang-bang controls. This meant that the population was either at its highest level of mixing or its lowest level of mixing at any point

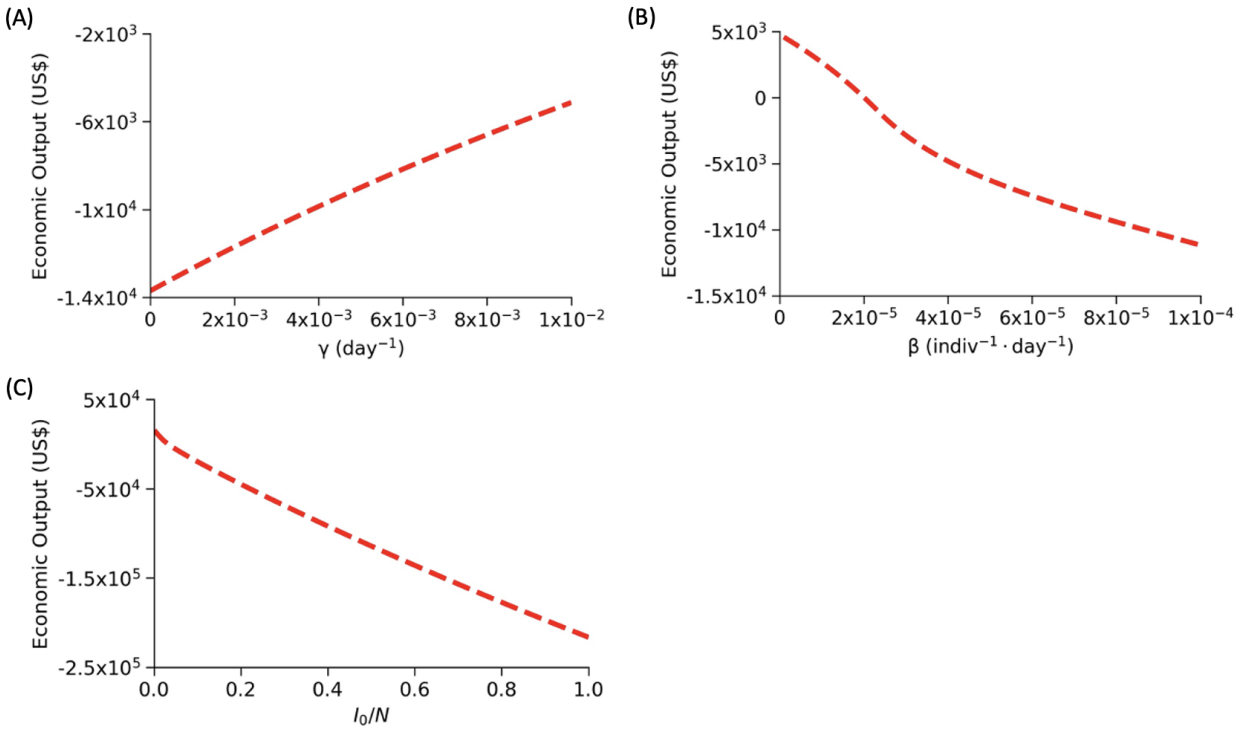

Figure 2.11: Changes in economic output due to changes in the disease parameters. Figure (A) shows the changes in economic output due to changes in γ. We see that as the per-capita recovery rate, γ, increases from $1.0 \times 10^{-6}(\text{day})^{-1}$ to $1.0 \times 10^{-2}(\text{day})^{-1}$, the economic output from the optimal reduced-mixing strategy also increases. Figure (B) shows the changes in economic output due to changes in β. We see that the economic output from the optimal reduced-mixing strategy decreases as we increase the transmission coefficient, β. Figure (C) shows the changes in economic output due to changes in I_0. We see that as the initial number of infectives, I_0, increases from $0.001N$ individuals to $1.0N$ individuals, the economic output from the optimal reduced-mixing strategy decreases.

in time. We also found that there was at most one switch and that the population had to be at the highest level of mixing at the time horizon. This meant that there was either one switch from low mixing to high mixing or the population remained at the higher level for all times.

We were able to determine analytical solutions for our optimal-control problem, but we were not able to solve for the switching time explicitly. We were, however, able to determine the ratio of the revenue and cost parameters as a function of the switching time. From this, we found that if the ratio of the revenue and cost parameters was small, the population remained at the lower mixing level for longer. As the ratio increased, the switching time occurred sooner. This result emphasizes the importance of correctly identifying the revenue

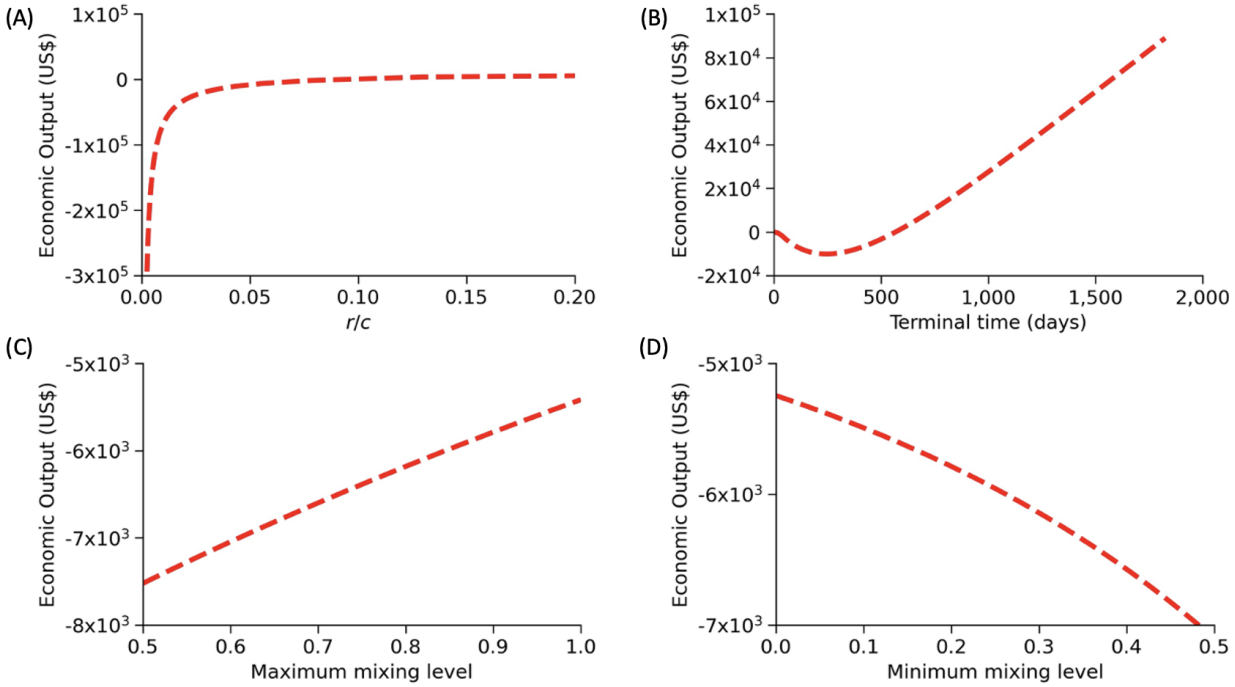

Figure 2.12: Changes in economic output due to changes in the optimal-control parameters. Figure (A) shows the changes in economic output due to changes in r/c. In this figure, we see that the economic output from the optimal reduced-mixing strategy quickly increases as r/c increases, initially. This increase occurs more gradually for $r/c > 0.05$. Figure (B) shows how the economic output from the optimal reduced-mixing strategy changes depending on the terminal time of the simulation, T . We see that as the terminal time increases, the economic output initially decreases then increases. In Figure (C), we increase the maximum mixing level, M, from 0.5 to 1 while holding m = 0.2 constant, and in Figure (D), we increase the minimum mixing level, m, from 0.01 to 0.5 while holding M = 0.9 constant. We find that the economic output from the optimal reduced-mixing strategy increases as M increases, but decreases as m increases.

and cost parameters when working with real-world examples.

Next, we studied *S. aureus* GTB transmission using both numerical methods and our analytical solutions. We saw that the economic output was maximized when mixing was reduced for about half of the simulation. Furthermore, for our example, we found that while mixing was reduced, the outbreak was controlled and that once the switch occurred, the number of cases began to increase. We again emphasize that we studied a mild disease. For a potentially fatal disease, the cost parameter should be chosen to properly account for loss of life.

Finally, we analyzed how changes in parameter values affected the optimal switching time. For our example, we found that the optimal switching time decreased as the ratio of the

revenue and cost parameters increased. Also, we found that when the revenue parameter was 0.2 times the cost parameter, no switch would occur. The optimal switching time increased as the values of the minimum and maximum mixing levels increased. This effect was stronger for the minimum mixing level. Also, the switching time increased with the time horizon. For our disease parameters, we saw that as the transmission coefficient increased, the switching time rapidly increased towards the terminal time, and the switching time significantly decreased as the per-capita rate of recovery increased. The results of the sensitivity analysis indicate that it is beneficial to employ further mitigation strategies such as improving treatment options or vaccinations. Another parameter that had a strong effect on the switching time was I_0, the initial infected population. Since the prevalence of *S. aureus* infections in a herd can be high, this is an important value to consider when implementing reduced-mixing control strategies.

An important component of this work is that we were able to determine closed-form analytic solutions for the optimal-control problem of maximizing economic output during an outbreak. These solutions, however, are for a simple disease model that assumes a constant population size, does not consider a discount term in the objective functional, and lacks classes such as exposed, vaccinated, or deceased. When performing a similar analysis on infectious diseases with more complex dynamics, it will be much more difficult to obtain closed-form solutions. Future work may include incorporating these more complex dynamics into our optimal-control problem and working with real-world data.

An assumption of our optimal-control problem that may be limiting is the assumption that infected individuals mix with the general population, but do not produce revenue. If isolation is not an option, mixing with the the general population may still occur. We assumed that individuals do not produce revenue when sick as they may be unable to work or to produce usable goods.

If infected individuals can be asymptomatic or can still be productive when symptoms are mild, we can include a parameter, $0 \leq \sigma \leq 1$, that represents disease severity. If $\sigma = 1$,

the disease is very severe, and if $\sigma = 0$, the disease is completely asymptomatic. We can then write the revenue produced by infected individuals as

$$\max_{m \le a(t) \le M} \int_0^T ra(t)[N - I(t)] + a(t)r(1-\sigma)I(t) - cI(t)dt. \tag{2.23}$$

In this paper, we assumed $\sigma = 1$.

We have recently begun analyzing optimal-control problems using objective functional (2.23) with various levels of disease severity. So far, we have found that the optimal control is still bang-bang. In this case, however, we have found instances where multiple, coexisting extremals are able to satisfy Pontryagin's maximum principle. Depending on the values of σ and I_0, some of these solutions have two switches. Theoretical studies suggest that optimal-control problems can routinely possess coexisting extremals [101, 102]. These have, however, rarely, if ever, been reported in numerical optimal-control studies of diseases.

In this study, we focused on determining how a population should behave during an outbreak in order to maximize economic output. The population size we used is on a business or farm level. This problem can be scaled up to represent a larger populations, such as a region or country, or scaled down to represent even smaller communities. The scale of the problem can be changed by changing parameters like the population size, the revenue parameter, and the cost parameter. A population of any size, however, is not homogeneous in risk of infection and in the consequences of infection. For example, an individual who is able to work from home may behave differently during an epidemic than an individual who must work in-person. Moreover, a large dairy farm in good financial standing may be able use different reduced-mixing strategies than a smaller dairy farm. Therefore, an interesting follow-up question to this research is what an individual's optimal strategy might be during an infectious-disease outbreak.

This is an Accepted Manuscript of an article published by Taylor & Francis in the Journal of Biological Dynamics on November 22, 2022, available at:
https://doi.org/10.1080/17513758.2022.214876.

Chapter 3

Maximizing Disease-Severity-Dependent Economic Output in an SIS Infectious-Disease Model

Scientists, policymakers, and those affected by policy decisions have debated the usefulness of costly disease-mitigation strategies [103–107]. An example of such debates concerns the use of lockdowns to reduce the spread of COVID-19. Most scientists [108, 109] agree that lockdowns were effective and necessary at the beginning of the pandemic. The effectiveness of later or prolonged lockdowns, however, is less clear.

Debates over the use of mitigation strategies that reduce both the spread of disease and economic output are not limited to the control of diseases in humans. For example, to combat the avian flu pandemic devastating the poultry industry, the United States is considering vaccinating commercial poultry [14]. The National Chicken Council, however, is against this strategy due to possible trade restrictions and fears of silent infections, which contaminate products and lead to revenue loss. Similarly, policymakers, researchers, and veterinarians

recommend the implementation of biosecurity measures, such as isolating sick or potentially infected animals and keeping equipment clean [110], to prevent the spread of infectious diseases in livestock. Many in industry, however, often ignore these recommendations due to the associated costs of implementation [111, 112]. This behaviour is commonplace in the dairy industry [113–115], which is the focus of this paper.

In this paper, we study the use of biosecurity measures to control the transmission of *Staphylococcus aureus* in dairy cows during lactation. *S. aureus* is a common cause of bovine mastitis and leads to great economic loss in the dairy industry [116, 117]. Bovine mastitis is an inflammation of the mammary gland and can be clinical, subclinical, or chronic. Clinical mastitis-cases typically produce visible abnormalities, such as watery milk with flakes or clots and a red and swollen udder, or fever [118]. Subclinical mastitis-cases, which are more common, lack visible abnormalities [6]. Cows with chronic mastitis have prolonged infections with flare-ups of clinical infections. All mastitis cases decrease milk production during and after infection, to differing degrees [5]. Subclinical mastitis, however, accounts for more financial loss than clinical mastitis due to its prevalence [119].

Mitigation strategies for preventing the spread of bovine mastitis within a herd include testing; separating sick and healthy cows; milking cows that are known to be infected, as well as cows with high somatic-cell counts (SCC), last or separately; feeding only pasteurized whole milk, waste milk, or colostrum to calves; preventing contamination from people, vehicles, or equipment; using teat-dip and dry-cow treatments; and maintaining udder hygiene [120, 121]. The level of implementation of these mitigation strategies is, however, low, due to factors such as the high cost of implementation, a lack of knowledge about current practices, and incomplete information about the effectiveness of mitigation strategies [113–115].

In Section 3.1, we introduce an optimal-control problem to determine the most economically beneficial measures and treatments for bovine mastitis. As cows may be re-infected with *S. aureus*, we use SIS (susceptible-infectious-susceptible) disease-dynamics to model the transmission. We assume that revenue is generated by both susceptible cows and, to a lesser

degree, infective cows. We also assume that sick infectives incur an economic cost. The economic output, or payoff, is the cumulative difference between the revenue and the cost, for a given time-horizon. We interpret the control variable as the level of mixing in the population, which is, in turn, affected by mitigation strategies such as biosecurity measures. We analyse solutions for several cases and find mixing strategies that improve economic output.

Then, in Section 3.2, we numerically solve our optimal-control problem with parameters for the transmission of *Staphylococcus aureus* in dairy cows. In Section 3.2.1, we explore the effects of varying key parameters, and we find that under certain conditions, multiple candidate-solutions, corresponding to radically different strategies, can coexist. Finally, in Section 3.3, we summarize our results and discuss the limitations and future directions of our research.

3.1 The Optimal-Control Problem

As in our previous work [3], we aim to maximize economic output during an infectious-disease outbreak that obeys SIS disease-dynamics. Individuals may, in other words, transition from a susceptible state to an infectious state and back. In contrast to our earlier work, however, we now consider how the severity of the disease affects the ability of cows to contribute economically, since economic output can depend strongly on the severity of the disease. For asymptomatic infections, there may be no loss in revenue, and for mild infections, there may only be a minor loss. In our example, subclinical bovine mastitis in dairy cows reduces milk quality, which does not prevent milk from being produced and sold, but does lower its price.

The ordinary differential equations (ODEs) for the SIS model include equations for the change in the number of susceptible individuals, $S(t)$, and for the number of infectious individuals, $I(t)$. In our model, $S + I = N$ for a population of size N. Thus, the system of ODEs,

$$\frac{dS}{dt} = -a(t)\beta SI + \gamma I, \qquad \frac{dI}{dt} = a(t)\beta SI - \gamma I, \tag{3.1}$$

reduces to the single state-equation,

$$\frac{dI}{dt} = a(t)\beta(N - I)I - \gamma I, \tag{3.2}$$

with an initial condition $I(0) = I_0$ such that $I_0 < N$.

As in our previous work [3], the control variable $a(t)$ represents the level of mixing in our population at time t and ranges between m and M. We assume that mitigation strategies reduce mixing and contacts with infectives, but that they also decrease revenue, per cow, due to the increased labour-costs, equipment-costs, and maintenance-costs needed for implementation. The parameter β is the transmission coefficient, for full mixing, and the parameter γ is the per-capita rate of recovery for infected individuals.

Although our state equation is the same as in our previous work [3], the objective functional that we will maximize,

$$\max_{m \le a(t) \le M} \int_0^T ra(t)[N - \sigma I(t)] - cI(t)dt, \tag{3.3}$$

is significantly different. The first term in the objective functional is the revenue produced by the saleable-milk-producing population, which includes individuals with mild or asymptomatic infections in addition to healthy individuals. The second term represents the cost due to infected individuals. The additional parameters in the objective functional include r, the revenue generated per healthy susceptible per day, c, the cost per sick infective per day, T, the terminal time, and σ, the severity of the disease.

The parameter σ, which we introduce in this work, ranges between 0 and 1 and affects how much revenue infected individuals can produce. This parameter can describe scenarios where individuals are less productive when infective or scenarios where only some proportion of infective individuals can contribute economically. For asymptomatic diseases, $\sigma = 0$, and

all individuals continue to produce revenue. For severe diseases, $\sigma = 1$, and infective individuals cannot produce revenue. Our model formulation, therefore, assumes that infective individuals may contribute economically, if they are not too sick. Additionally, infective individuals are able to interact with the population. Both the ability to produce revenue and the ability to mix with other individuals depends on the value of the control variable.

As our ODEs are simple, we were able to analyse the solutions for the optimal-control problem. We found that solutions to our optimal-control problem are bang-bang, meaning that the value of the control, $a(t)$, must be at either its lowest or its highest possible value at any given time. Details for the analysis of the optimal-control problem are provided in the Supplementary Material.

After exploring appropriate phase-plots for various initial conditions, we found that there are three possible types of solutions: those with no switch, one switch, or two switches. Surprisingly, we also found that, for some parameter values, several candidate-solutions can satisfy the necessary conditions of Pontryagin's maximum principle. This is in sharp contrast to our previous work [3], which found that only one candidate solution, which was either a no-switch or a one-switch solution, was possible when disease severity was not considered.

Figure 3.1 shows no-switch and two-switch solutions and shows a typical (I, λ) phase-portrait, on both sides of the switching function. Here, λ is the adjoint variable for the optimal-control problem (in the Supplementary Material), and the black curve shows the switching function. Above this curve, the control is at the maximum level of mixing, $a(t) = M$, and below this curve, the control is at the minimum level of mixing, $a(t) = m$. No-switch solutions are solution curves that never cross the switching function and that stay at the maximum mixing-level. These solutions correspond to a minimal use of biosecurity measures. A one-switch solution crosses the switching function once and can have a long period of minimal mixing. These solutions can have a period of maximal use of biosecurity measures followed by a period of minimal use. A two-switch solution crosses the switching function twice and can also have a long period of minimal mixing. These solutions have long

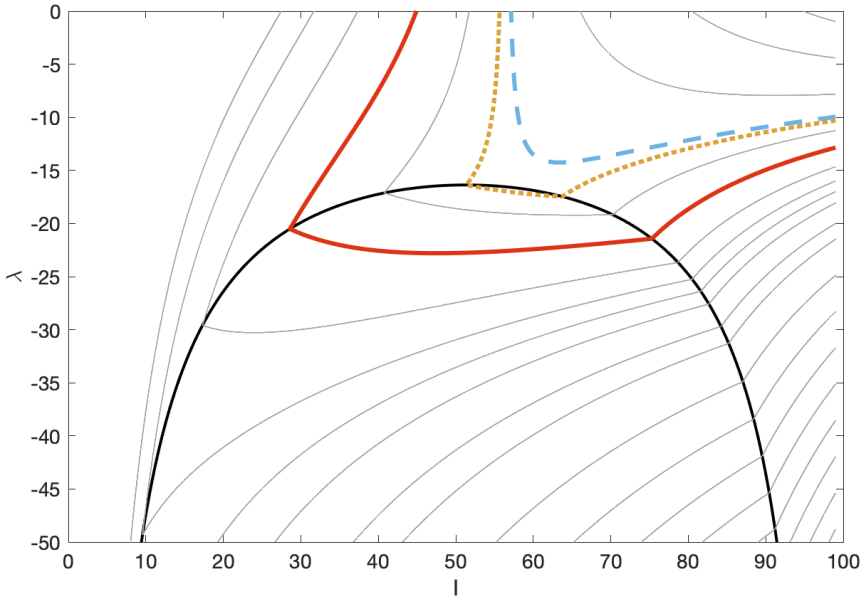

Figure 3.1: Phase portrait of the optimal-control problem. In this figure, we see the behaviour of λ, the adjoint variable (grey curves), and the switching function (black curve) as a function of I, the number of infective individuals. Above the switching curve, the control is at the maximum level of mixing, $a(t) = M$, and below, the control is at the minimum level of mixing, $a(t) = m$. Each of the grey lines is from an evaluation of the optimal-control model for a different terminal time. The solid red, dashed blue, and dotted yellow lines show three candidate-solutions with the same terminal time, $T = 305$. In this figure, we can see that the adjoint variable crosses the switching function at most twice for each simulation. We also see that there may be multiple candidate-solutions for the same parameter set. In this figure, we use the parameters $(m, M, N, I_0, \beta, \gamma, r, c, \sigma) = (0.2, 0.9, 100, 99, 0.0232/N, 1/110, 0.1, 0.2, 0.1)$.

periods of maximal use of biosecurity measures both preceded and followed by periods of minimal use.

Figures 3.1 and 3.2 also show an example of a case where multiple candidate-solutions exist. These figures emphasize the difference from [3], where two-switch solutions and multiple candidate-solutions were not possible.

3.2 Numerical Analyses

In our numerical analysis of the bovine mastitis problem, most of the parameters we use are from the literature. Table 1 in the Supplementary Information provides detailed information about the parameter values. For the new disease-severity parameter, we used the proportion

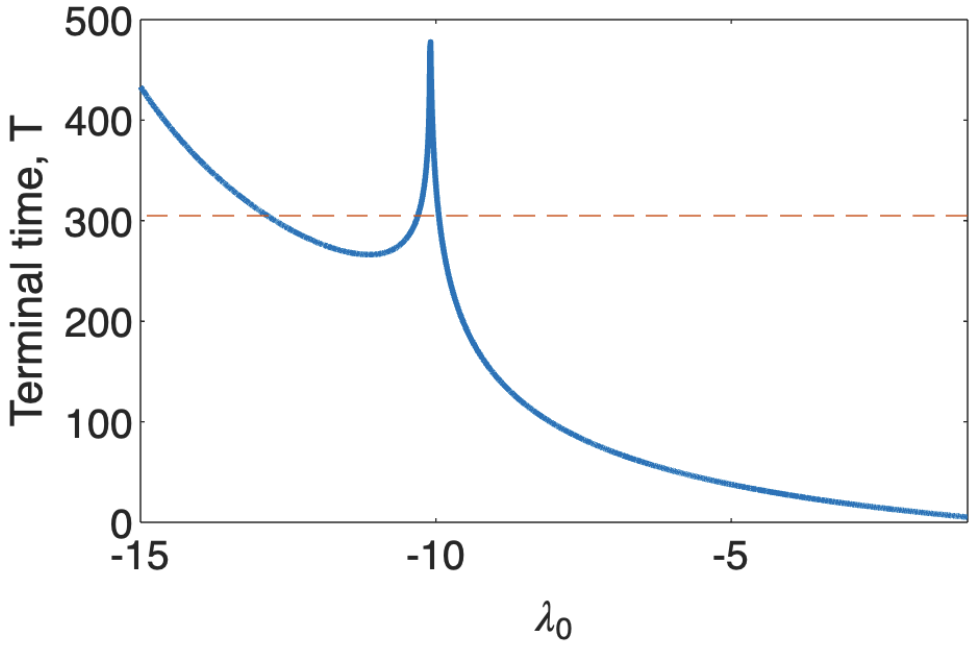

Figure 3.2: Multiple candidate-solutions in the (λ_0, T) space. In this figure, we use the parameters $(m, M, N, I_0, \beta, \gamma, r, c, \sigma) = (0.2, 0.9, 100, 99, 0.0232/N, 1/110, 0.1, 0.2, 0.1)$ and vary the initial value for the adjoint variable, $\lambda(0) = \lambda_0$. We solve both the state and adjoint equations forward in time, and end the simulation when the transversality condition, $\lambda(T) = 0$, is met. We see that three values for λ_0 result in a terminal time of $T = 305$. This shows that there are multiple candidate-solutions that satisfy the first-order necessary conditions of Pontryagin's maximum principle.

of mastitis cases that are categorized as clinical [6], which is $\sigma = 0.05$. This means that most cows with mastitis are still able to produce saleable milk (if not treated with antibiotics), which is a very different assumption than that made in [3].

By numerically solving our optimal-control problem using the forward-backward sweep method [32, 34–36], we find that, to maximize economic output, there should be one switch from the lowest possible level of mixing to the highest, after about 260 days. Figure 1 in the Supplementary Information shows the dynamics of this solution. Although this is the solution for the parameters in Table 1 in the Supplementary Information, there is a significant amount of uncertainty in the values for the parameters found in the literature. For example, [122] finds the average duration of infection to be 30 days, which is significantly different from the value reported by [2]. Moreover, there is great variation in the transmission rates reported in the literature [1, 2, 122]. Therefore, the next step in our analysis is to observe

the effects of varying key parameters and how this can lead to multiple candidate-solutions.

To numerically analyze the multiple candidate-solutions, we solve both the state and adjoint equations forward in time using standard ODE solvers. To determine values for initial condition of the adjoint variable that satisfy the necessary conditions of Pontryagin's maximum principle, we use root-finding methods.

3.2.1 Multiple candidate-solutions

In Figure 3.1, we saw that multiple candidate-solutions may exist for certain parameter-sets. To determine the source of this behaviour, we looked at three candidate-solutions (Figures 3.3(A-C)) and their associated surface-plots (Figures 3.3(D-F)), which show the payoffs for different switching times. In these plots, we increased the revenue relative to the cost, and in Figures 3.3(D-F), we saw that small changes in parameter values can easily lead to very different strategies having similar economic outputs. We also looked at plots of the corresponding candidate-solutions in the (I,λ) plane in Figures 3.3(A-C) and saw that the behaviour of the candidate solutions can differ greatly.

Each of the parameter sets used to produce Figure 3.3 have multiple candidate-solutions that satisfy the necessary conditions of Pontryagin's maximum principle. We see in Figure 3.3(A-C) that two of these candidate-solutions have two switches, and the third has no switches. In each case, the candidate solution with the longest reduced-mixing period, or period where $a(t) = m$, (solid red lines) and the candidate solution with no reduced-mixing, meaning $a(t) = M$ at all times, (dashed blue lines) are local maxima in Figures 3.3(D-F). In Figures 3.3(D) and 3.3(E), the global maximum is the candidate solution with the longest reduced-mixing period. In Figure 3.3(F), however, the global maximum is the candidate solution with no reduced-mixing period. The candidate solutions shown by the yellow dotted lines in 3.3(A-C) are intermediate values that are neither local maxima nor local minima in Figures 3.3(D-F). We also see that these candidate-solutions become more similar to the no-switch candidate-solutions as the revenue increases relative to the cost.

We continue this sensitivity analysis in Figure 3.4 using the parameter set $(m, M, N, I_0, \beta, \gamma, r, c, \sigma) = (0.2, 0.9, 100, 99, 0.0232/N, 1/110, 0.1, 0.2, 0.1)$ as a baseline. From this figure, we see that there is a wide range of parameter values for which three candidate-solutions may coexist. For example, the minimum (m) and maximum (M) mixing-levels and the transmission coefficient (β) have relatively large ranges of realistic values for which three candidate-solutions exist. For the time horizon (T) and the ratio of the revenue and cost parameters (r/c), however, three candidate-solutions exist for only relatively small ranges of realistic values.

Figure 3.4 also shows where the candidate solutions trade off in optimality and how similar they may be in terms of economic output, or payoff. For example, Figure 3.4F shows the effects of varying the per-capita recovery rate, γ. In this subfigure, the optimal candidate-solution switches from a no-switch solution to a two-switch solution at about $\gamma \approx 0.008$. We also see that three candidate-solutions coexist for values of γ ranging from 0.007 to 0.0125. The economic output from these candidate-solutions is, however, very similar. In Figure 3.4C, we see the effect of varying the disease severity parameter, σ, which is especially important. When σ is greater than 0.27, meaning that more than 27% of infections lead to severe symptoms, only two-switch solutions occur. This means that the possibility of having three candidate-solutions, including the no-switch case, only occurs for mild diseases. Moreover, we see that a no-switch solution may only be optimal for very mild diseases.

From Figure 3.4, we can see which parameter values have the greatest effect on overall economic output. The payoff (y-axes of Figure 3.4) varies greatly with the transmission coefficient, the per-capita recovery rate, and, to a lesser extent, the ratio of the revenue and cost parameters. The change in the payoff when varying the minimum and maximum mixing-levels and the time horizon is smaller.

From our numerical analysis, we suspect that the coexistence of three candidate-solutions is due to the presence of a cusp catastrophe. Although the literature on the topic of catastrophes in optimal-control problems is sparse, we were able to find examples of such occurrences.

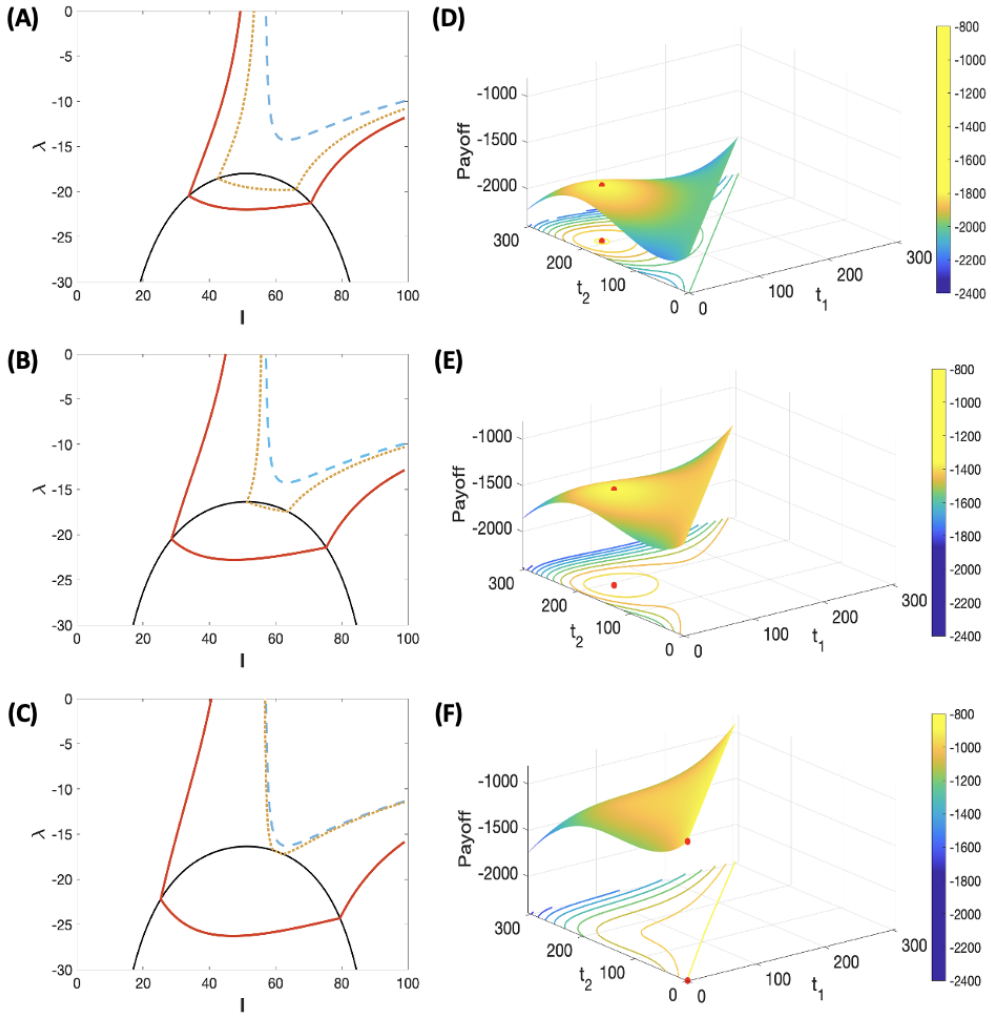

Figure 3.3: Effects of parameter variations on the payoff of different mitigation-strategies and candidate-solutions. Figures (A-C) show the three candidate-solutions, in the (I,λ) plane, corresponding to Figures (D-F). Figures (D-F) show the economic output for different combinations of switching times, t_1 and t_2. The first switching-time, t_1, is a switch from the maximum mixing-level to the minimum mixing-level. The second switching-time, t_2, is a switch from the minimum mixing-level to the maximum mixing-level. If $t_1 = 0$, the population will start at the minimum mixing-level, and there will be one switch to the maximum mixing-level. If $t_1 = t_2$, then the switch from the maximum mixing-level to the minimum mixing-level occurs at the same time as the switch from the minimum mixing-level back to the maximum mixing-level. Therefore, there will be no switch. The red dots on the surface and contour plots show the maximum payoff. The middle figures, (B) and (E), are for the parameter set $(m, M, N, I_0, \beta, \gamma, r, c, \sigma) = (0.2, 0.9, 100, 99, 0.0232/N, 1/110, 0.1, 0.2, 0.1)$. The figures above, (A) and (D), show what happens when we decrease the cost to $c = 0.23$, and the figures below, (C) and (F), show what happens if we increase the revenue to $r = 0.11$. Each surface-plot has two local maxima. The local maximum along the line $t_1 = t_2$ corresponds to the no-switch candidate-solution, and the second local maximum corresponds to a two-switch candidate-solution. The dashed blue and solid red lines, respectively, show these candidate-solutions in Figures (A-C). The dotted yellow lines in Figures (A-C) correspond to an intermediate candidate-solution, which is neither a local minimum nor a local maximum.

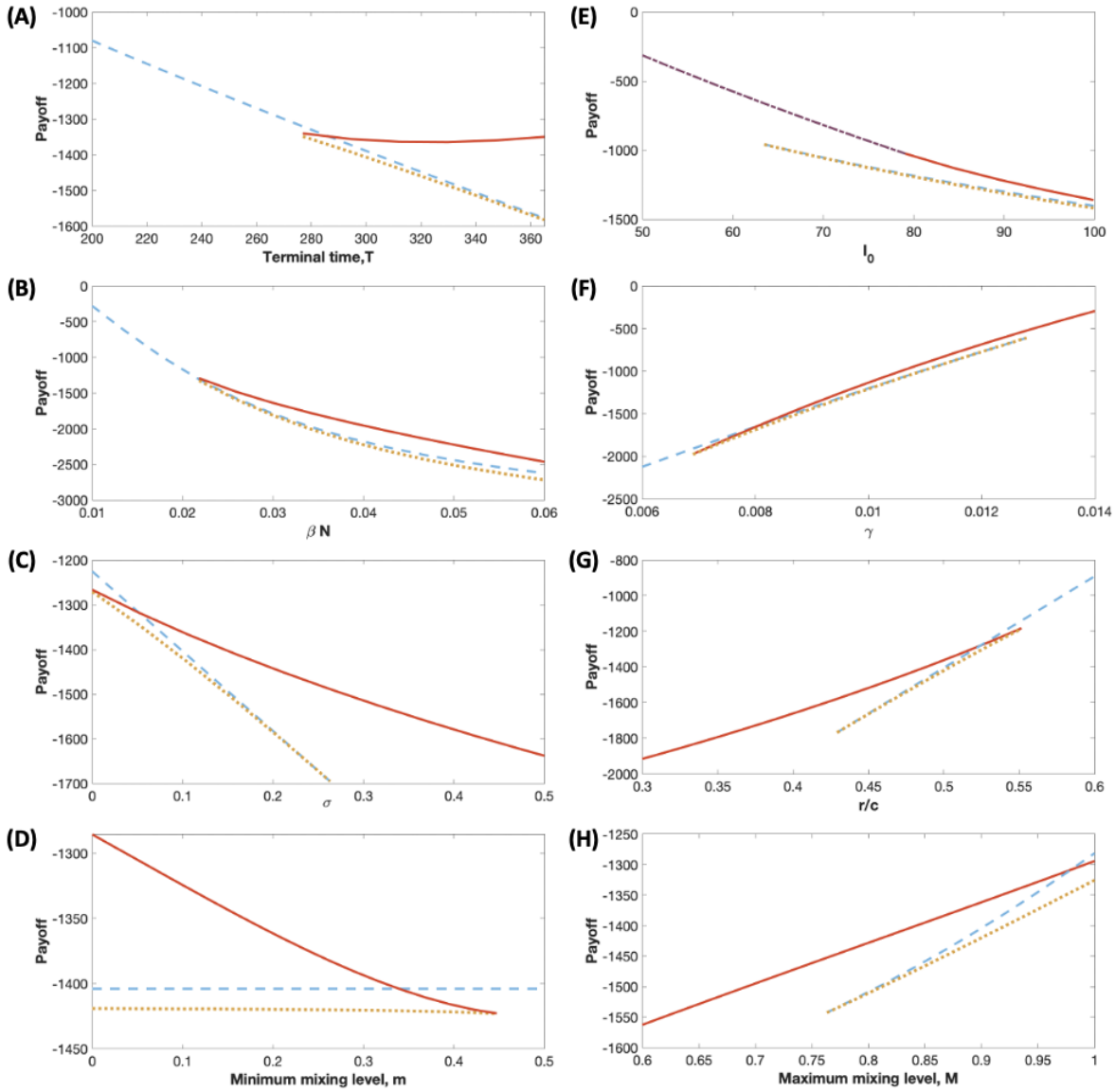

Figure 3.4: Changes in payoff and candidate solutions due to changes in parameter values. In this figure, we vary key parameters, from the values $(m, M, N, I_0, \beta, \gamma, r, c, \sigma) = (0.2, 0.9, 100, 99, 0.0232/N, 1/110, 0.1, 0.2, 0.1)$, and observe the associated changes in the payoff for each of the three candidate-solutions. We also see for which parameter sets three candidate-solutions exist. In each figure, the solid red line shows the two-switch candidate-solution that is a local maximum and the dotted yellow line shows the two-switch candidate-solution that is neither a local minimum nor a local maximum. The dashed blue line shows the no-switch candidate-solution, which is also a local maximum. If we reduce I_0, we also have the possibility of one-switch candidate-solutions. The purple dashed line shows the one-switch candidate-solution in Figure (E).

For example, in their 2021 paper, Offen and Ober-Blöbaum [123] observed that bifurcations in solutions to optimal-control problems are related to classical catastrophes. Moreover, these bifurcations can lead to the existence of multiple solutions satisfying the first-order

necessary conditions of Pontryagin's maximum principle.

3.3 Discussion

In this study, we explored the trade-off between economic output and the use of activity-reducing disease-mitigation strategies. To do this, we formulated an optimal-control problem with the goal of maximizing overall economic output during an infectious-disease outbreak that obeys SIS disease-dynamics. In our objective functional, revenue is produced by susceptibles and some proportion of infectives, and there is an economic cost associated with infectives. We assume the severity of the disease determines the proportion of infectives that are able to produce revenue.

We found that the solution to our optimal-control problem is bang-bang, and, although we were not able to determine a closed-form solution, we were able to analyse three possible cases for the solution: the no-switch case, the one-switch case, and the two-switch case. In the no-switch case, the population remains at the maximum mixing-level, with the minimal use of biosecurity measures. In the one-switch case, there is one switch from the minimum mixing-level to the maximum mixing-level, meaning biosecurity measures are strictly adhered to at the beginning of the time frame but relaxed at the switching time. In the two-switch case, there is a switch from the maximum to the minimum mixing-level followed by a second switch from the minimum to the maximum mixing-level. In this case, biosecurity measures are used minimally at the beginning and end of the time frame but are used maximally during a long period in the middle of the time frame. The model parameters determine which of these three cases leads to the largest economic output.

We applied our model to the transmission of *S. aureus* in dairy cows and found that the optimal solution has one switch from the minimum mixing-level to the maximum mixing-level after about 260 days. This means that it was economically beneficial to employ reduced-mixing mitigation-strategies, such as the implementation of biosecurity measures, for most

of the lactation period.

For other circumstances, the optimal strategy may not be so clear. When analysing the effects of varying key parameter values, we found that some sets of parameters lead to the existence of multiple candidate-solutions that satisfy the first-order necessary conditions for Pontryagin's maximum principle. These candidate-solutions often exhibited very different behaviours and traded off in optimality with small changes in parameter values. Moreover, we found that candidate solutions with drastically different behaviours could produce similar economic payoffs.

The possibility that a disease-mitigation strategy with a long period of reduced mixing can have a similar economic output to a strategy with no reduced mixing emphasizes the importance of seeing the full picture during decision making. For example, if this scenario were to occur in an agricultural setting, farmers might decide that a small increase in economic output is not worth the difficulties of implementing new practices or procedures. In human populations, if the economic output under reduced-mixing strategies is similar to that without reduced mixing, it would indicate the to need take more factors into consideration. For a severe disease in human populations, a scenario where economic outputs are similar with or without reduced mixing would provide further motivation for the use of mitigation strategies to reduce morbidity and mortality, as the improvement in overall public health would outweigh the small reduction in economic output. Alternatively, for a mild disease in human populations, a scenario where economic outputs are similar with or without reduced mixing could indicate the need to consider the possible negative societal impacts of reduced-mixing strategies, like setbacks in education or a decline in mental health.

In this paper, we have studied a scenario in which mitigation strategies for bovine mastitis reduce contacts between susceptible and infected cows. In future work, we hope to instead study scenarios where mitigation strategies increase the recovery rate, such as the use of antibiotics to treat mastitis. The use of antibiotics is generally recommended in the case of clinical mastitis and may also be used to treat subclinical mastitis [124]. The use of

antibiotics for subclinical mastitis is, however, a subject of debate. Due to high costs and poor cure-rates, treating subclinical mastitis may not be considered economical or effective [124]. In contrast, several studies [125–127] claim that the treatment of subclinical mastitis reduces SCC and reduces the incidence of clinical mastitis. Moreover, recent studies have found that a longer duration or higher frequency of treatment and the development of new drugs may improve cure rates [128–130]. It is important to note, however, that when treating a cow with antibiotics, dairy farmers must withhold that cow's milk from the market for a recommended withdrawal-period.

To study the dynamics of antibiotic treatment, we may adapt our optimal-control model by applying the control to the per-capita recovery rate instead of to the transmission coefficient in the SIS disease-model,

$$\frac{dS}{dt} = -\beta SI + [\gamma_0 + a(t)\gamma_1]I, \tag{3.4}$$

$$\frac{dI}{dt} = \beta SI - [\gamma_0 + a(t)\gamma_1]I. \tag{3.5}$$

Here, the control $a(t)$ represents the proportion of infective cows treated with antibiotics and can range from 0 to 1. When the control is at its minimum value, $a(t) = 0$, no antibiotics are used to treat infective cows. When the control is at its maximum value, $a(t) = 1$, antibiotics are used to treat all infective cows. The parameter γ_0 is the per-capita recovery rate when $a(t) = 0$, and the sum $\gamma_0 + \gamma_1$ is the per-capita recovery rate when $a(t) = 1$.

We would also change our objective functional so that the control only affects the revenue from infective cows,

$$\max_{m \le a(t) \le M} \int_0^T r[N - I(t)] + r[1 - a(t)](1 - \sigma)I(t) - cI(t)dt. \tag{3.6}$$

In this formulation of the model, when $a(t) = 0$, the revenue would not be affected by the control. As $a(t)$ is increased, the number of cows with the faster per-capita recovery rate, $\gamma_0 + \gamma_1$, will increase, but revenue will decrease due to the loss of saleable product. If $a(t) = 1$,

antibiotics are used on all infective cows, and the milk produced by all infective cows will not be saleable.

An analysis of the economic trade-off associated with antibiotic use for the treatment of bovine mastitis, similar to the one done in this paper for biosecurity measures, may help to answer questions about the cost-effectiveness of this mitigation-strategy. Moreover, if this problem has similar dynamics to what we have seen in this paper, results may indicate that factors besides economic output, such as antibiotic resistance, would need to be taken into consideration.

3.4 Appendix

3.4.1 Details of the analytical analyses

We analyse solutions to the optimal-control problem, with control $a(t)$ and described by the state equation,

$$\frac{dI}{dt} = a(t)\beta(N - I)I - \gamma I, \tag{3.7}$$

and the objective functional

$$\max_{m \le a(t) \le M} \int_0^T ra(t)[N - \sigma I(t)] - cI(t)dt, \tag{3.8}$$

using Pontryagin's maximum principle [33]. First, we define the control Hamiltonian, H as

$$\begin{aligned} H &= f(t, I, a) + \lambda g(t, I, a) \\ &= a(t)\left[r(N - \sigma I) + \lambda\beta(N - I)I\right] - I(c + \lambda\gamma), \end{aligned} \tag{3.9}$$

where $f(t, I, a)$ is the integrand of objective functional (3.8) and $g(t, I, a)$ is the right-hand side of state equation (3.7).

For the problem given by equations (3.7) and (3.8), the maximum principle tells us that,

for the optimal trajectories $I^*(t)$ and $a^*(t)$, there exists a piecewise-differentiable adjoint variable, $\lambda(t)$, obeying the differential equation

$$\begin{aligned}\dot{\lambda}(t) &= -\frac{\partial H(t, I^*(t), a^*(t), \lambda(t))}{\partial I} \\ &= a\left[r\sigma - \lambda\beta(N - 2I)\right] + c + \lambda\gamma\end{aligned} \tag{3.10}$$

and the transversality condition $\lambda(T) = 0$. The maximum principle also tells us that

$$H(t, I^*(t), a(t), \lambda(t)) \leq H(t, I^*(t), a^*(t), \lambda(t)) \tag{3.11}$$

for all possible a at time t [32, 95].

The ODEs, with an initial condition for the state equation and a terminal condition for the adjoint equation, form a two-point boundary-value problem. To solve this boundary-value problem, we want to solve the state equation forwards in time and the adjoint equation backwards in time.

To begin to solve the problem, we first observe that the Hamiltonian is linear in the control variable,

$$H = a\phi(t) - (c + \lambda\gamma)I, \tag{3.12}$$

where

$$\phi = r(N - \sigma I) + \lambda\beta(N - I)I \tag{3.13}$$

is known as the switching function.

The above linearity implies that the form of the optimal control that maximizes the Hamiltonian is bang-bang. If the switching function is either positive or negative, the optimal control is

$$a(t) = \begin{cases} m, & \phi(t) < 0, \\ M, & \phi(t) > 0. \end{cases} \tag{3.14}$$

A switch occurs when $\phi = 0$ or when

$$\lambda = -\frac{r(N - \sigma I)}{\beta(N - I)I}. \tag{3.15}$$

So, if $\phi(t) > 0$,

$$\lambda > -\frac{r(N - \sigma I)}{\beta(N - I)I}, \tag{3.16}$$

and if $\phi(t) < 0$,

$$\lambda < -\frac{r(N - \sigma I)}{\beta(N - I)I}. \tag{3.17}$$

To determine if the optimal-control model has a singular solution, we set the derivative of λ, obtained from the switching condition (3.15), equal to equation (3.10) at the time of the switch. We find that a singular solution is possible if

$$c = \frac{r\gamma(1 - \sigma)N}{\beta(N - I)^2}. \tag{3.18}$$

Therefore, a singular solution may exist.

To find the possible singular solution, we plug equation (3.15) into adjoint equation (3.10) to get

$$\dot{\lambda}(t) = c + \frac{r\left[a\beta\left(N^2 - 2NI + \sigma I^2\right) - \gamma(N - \sigma I)\right]}{\beta I(N - I)}. \tag{3.19}$$

Setting this equal to the derivative of (3.15) with respect to time, we find the solution to the state equation along the singular arc to be

$$I^*(t) = N - \sqrt{\frac{Nr\gamma(1 - \sigma)}{c\beta}}. \tag{3.20}$$

Then, noting that $\dot{I} = 0$ during the singular interval, we plug equation (3.20) into the state equation to get the singular control

$$a^*(t) = \frac{c\gamma}{\sqrt{cNr\beta\gamma(1-\sigma)}}, \tag{3.21}$$

which may exist when the singular control is within the bounds $m < a < M$.

The optimal control is then

$$a = \begin{cases} m, & \phi < 0, \\ \dfrac{c\gamma}{\sqrt{cNr\beta\gamma(1-\sigma)}}, & \phi = 0, \\ M, & \phi > 0. \end{cases} \tag{3.22}$$

To determine if the singular control is optimal, we check the generalized Legendre-Clebsch optimality condition [131],

$$(-1)^q \left\{ \frac{\partial}{\partial a} \left[\frac{\partial^{2q}}{\partial t^{2q}} \left(\frac{\partial H}{\partial a} \right) \right] \right\} \leq 0, \qquad \text{for } q = 0, 1, 2, \ldots \tag{3.23}$$

For $q = 1$, this reduces to

$$c\beta^2 (I^*)^2 \sqrt{\frac{Nr\gamma(1-\sigma)}{c\beta}} \leq 0, \tag{3.24}$$

which is false. Therefore, the singular control will never be optimal, and our optimal control is

$$a = \begin{cases} m, & \phi < 0, \\ M, & \phi > 0. \end{cases} \tag{3.25}$$

Although we cannot find a general, closed-form, analytical solution, we are able to analyse solutions for several cases. For the no-switch, one-switch, and two-switch cases, we are able to find solutions for the state and adjoint equations, but we are not able to find expressions for the switching times.

No-switch case

In the no-switch case, the population is active ($a = M$) for all time. The solution for the state equation for this case is

$$I(t) = \frac{\delta_M I_0}{M\beta I_0 + (\delta_M - M\beta I_0)\, e^{-\delta_M t}},$$

where

$$\delta_M = MN\beta - \gamma. \tag{3.26}$$

The solution for the adjoint equation in this case is

$$\lambda(t) = \frac{(Mr\sigma + c)\left(1 - e^{-\delta_M (T-t)}\right) u(t)}{\delta_M u(T)} \tag{3.27}$$

where

$$u(t) = \delta_M + M\beta I_0 \left(e^{\delta_M t} - 1\right). \tag{3.28}$$

One-switch case

In the one-switch case, there is one switch from low activity to high activity. In other words, $a(0) = m$, and there is a switch at time t_1 such that $a(T) = M$. Before the switch, the solution to the state equation is

$$I(t) = \frac{\delta_m I_0}{m\beta I_0 + (\delta_m - m\beta I_0)e^{-\delta_m t}}, \tag{3.29}$$

where

$$\delta_m = mN\beta - \gamma. \tag{3.30}$$

After the switch at $t = t_1$, the solution to the state equation is

$$I(t) = \frac{\delta_M I_1}{M\beta I_1 + (\delta_M - M\beta I_1)e^{-\delta_M(t-t_1)}}, \tag{3.31}$$

where $I_1 = I(t_1)$. We use equation (3.29) to find $I(t_1)$.

After the switch, the solution to the adjoint equation is

$$\lambda(t) = \frac{(Mr\sigma + c)u(t)\left[1 - e^{\delta_M(T-t)}\right]}{\delta_M u(T)} \tag{3.32}$$

where

$$u(t) = \delta_M + M\beta I_1\left(e^{\delta_M(t-T)} - 1\right). \tag{3.33}$$

Before the switch, the solution to the adjoint equation is

$$\lambda(t) = \frac{v(t)\left\{\lambda_1 v(t) - (mr\sigma + c)\left[1 - e^{\delta_m(t-t_1)}\right]\right\}}{\delta_m^2 e^{\delta_m(t-t_1)}}, \tag{3.34}$$

where

$$v(t) = \delta_m + m\beta I_0\left(e^{\delta_m(t-t_1)} - 1\right), \tag{3.35}$$

and $\lambda_1 = \lambda(t_1)$.

Two-switch case

In the two-switch case, there is one switch from high activity to low activity, followed by a second switch from low activity to high activity. This means $a(0) = M$, there is a switch to $a = m$ at time t_1, and there is another switch to $a = M$ at time t_2.

The solution for the state equation from $t = 0$ to $t = t_1$ is

$$I(t) = \frac{\delta_M I_0}{M\beta I_0 + (\delta_M - M\beta I_0)\, e^{-\delta_M(t)}}. \tag{3.36}$$

From $t = t_1$ to $t = t_2$, the solution to the state equation is

$$I(t) = \frac{\delta_m I_1}{m\beta I_1 + (\delta_m - m\beta I_1)\, e^{-\delta_m (t-t_1)}}, \tag{3.37}$$

where equation (3.36) gives I_1 at time t_1. From $t = t_2$ to $t = T$, the solution to the state equation is

$$I(t) = \frac{\delta_M I_2}{M\beta I_2 + (\delta_M - M\beta I_2)\, e^{-\delta_M (t-t_2)}}, \tag{3.38}$$

where equation (3.37) gives I_2 at time t_2.

The solution to the adjoint equation from $t = T$ to $t = t_2$ is

$$\lambda(t) = \frac{(Mr\sigma + c)u(t)\left[1 - e^{\delta_M (T-t)}\right]}{\delta_M u(T)}, \tag{3.39}$$

where

$$u(t) = \delta_M + M\beta I_2 \left(e^{\delta_M (t-t_2)} - 1\right). \tag{3.40}$$

The solution to the adjoint equation from $t = t_2$ to $t = t_1$ is

$$\lambda(t) = \frac{v(t)\left\{\lambda_2 v(t) - (mr\sigma + c)\left[1 - e^{\delta_m (t-t_1)}\right]\right\}}{\delta_m^2 e^{\delta_m (t-t_1)}}, \tag{3.41}$$

where

$$v(t) = \delta_m + m\beta I_1 \left(e^{\delta_m (t-t_1)} - 1\right), \tag{3.42}$$

and λ_2 is given by (3.39) at time t_2. The solution to the adjoint equation from $t = t_1$ to $t = 0$ is

$$\lambda(t) = \frac{w(t)\left\{\lambda_1 w(t) - (Mr\sigma + c)\left[1 - e^{\delta_M (t)}\right]\right\}}{\delta_M^2 e^{\delta_M (t)}}, \tag{3.43}$$

where

$$w(t) = \delta_M + M\beta I_0 \left(e^{\delta_M(t)} - 1\right), \tag{3.44}$$

and λ_1 is given by (3.41) at time t_1.

3.4.2 Supplementary tables and figures

Table 3.1. Realistic parameters for the optimal-control problem. We adapted the transmission rate, β, from [1]. Moreover, like [1], we used the arithmetic mean-duration of *S. aureus* infection of 110 days from [2] to get the per-capita recovery-rate, γ. Barlow et al. (2009) based this value on the assumption that 74% of mastitis cases become chronic. We chose a time horizon, T, that reflects the standard milk-yield period of the lactation cycle. This model, therefore, is better suited to a standard farm environment than the pasture-based dairy operations modeled in [3]. Furthermore, we determined the revenue per cow per day using 2020 data [4], and we calculated the cost per case of mastitis per day by adapting the value given by [5] using the average duration of infection. We use the proportion of mastitis cases that are categorized as clinical [6] for the disease severity parameter, σ, and we use the cow-level prevalence of mastitis from [6] to determine the initial infected population. The values of the parameters m and M are unknown, and we assume the values $m = 0.2$ and $M = 0.9$ as in [3].

Parameter	**Value**	**Meaning**	Source
β	$\frac{0.0232}{N}$ $(\text{indiv}\cdot\text{day})^{-1}$	Transmission coefficient	[1]
γ	$\frac{1}{110}$ $(\text{day})^{-1}$	Per-capita recovery-rate	[2]
T	305 days	Standard lactation-period	
r	0.20 $\frac{\text{USD}}{\text{indiv}\cdot\text{day}}$	Revenue per milk-producing cow per day	[4]
c	1.41 $\frac{\text{USD}}{\text{indiv}\cdot\text{day}}$	Cost per infective per day	[2, 5]
σ	0.05	Cow-level prevalence of clinical mastitis	[6]
m	0.2	Minimum mixing-level	
M	0.9	Maximum mixing-level	
I_0	63 individuals	Cow-level prevalence of mastitis	[6]
N	100 individuals	total population-size	

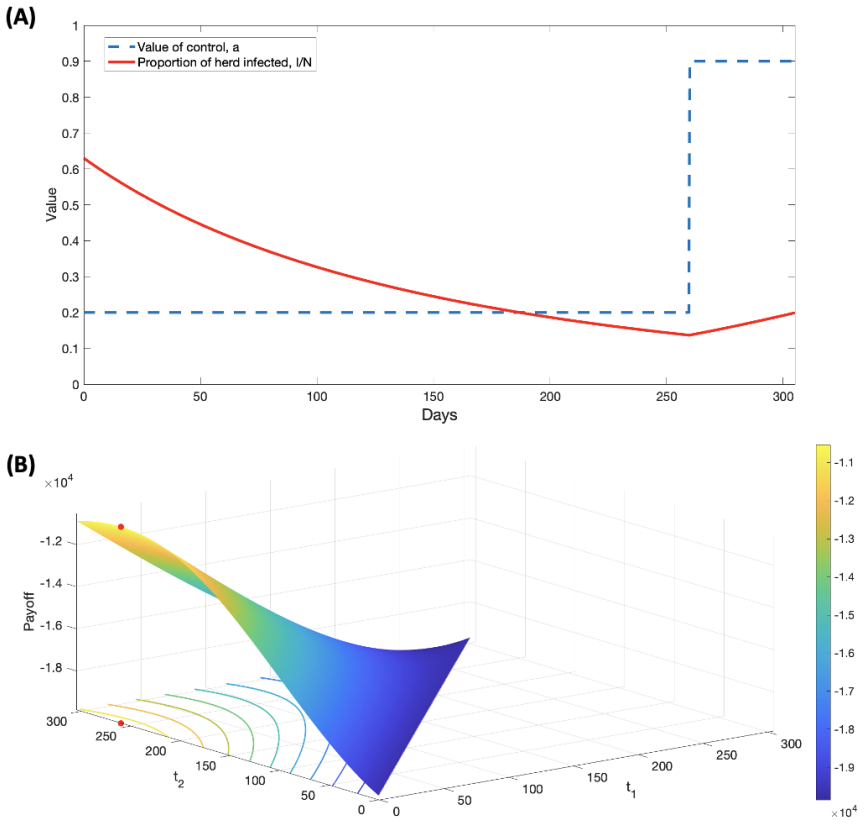

Figure 3.5: Solution of the optimal-control problem with parameters from Table 2.1. Figure (A) shows how the value of the control (dashed blue line) and the proportion of the herd infected (solid red line) change over time. We see that reduced-mixing strategies should be used for about 260 days in order to maximize profit. Figure (B) shows the payoff as a function of the switching times, t_1 and t_2. The first switching-time, t_1, is a switch from the maximum mixing-level to the minimum mixing-level. The second switching-time, t_2, is a switch from the minimum mixing-level to the maximum mixing-level. If $t_1 = 0$, the population will start at the minimum mixing-level, and there will be one switch from the minimum mixing-level to the maximum mixing-level. If $t_1 = t_2$, then the switch from the maximum mixing-level to the minimum mixing-level occurs at the same time as the switch from the minimum mixing-level back to the maximum mixing-level. Therefore, there will be no switch. In this figure, the maximum payoff occurs when there is only one switch from low to high activity after 260 days ($t_1 = 0$ and $t_2 = 260$). The red dots on the surface and contour plots show the maximum payoff.

Chapter 4

Retrospective Analysis of Equity-Based Optimization for COVID-19 Vaccine Allocation

The COVID-19 pandemic has highlighted and exacerbated the inequities of the health care system in the United States (US) and other countries in the world. In the US, over the course of the pandemic, there have been significant inequities in cases, hospitalizations, and deaths according to race and ethnicity, with those in marginalized communities carrying the most burden of the pandemic. In the state of Oregon, racially marginalized communities in every age group have experienced disproportionate mortality rates. For example, the Non-Hispanic (NH) American Indian or Alaska Native (AIAN) population had the highest risks of COVID-19 infection, hospitalization, and death and were 2.7, 3.6, 3.2 times more likely to be infected, hospitalized, or die when compared to a white person of the same age in 2020 [132]. Moreover, the BIPOC persons (consisting of NH black or African-American persons, NH Asian persons, NH AIAN persons, and Hispanic or Latino persons) aged 20-59 have experienced mortality rates 5.7 times higher than their white counter parts, those aged 60-69 have experienced 4 times higher rates, and individuals aged 0-19 and 70+ have experienced

mortality rates that are 1.8 times higher. Data has shown similar disparities nationally [133]. Studies have shown that this is due, in part, to systemic racism and inequities leading to differences in comorbidities, access to health care, and occupation [133–152]. For example, BIPOC persons are more likely to be employed in front-line work, leading to more exposure, and decreasing the effectiveness of mitigation strategies like shelter-in-place for these groups [153–157].

In the summer of 2020, the National Academies of Science, Medicine and Engineering (NASEM) and the World Health Organization (WHO) released frameworks for equitable vaccine allocation [158, 159]. However, allocating the vaccine in an equitable way proved to be difficult, as there were many obstacles, including differences in vaccine perception [160] and inequities in access [153, 161], resulting in large differences in vaccination rates between racial groups, particularly during the first few months of the vaccination campaigns [162–165]. These inequities have further compounded disparities in COVID-19 outcomes [166]. Hence, the need to create health policies, including vaccination strategies, that promote equity through the use of targeted, community-based interventions is increasingly evident [144, 153, 167, 168].

Previous work addressing vaccine prioritization for COVID-19 vaccines has predominantly been age-centered (e.g. [169–175]) with only a few studies including social variables [176]. Most of these studies evaluate vaccination success as the reduction of the overall disease burden (mortality, hospitalizations, or infections) without accounting for projected equity gaps. A few studies include inequity outcomes, mostly focusing on geographic distribution of vaccines among countries, states, or affected regions [177, 178], and only a handful discuss reducing inequities in access or disparities in outcomes between racial groups [179–181].

In the present work, we explore a race conscious, as opposed to colorblind, approach to determine mathematically optimal vaccine allocation strategies that not only minimize overall disease burden (mortality or years of life lost, YLLs) but also minimize the inequity in COVID-19 outcomes between racial groups, which we measure using several metrics. To

that end, we develop an age-and-race-stratified mathematical model, and apply optimization algorithms, which account for both disease burden and equity, to determine the optimal distribution of available vaccine doses across age and race groups under different disease and equity metrics. We retrospectively analyze data from Oregon for the first four months of 2021, when vaccine supplies were extremely limited and SARS-CoV-2 was relatively stable, and explore counterfactual vaccine allocations. To be clear, we are not suggesting allocating vaccine based on race, but given the fact that the data itself is race-stratified, we use race as an incomplete proxy for systemic inequities, such as disparities in social determinants of health (SDOH), affecting BIPOC communities. Nevertheless, we recognize that considering race alone does not grant us full understanding of the systemic inequities caused by multiple axes of oppression [182] and that no mathematical model or vaccine allocation strategy alone could be sufficient to resolve the profound and complex problem of racism and centuries-long systemic inequities experienced in the US. Policy makers are faced with extreme pressure during a public health emergency, such as a pandemic, where they need to make decisions affecting all aspects of our lives. Our hope is to provide a framework to learn from the inequities observed during the COVID-19 pandemic, and that other public health interventions, present and future, might benefit from a quantitative approach addressing both disease burden and inequity reduction. Our analysis suggests that when vaccine supply is very limited, there is a trade-off between diminishing overall mortality and reducing inequity resulting in significantly high, and likely unacceptable, levels of burden in one or the other. However, this trade-off lessens as more vaccine becomes available.

4.1 The mathematical model

We construct a deterministic mathematical model of SARS-CoV-2 transmission and vaccination. The structure of our model accommodates the available case data from the state of Oregon. This data includes information about hospitalization and death after infection

as well as demographic information about age and race or ethnicity. Although much of the inequity in COVID-19 outcomes between racial or ethnic groups is due to systemic disparities in SDOH such as access to healthcare, income, and education, this information is not regularly collected along with case data. Therefore, we use the race and ethnicity variable as a proxy for SDOH and these systematic disparities to gain insight into counteracting or preventing inequities in resource allocation and disease outcomes [183].

In our model, individuals can be either unvaccinated or vaccinated. Once infected, susceptible individuals become latent, meaning they are infected but not yet infectious. Once the latency period has ended, individuals may become either symptomatic or asymptomatic. All asymptomatic individuals eventually recover, but symptomatic individuals may become hospitalized before recovering or dying.

We stratified the population into five age groups: children and young adults (aged 0-19), adults aged 20-49, adults aged 50-59, adults aged 60-69 years old, and adults aged 70 and older. We chose not to vaccinate the youngest age group, which mostly consists of children, in our model as vaccines were not available for children at the beginning of 2021. We consider two racial groups: non-Hispanic white persons (referred to as white) and persons belonging to other racial or ethnic groups as preestablished in the fitted data (including non-Hispanic black or African-American persons, non-Hispanic Asian persons, non-Hispanic American-Indian or Alaska-Native persons, and Hispanic or Latino persons), referred to as BIPOC below. For each age group, the BIPOC racial group was computed as a weighted average of the racial/ethnic groups mentioned above, reflecting the composition of the population in Oregon in 2020-2021 according to census data for the white and BIPOC groups [184]. The population distribution is shown in Figure 4.1(D).

Mortality and hospitalization rates by age were estimated from published sources [185] and [186]. Using data from Oregon, we computed per-capita mortality rate ratios between the BIPOC and white groups for each age group and use these ratios to estimate the differences in health outcomes between racial groups.

In our model, individuals come into contact with each other in four locations: home, school, work, and community. Using data given in [187, 188] and [189], we adapted the contact matrices from [190] for home and work, respectively, to reflect different contact patterns across racial groups. Figure 4.1 shows the resulting contact patterns stratified by race used to adapt the work (B) and home (C) contacts. We assume community and school contacts are not different for racial groups, but these contacts are proportional to the population size of each group. The overall contact matrix is found by summing the location-specific contact matrices.

Following the ideas of [191, 192], we consider three vaccine effects: reduction on the susceptibility to infection (set to 70%), reduction on symptomatic infection (set to 66%) and reduction on hospitalization and death (set to 90%). These values reflect the vaccine

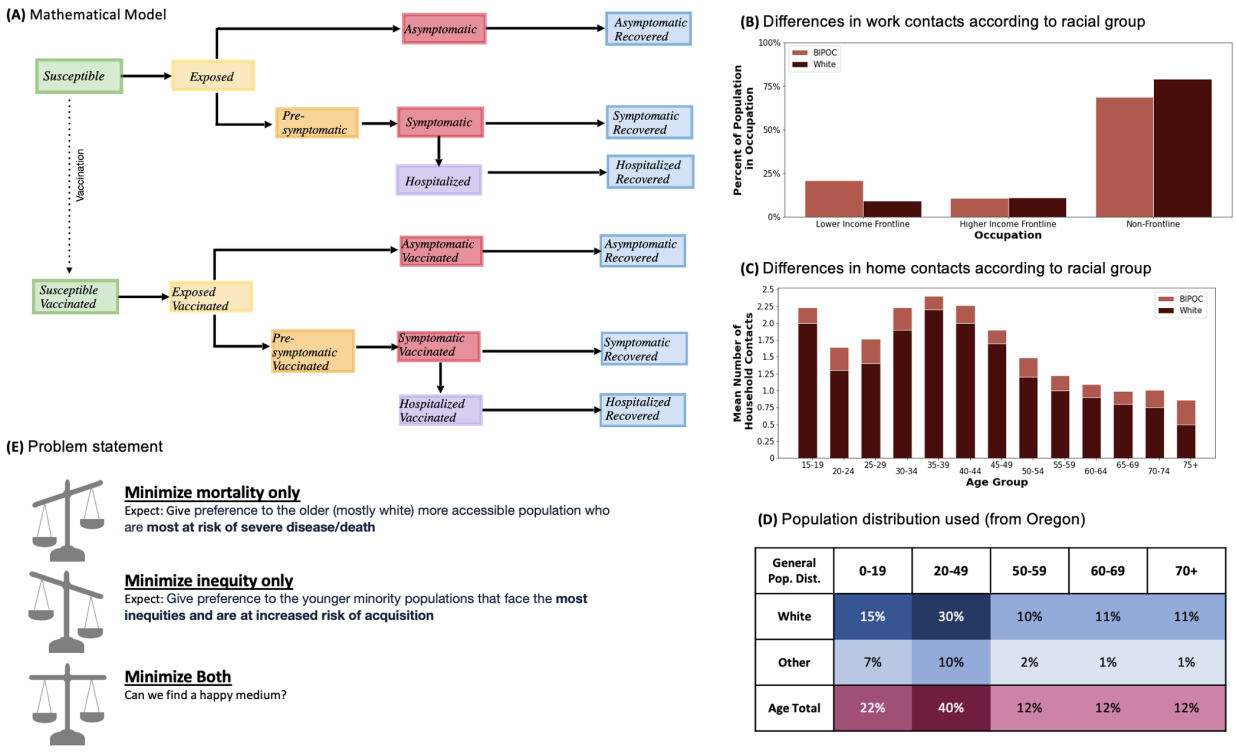

(D) Population distribution used (from Oregon)

General Pop. Dist.	0-19	20-49	50-59	60-69	70+
White	15%	30%	10%	11%	11%
Other	7%	10%	2%	1%	1%
Age Total	22%	40%	12%	12%	12%

Figure 4.1: Model description and demographic information. This figure includes the model diagram (A), the differences in occupation type according to racial group [189] (B), the differences in home contacts according to racial group [187] (C), the population distribution of the population under study (D), and the problem statement (E).

effectiveness estimated as of January 2021 [191, 193–196]. We assume that natural immunity, which is completely effective, and vaccine-induced immunity last for the entirety of the simulated period of four months with no new strains of COVID-19 introduced during that time.

4.1.1 The optimization problem

Our goal is to distribute available vaccines to the four, adult age groups in the two racial groups aiming to minimize different objective functions including measures of disease burden (mortality and YLLs), measures of inequity (Table 4.1), and joint disease burden and inequity measures. For the combined measures, the inequity measure is weighted to match the scale of the measure of disease burden. To calculate YLLs, the number of deaths in each group is multiplied by the average remaining life expectancy in that group. Therefore, YLLs assign higher values to the lives lost in the younger populations [197, 198]. This is worth noting as the proportion of the BIPOC population in the younger age-groups is greater than that of the white population.

We consider five measures of inequity, described in Table 4.1. These include the relative and absolute disparity in mortality rates between racial groups calculated on age-group basis. The first of these measures is minimized when the two racial groups have the same age-matched mortality rate and weights all age groups equally. The second is also minimized when the two racial groups have the same age-matched mortality rate, but may give more weight to older age groups with much higher mortality rates. We also include the absolute disparity in YLLs between racial groups and the indices of disparity in mortality and YLLs based on race/ethnicity [199]. These indices are commonly used to study disparities in disease outcomes [200, 201].

For our optimization routine, we develop a coarse global search algorithm to find the vaccination strategy that minimizes a given objective function with a fixed amount of resources (vaccine doses) over a time frame of four months. Vaccination strategies are represented

Table 4.1. Measures of Inequity.

Name	Formula	Meaning
Relative disparity in mortality	$\sum_{a \in \text{ages}} \lvert \frac{m_{a,B}}{m_{a,W}} - 1 \rvert$	Estimating how distant the set of mortality rate ratios across age groups is from perfect equity (all ones).
Absolute disparity in mortality	$\sum_{a \in \text{ages}} \lvert m_{a,B} - m_{a,W} \rvert$	Estimating the difference between mortality rates by race across age groups.
Index of disparity (mortality)	$\sum_{a \in \text{ages}} \frac{1}{2} \cdot \frac{\sum_{R \in \text{races}} \lvert m_{a,R} - \overline{m}_a \rvert}{\overline{m}_a} \cdot 100$	Inequity measure giving the sum of the indices of disparity for mortality rates for each age group.
Absolute disparity in YLLs	$\sum_{a \in \text{ages}} \lvert YLL_{a,B} - YLL_{a,W} \rvert$	Inequity measure giving the sum of the differences in years of life lost between racial groups for each age group.
Index of disparity (YLLs)	$\sum_{a \in \text{ages}} \frac{1}{2} \cdot \frac{\sum_{R \in \text{races}} \lvert YLL_{a,R} - \overline{YLL_a} \rvert}{\overline{YLL_a}} \cdot 100$	Inequity measure giving the sum of the indices of disparity for YLLs for each age group.

Note: The values $m_{a,B}$ and $m_{a,W}$ are the resulting mortality rates for the BIPOC and white populations, respectively, by age. The value $m_{a,R}$ is the resulting mortality rates for race group R (either BIPOC or white population) by age. The value $\overline{m}_a$ is the mean mortality rate by age.

by vectors of the proportion of each group to be vaccinated (ranging from 0 to 1). Similar to [169], we performed the optimization routine in two steps. First, we generate 10,000 random vaccination vectors and evaluate the objective function using each. We select the 20 best vectors and use them, together with four educated-guesses, as starting points for three constrained optimization algorithms: trust-region constrained, SLSQP, and adapted Nelder-Mead. We report the optimal allocation strategy to be the best solution among the

24 solutions calculated

We focus on a scenario where vaccine availability is very constrained similar to the situation in the United States in January 2021. We explored scenarios with enough vaccine to cover 10%, 20%, or 30% of the entire population.

4.2 Results

4.2.1 Model fitting

We calibrate our model to the number of deaths reported in Oregon in 2020 by fitting the percentage of contacts maintained when social distancing policies were implemented as well as the rates of asymptomatic infection by age. Given our interest in the disparities in severe COVID-19 outcomes between different races, we also fit to the mortality rates ratios between the white and BIPOC populations in each age group. Our resulting fit has the same number of deaths as the reported data as well as a similar distribution of deaths. Figure 4.5 and Table 4.3 show the detailed results of model fitting and can be seen in the Supplementary Information.

4.2.2 Allocating vaccines

We start with a scenario in which vaccine supply is very limited by assuming that available vaccine doses in the beginning of 2021 are enough to cover 10% of the population. We simulate a baseline case where vaccines are randomly allocated to serve as a basis for comparison to the allocation strategies found through optimization, referred as optimal strategies below. In the baseline case, the burden of disease, measured by the number of deaths or YLLs, is concentrated in the oldest age groups. Moreover, individuals aged 70+ from the BIPOC group die at 2.4 times higher rates than their white counterparts. The most extreme racial inequities in burden of disease, however, are in the young and middle-aged adult groups, where there is a maximum relative difference in mortality of 6.2 in those aged 20-49 years

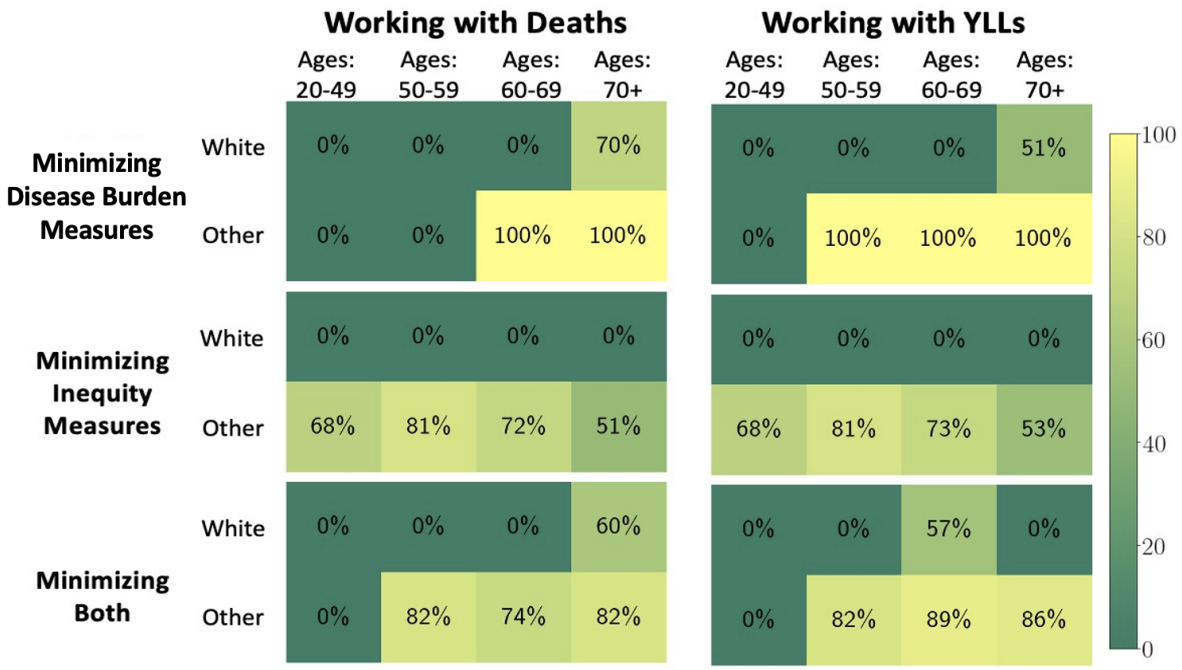

Figure 4.2: Vaccine allocation with resources to vaccinate 10% of the population. The first column in this figure contains the results of minimizing deaths (row 1), relative disparity in deaths (row 2), and deaths and relative disparity in mortality (row 3). The second column in this figure contains the results of minimizing YLLs (row 1), absolute disparity in YLLs (row 2), and YLLs and the absolute disparity in YLLs.

old and the highest index of disparity (134) in those aged 50-59.

We then allocate vaccines by minimizing each of the objective functions defined above. When minimizing only measures of disease burden (deaths or YLLs) or only measures of inequity, the optimal allocation strategy is to prioritize either the older population (who are most at risk of severe disease and death) or the younger, BIPOC population (who face the most inequities), respectively (Figure 4.2). To minimize combinations of measures, the optimal strategy is to strike a balance between the objectives. For example, to minimize both deaths and relative inequity in mortality, a significant amount of the available vaccine (about 73%) is allocated to the older population to reduce mortality, and the remaining vaccine (about 27%) is allocated to the younger BIPOC population to reduce inequity. In this case, neither population is completely prioritized over the other.

All of our optimal vaccine-allocation strategies improve COVID-19 outcomes, in both

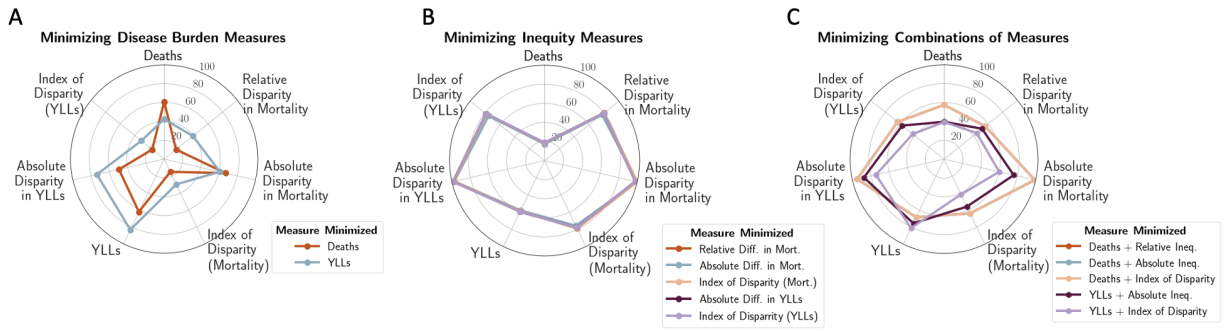

Figure 4.3: Summary of COVID-19 outcomes when allocating vaccine to 10% of the population. The vaccine allocation strategies that minimize measures of disease burden (A), inequity measures (B), and combinations of measures (C) are evaluated. The results are reported as the percent averted from the base (random allocation) case. Each of the colorful lines represent a vaccination strategy for minimizing the measure shown in the legend. The axes in each circle plot correspond to the disease burden or inequity measures and the gray circles correspond to the percent averted in each measure.

disease burden and inequity measures, when compared to the baseline scenario (Figure 4.3), but the amount of improvement in disease burden or inequity is different depending which measure is minimized. There is a trade-off: Minimizing only measures of disease burden results in vaccine allocation strategies with larger inequity and vice versa. This holds for any optimization based on a single metric (disease burden or inequity) and for all the inequity metrics considered (Table 4.1, Figure 4.3A vs Figure 4.3B). For example, minimizing overall deaths reduces mortality by 61% from the baseline scenario, but minimizing relative inequity in mortality reduces overall mortality by only 16%.

The optimal allocation strategies that minimize different metrics of inequity yield very similar outcomes (Figure 4.3B). When comparing between measures of disease burden, minimizing only YLLs is more equitable than minimizing only deaths and results in a greater percentage of inequity averted for four of the five measures of inequity (Figure 4.3A). As expected, minimizing YLLs leads to more deaths (42% deaths averted when compared to baseline versus 61% when minimizing deaths), but significantly decreases the number of YLLs (83% YLLs averted versus 62% when minimizing deaths).

Allocation strategies minimizing combined measures of disease burden and inequity produce middle-ground solutions improving both. For instance, when the overall number of

deaths is minimized along with any of the measures of inequity in mortality, mortality is reduced by 57% and the relative disparity in mortality is reduced by 56% from the baseline. This results in 4 percentage points less deaths averted than when minimizing mortality alone and 25 percentage points less inequity averted than when minimizing inequity alone (Figure 4.3C). Minimizing both YLLs and measures of inequity based on YLLs results in a 75% reduction in YLLs, and an 87% reduction in absolute disparity in YLLs when compared to baseline. This shows a similar trade-off when compared to single-measure optimizations minimizing YLLs (83% reduction in YLLs) or inequity in YLLs only (99% reduction in absolute disparity in YLLs). Minimizing both YLLs and the index of disparity in YLLs leads to a greater reduction in YLLs, but averts less inequity than any other combination of measures.

Our analysis highlights the importance of accounting for both disease burden and inequity, when vaccine supply is limited. As more vaccine doses become available, the trade-off between equity and mortality lessens. With enough resources to vaccinate 20% of the population, there are more vaccination strategies significantly reducing both equity and mortality simultaneously, and combined optimization yields similar impact in minimizing both outcomes as minimizing each one individually. For example, the optimal allocation strategy minimizing both overall deaths and relative inequity in mortality reduces mortality by 83% and inequity by 71% from the baseline scenario. This is comparable to the 89% and 85% reduction in deaths and inequity in mortality obtained when minimizing each alone (Figure 4.4). With a further increase of available resources (enough to vaccinate 30% of the population) the difference between the combined and single-measure optimizations is almost entirely eliminated. In this case, minimizing both overall deaths and relative inequity in mortality results in comparable reduction in mortality with minimizing only deaths (94% vs 97%) while preserving the majority of the inequity reduction (78%) compared to scenarios minimizing only inequity (85%).

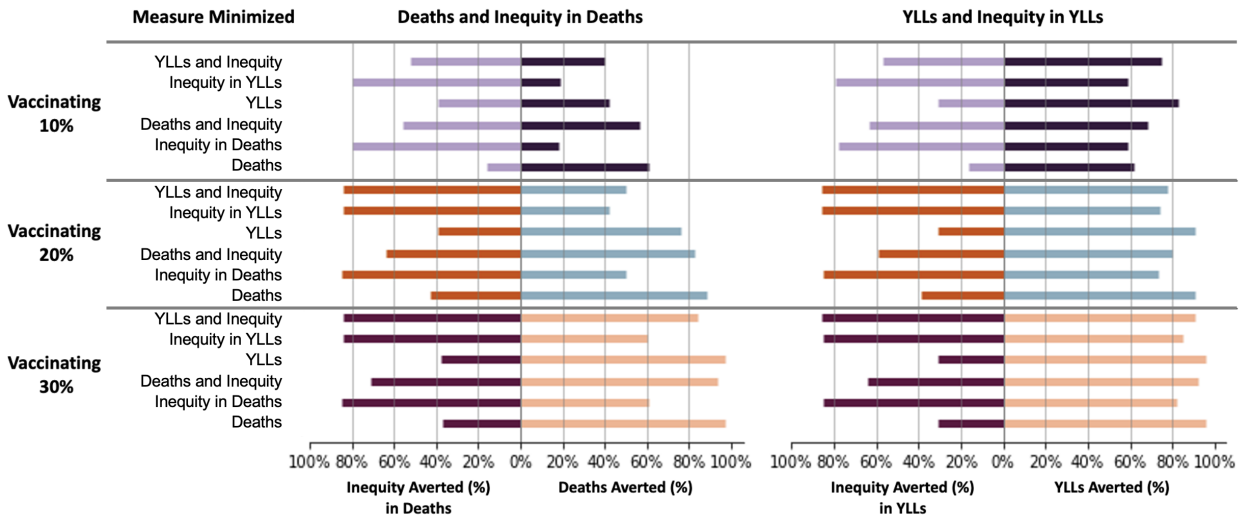

Figure 4.4: Performance of optimal vaccination strategies for six minimization objectives when there is enough vaccine to cover 10%, 20% or 30% of the population. Each strategy is evaluated for four metrics: overall deaths, YLLs, inequity in deaths (measured by the index of disparity in mortality), and inequity in YLLs (measured by the index of disparity in YLLs). Performance is reported as the percent averted compared to the baseline scenario with random vaccination.

4.3 Discussion

During late 2020 and early 2021, different voices proposed vastly different vaccine allocation strategies [202]. Some argued that protecting the older population, which is mostly white and at the highest risk for severe disease, needed to be prioritized [203, 204]. Others argued that vaccines needed to be allocated to communities experiencing the greatest inequities in access and disparities in outcomes, usually younger BIPOC populations, working more often in essential occupations [205–208]. Here, we are not advocating for the allocation of vaccines based on race or ethnicity. We instead use race and ethnicity as a proxy for social determinants of health such as access to healthcare and occupation for which data is not usually collected along with case information. While racial identity is a poor proxy for analyzing and addressing systemic inequities in vaccine allocation and disparities in YLLs or mortality, it allows a race conscious data-driven analysis that can be incorporated into broader societal decisions about how to best allocate vaccine in urgent conditions of scarcity, such as those experienced early in the SARS-CoV-2 pandemic. For example, the results when minimizing inequity support prioritizing marginalized communities. This could be

interpreted as implementing mitigation strategies such as setting up more vaccination clinics in underserved communities, using community-engaged public health approaches, or first vaccinating frontline workers. An example of such a strategy is given by [209], and describes a method for increasing vaccination rates in black communities by engaging community leaders, embracing low/tech platforms, and reimmagining clinic flows. Our analysis also highlights the urgent need to collect better data regarding social variables, so that further analyses can be refined.

In the present work, we used an age-and-race-structured mathematical model to study counterfactual scenarios of COVID-19 vaccine allocation in early 2021 in the United States, when very limited amounts of vaccine were available. Our results are not meant to be construed as a critique of the COVID-19 vaccine allocation during the pandemic, but rather as a theoretical exercise to quantify equity in public health resource distribution. Indeed, our results are aligned with the prioritization followed by most regions worldwide when vaccine availability was extremely low, where older adults were given vaccine first to minimize mortality. To better understand the effect of different vaccination policies on inequity, we analyzed five measures of inequity. Our results suggest that when vaccine is very limited, there is a trade-off between minimizing inequity and minimizing overall mortality (or YLLs). If minimizing overall mortality, vaccine was allocated to the oldest population, with those in racially marginalized older groups being prioritized. In contrast, when minimizing inequity, irrespective of the metric used, vaccine was allocated to those in the, usually younger, BIPOC group. This resulted in additional deaths in older age groups, including in BIPOC communities. This trade-off, however, lessens as more resources become available, and our optimization work shows that it is possible to minimize both mortality and inequity if vaccine is allocated optimally.

The trade-off between equity and mortality is exaggerated due to the nature of COVID-19 disease profile: the burden of severe disease and mortality is concentrated in the oldest population, which is disproportionately white due to racism leading to inequities in access

to care and disparities in morbidity/mortality at baseline. As vaccines become more readily available, the potential to address both age-and-racial/ethnic inequities mathematically, becomes more balanced. Translation of this potential then needs to shift to evaluation of systemic biases that impact vaccination allocation policies, implementation strategies, and conscious and unconscious bias that impact vaccine distribution. In that sense, our work suggests that for other infectious diseases which do not have a strong age-dependent mortality pattern (e.g., mpox or HIV), resources can be allocated to reduce overall disease burden and inequity simultaneously, even when they are scarce.

Our work, like any mathematical model, is subject to limitations. First, due to data limitations, we use race and ethnicity as a proxy for factors that lead to differences in health outcomes such as social determinants of health and racism in society. Therefore, our results may serve as an indication of which groups to prioritize for vaccine distribution, but do not tell us which factors have the most influence. For example, we are not able to determine if individuals with low access to healthcare should be prioritized over those in essential occupations. Furthermore, we only included two racial/ethnic groups. However, the BIPOC group was calculated to match the proportions in Oregon of each of the five racial/ethnic groups defined in [133], and we believe that the inclusion of more racial/ethnic groups will not significantly alter the results. While these proportions closely match the national average, the optimal vaccination strategies could potentially be different in other cities where the composition of the population is very different.

In the first few months of 2021, the majority of the population was unvaccinated, SARS-CoV-2 reinfections were very uncommon, and the virus was relatively stable. Therefore, we did not include waning immunity from previous infections, or from vaccinations, or booster vaccinations. Furthermore, we currently vaccinate all individuals simultaneously at the beginning of our simulation. This allows us to compare different vaccination strategies without additional confounders (e.g., vaccination rates). Implementing a vaccination campaign would be more realistic but would require us to also optimize the order in which individuals are

vaccinated. We quantified inequity in five different ways and combined them with mortality or YLLs, but other measures or combinations might be more appropriate. In particular, using Pareto optimization instead of adding these measures might be a better way to explore the trade-offs between reduction in overall mortality and minimizing inequitable outcomes. Much of the inequity in disease outcomes is the result of profound systemic inequities that cannot be overcome through vaccine allocation alone. Therefore, absolute equity is not achievable.

Our results show that public health decisions in the midst of a pandemic are intrinsically difficult and that trade-offs might be unavoidable when public health crises arise in a society that is inequitable and rooted in racially biased systems at baseline. Indeed, decision-makers need to consider societal, economic, and political factors to understand and address the trade-offs that arise. While counteracting racial inequities and underlying racism is complex and can be emotionally charged, our work may help to provide a quantitative framework to measure the impact of public health interventions on equity. Specifically, it offers quantitative methodology to evaluate strategies for counteracting racial/ethnic inequities in the distribution of resources and in outcomes. We hope that this framework will help inform future discussions about how to equitably protect those at highest risk of harm in public health emergencies.

This is an Accepted Manuscript of an article published in PNAS Nexus in September, 2023, available at: https://doi.org/10.1093/pnasnexus/pgad323.

4.4 Supplementary information

4.4.1 Model equations

The model equations for the deterministic age-structured mathematical model of SARS-CoV-2 transmission stratified by both age and race for the unvaccinated population are

$$
\begin{aligned}
\dot{S}_i &= -\lambda S_i, \\
\dot{E}_i &= \lambda S_i - \gamma_E E_i, \\
\dot{A}_i &= \gamma_E(1-a_i)E_i - \gamma_A A_i, \\
\dot{P}_i &= \gamma_E a_i E_i - \gamma_P P_i, \\
\dot{I}_i &= \gamma_P P_i - (1-h_i)\gamma_I I_i - \sigma h_i I_i, \\
\dot{H}_i &= \sigma h_i I_i - \gamma_H H_i, \\
\dot{R}_i &= (1-h_i)\gamma_I I_i, \\
\dot{RA}_i &= \gamma_A A_i, \\
\dot{RH}_i &= (1-d_i)\gamma_H H_i.
\end{aligned}
\tag{4.1}
$$

For the vaccinated population, the model equations are

$$
\begin{aligned}
\dot{S}v_i &= -\theta_V \lambda S v_i, \\
\dot{E}v_i &= \theta_V \lambda S v_i - \gamma_E E v_i, \\
\dot{A}v_i &= \gamma_E(1-\phi_V a_i)E v_i - \gamma_A A v_i, \\
\dot{P}v_i &= \gamma_E \phi_V a_i E v_i - \gamma_P P v_i, \\
\dot{I}v_i &= \gamma_P P v_i - (1-\rho_V h_i)\gamma_I I v_i - \sigma \rho_V h_i I v_i, \\
\dot{H}v_i &= \sigma \rho_V h_i I v_i - \gamma_H H v_i, \\
\dot{R}v_i &= (1-h_i)\gamma_I I v_i, \\
\dot{RA}v_i &= \gamma_A A v_i, \\
\dot{RH}v_i &= (1-\delta_V d_i)\gamma_H H v_i.
\end{aligned}
\tag{4.2}
$$

The force of infection is

$$
\lambda = \sum_{i=1}^{10} \frac{r_i C \beta}{N_i} \left[r_A(A_i + \psi_V A v_i) + r_P(P_i + \psi_V P v_i) + (I_i + \psi_V I v_i) + r_H(H_i + \psi_V H v_i) \right].
\tag{4.3}
$$

The age-and-race-stratified contact matrix, C, is adapted from the age-specific contact matrix for the US given in [190], and we calculate β by assuming $R_0 = 3$. The parameters used for this model are described in Table S1.

4.4.2 Supplementary figures and tables

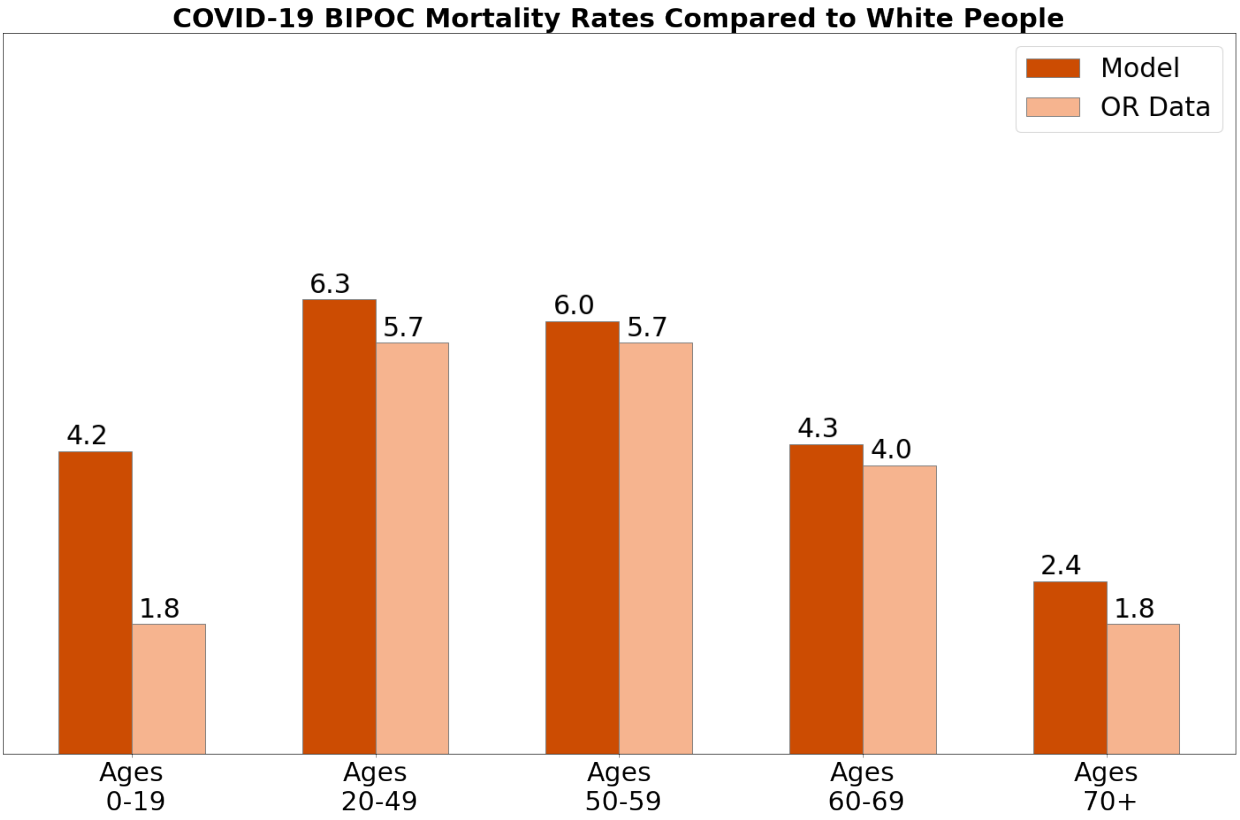

Figure 4.5: Mortality rate ratios from model fitting compared to data.

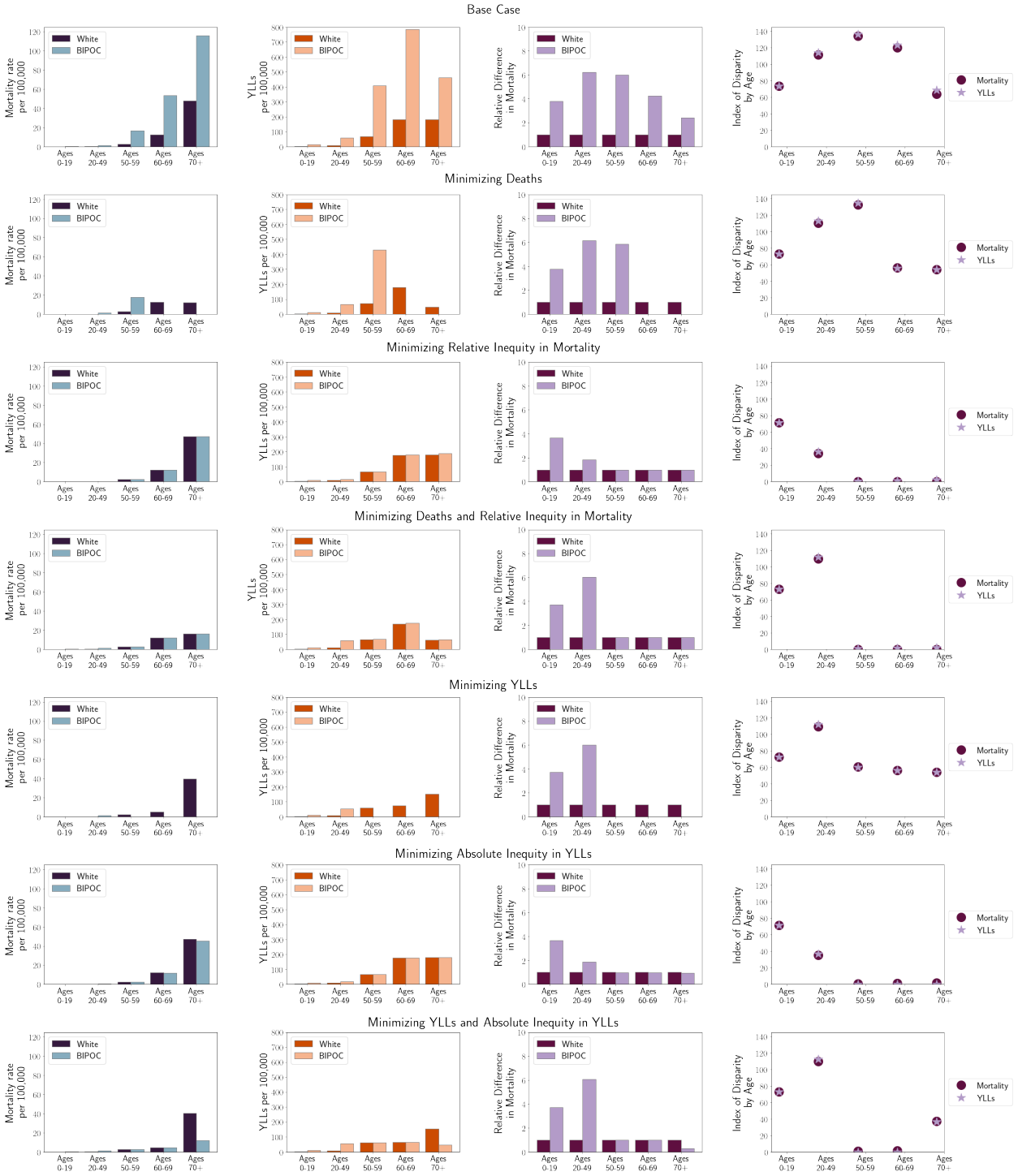

Figure 4.6: Summary of COVID-19 outcomes by-age when allocating vaccine to 10% of the population. The vaccine allocation strategies that minimize measures of disease burden (rows 2 and 5), inequity measures (rows 3 and 6), and combinations of measures (rows 4 and 7) are evaluated for comparison to the base case (row 1). Outcomes including mortality per 100,000 (column 1), YLLs (column 2), relative disparity in mortality (column 3), and the index of disparity in mortality and YLLs (column 4) are shown.

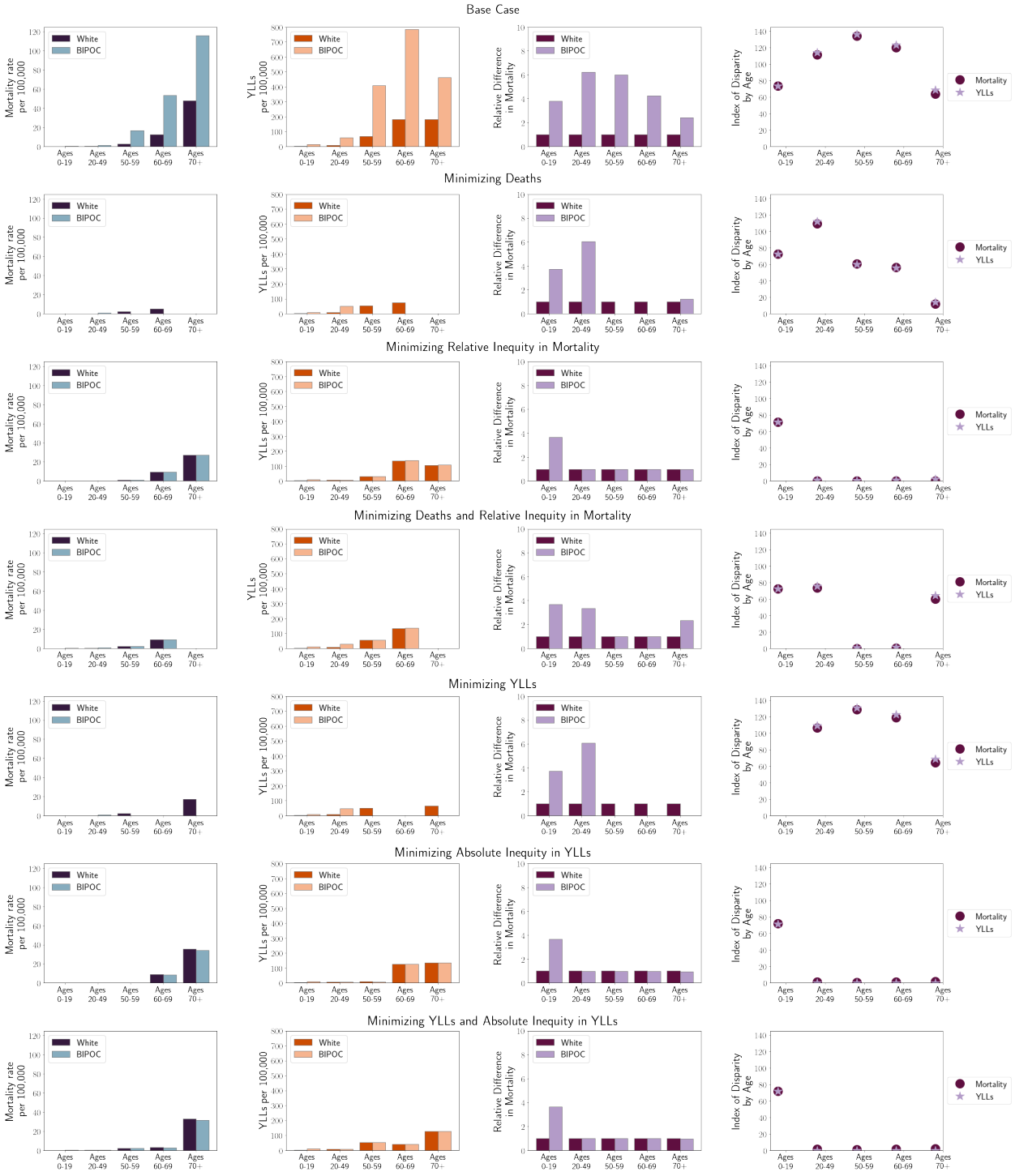

Figure 4.7: Summary of COVID-19 outcomes by-age when allocating vaccine to 20% of the population. The vaccine allocation strategies that minimize measures of disease burden (rows 2 and 5), inequity measures (rows 3 and 6), and combinations of measures (rows 4 and 7) are evaluated for comparison to the base case (row 1). Outcomes including mortality per 100,000 (column 1), YLLs (column 2), relative disparity in mortality (column 3), and the index of disparity in mortality and YLLs (column 4) are shown.

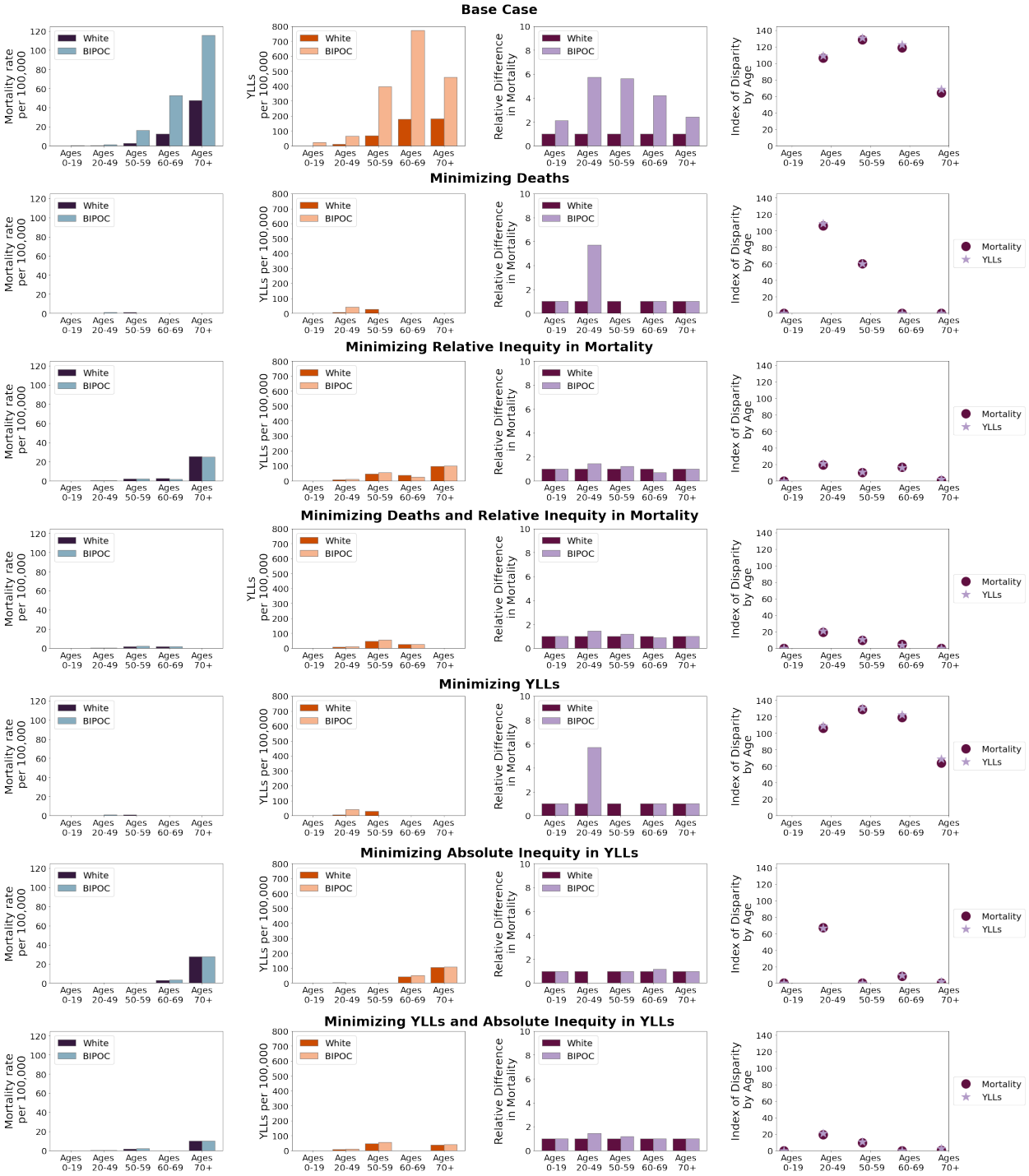

Figure 4.8: Summary of COVID-19 outcomes by-age when allocating vaccine to 30% of the population. The vaccine allocation strategies that minimize measures of disease burden (rows 2 and 5), inequity measures (rows 3 and 6), and combinations of measures (rows 4 and 7) are evaluated for comparison to the base case (row 1). Outcomes including mortality per 100,000 (column 1), YLLs (column 2), relative disparity in mortality (column 3), and the index of disparity in mortality and YLLs (column 4) are shown.

Table 4.2. Parameter values used in mathematical model.

Parameter	Meaning	Value	Source
$1/\sigma$	mean time from symptom onset to hospitalization	3.8 days	[210]
$1/\gamma_E$	mean latent period	3 days	[211, 212]
$1/\gamma_P$	mean pre-symptomatic period	2 days	[213]
$1/\gamma_A$	mean infectious period of asymptomatic infectives	6 days	assumed
$1/\gamma_I$	mean infectious period of symptomatic infectives, after developing symptoms	4 days	[214, 215]
$1/\gamma_H$	mean duration of hospitalization	W:(1/3,1/3,1/4,0.21,1/6), O:(1/3,1/3,1/4,0.22,1/6)	[216]
a	proportion of infections that are asymptomatic	age-stratified	fitted
h	proportion of symptomatic infections requiring hospitalization	W:(0.002,0.03,0.1,0.17,0.25), O:(0.007,0.12,0.46,0.79,0.68)	[186]
d	hospitalization fatality ratio	W:(0.08, 0.03 , 0.11 , 0.17, 0.23), O:(0.08, 0.04, 0.12, 0.13, 0.18)	[185]
r_A	relative infectiousness of asymptomatic infections	0.75	[216]
r_P	relative infectiousness of pre-symptomatic infections	1	[217]
r_H	relative infectiousness of hospitalized infections	0	assumed
R_0	basic reproductive number	3	[218, 219]
β	transmission coefficient	calculated	
C	contact matrix	-	
N	total population	4060795	[184]

Table 4.3. Comparison of deaths from model fitting to data from Oregon.

Deaths Per-Group	**0-19**	**20-49**	**50-59**	**60-69**	**70+**
Data: White	0	17	49	173	1130
Data: Other	1	33	55	76	170
Data Total: 1704					
Model: White	1	11	50	253	968
Model: Other	2	24	62	132	202
Model Total: 1704					

Table 4.4. Deaths per-group (% averted from base case) when minimizing measures of disease burden, measures of inequity, and combinations of measures with enough vaccine to vaccinate 10% of the total population. When minimizing inequity in deaths and when minimizing deaths and inequity, the relative inequity in deaths is used. When minimizing inequity in YLLs and when minimizing YLLs and inequity, the absolute inequity in YLLs is used.

Age-Group	0-19	20-49	50-59	60-69	70+
Base Case:					
White	0	3	12	58	220
Other	1	6	14	30	46
Minimizing Deaths: 61% total deaths averted					
White	0 (0%)	3 (0%)	12 (0%)	58 (0%)	56 (75%)
Other	1 (0%)	6 (0%)	15 (-7%)	0 (100%)	0 (100%)
Minimizing Inequity in Deaths: 18% total deaths averted					
White	0 (0%)	3 (0%)	11 (8%)	57 (2%)	218 (1%)
Other	0 (100%)	2 (67%)	2 (86%)	7 (77%)	19(59%)
Minimizing Both Deaths and Inequity: 57% total deaths averted					
White	0 (0%)	3 (0%)	11 (8%)	55 (5%)	75 (66%)
Other	0 (100%)	5 (17%)	2 (86%)	7 (77%)	6 (87%)
Minimizing YLLs: 42% total deaths averted					
White	0 (0%)	2 (33%)	10 (17%)	24 (59%)	183 (17%)
Other	0 (100%)	5 (17%)	0 (100%)	0 (100%)	0 (100%)
Minimizing Inequity in YLLs: 19% total deaths averted					
White	0 (0%)	3 (0%)	11 (8%)	57 (2%)	217 (1%)
Other	0 (100%)	2 (67%)	2 (86%)	7 (77%)	18 (61%)
Minimizing Both YLLs and Inequity: 40% total deaths averted					
White	0 (0%)	2 (33%)	10 (17%)	21 (64%)	186 (15%)
Other	0 (100%)	5 (17%)	2 (86%)	3 (90%)	5 (89%)

Table 4.5. YLLs per-group (% averted from base case) when minimizing measures of disease burden, measures of inequity, and combinations of measures with enough vaccine to vaccinate 10% of the total population. When minimizing inequity in deaths and when minimizing deaths and inequity, the relative inequity in deaths is used. When minimizing inequity in YLLs and when minimizing YLLs and inequity, the absolute inequity in YLLs is used.

Age-Group	0-19	20-49	50-59	60-69	70+
Base Case:					
White	3	9	67	180	182
Other	13	60	408	784	460
Minimizing Deaths: 62% total YLLs averted					
White	3 (0%)	10 (-11%)	72 (-7%)	180 (0%)	47 (74%)
Other	12 (8%)	65 (-8%)	429 (-5%)	0 (100%)	0 (100%)
Minimizing Inequity in Deaths: 59% total YLLs averted					
White	3 (0%)	9 (0%)	65 (3%)	177 (2%)	180 (1%)
Other	11 (15%)	17 (72%)	66 (84%)	181 (77%)	188 (59%)
Minimizing Both Deaths and Inequity: 68% total YLLs averted					
White	3 (0%)	9 (0%)	66 (1%)	170 (6%)	62 (66%)
Other	11 (15%)	59 (2%)	67 (84%)	174 (78%)	65 (86%)
Minimizing YLLs: 83% total YLLs averted					
White	3 (0%)	9 (0%)	59 (12%)	74 (59%)	151 (17%)
Other	11 (15%)	54 (10%)	0 (100%)	0 (100%)	0 (100%)
Minimizing Inequity in YLLs: 59% total YLLs averted					
White	3 (0%)	9 (0%)	65 (3%)	176 (2%)	180 (1%)
Other	11 (15%)	17 (72%)	65 (84%)	176 (78%)	180 (61%)
Minimizing Both YLLs and Inequity: 75% total YLLs averted					
White	3 (0%)	9 (0%)	61 (9%)	66 (63%)	154 (15%)
Other	11 (15%)	55 (8%)	61 (85%)	66 (92%)	48 (90%)

Table 4.6. Deaths per-group (% averted from base case) when minimizing measures of disease burden, measures of inequity, and combinations of measures with enough vaccine to vaccinate 20% of the total population. When minimizing inequity in deaths and when minimizing deaths and inequity, the relative inequity in deaths is used. When minimizing inequity in YLLs and when minimizing YLLs and inequity, the absolute inequity in YLLs is used.

Age-Group	0-19	20-49	50-59	60-69	70+
Base Case:					
White	0	3	12	58	220
Other	1	6	14	30	46
Minimizing Deaths: 89% total deaths averted					
White	0 (0%)	2 (33%)	9 (25%)	24 (59%)	0 (100%)
Other	0 (100%)	5 (17%)	0 (100%)	0 (100%)	0 (100%)
Minimizing Inequity in Deaths: 50% total deaths averted					
White	0 (0%)	2 (33%)	5 (58%)	44 (24%)	126 (43%)
Other	0 (100%)	1 (83%)	1 (93%)	5 (83%)	11 (76%)
Minimizing Both Deaths and Inequity: 83% total deaths averted					
White	0 (0%)	2 (33%)	9 (25%)	43 (26%)	0 (100%)
Other	0 (100%)	3 (50%)	2 (86%)	5 (83%)	0 (100%)
Minimizing YLLs: 76% total deaths averted					
White	0 (0%)	2 (33%)	9 (25%)	0 (100%)	80 (64%)
Other	0 (100%)	4 (33%)	0 (100%)	0 (100%)	0 (100%)
Minimizing Inequity in YLLs: 42% total deaths averted					
White	0 (0%)	2 (33%)	1 (92%)	41 (29%)	164 (25%)
Other	0 (100%)	1 (83%)	0 (100%)	5 (83%)	14 (70%)
Minimizing Both YLLs and Inequity: 50% total deaths averted					
White	0 (0%)	2 (33%)	9 (25%)	13 (78%)	153 (30%)
Other	0 (100%)	1 (83%)	2 (86%)	2 (93%)	13 (72%)

Table 4.7. YLLs per-group (% averted from base case) when minimizing measures of disease burden, measures of inequity, and combinations of measures with enough vaccine to vaccinate 20% of the total population. When minimizing inequity in deaths and when minimizing deaths and inequity, the relative inequity in deaths is used. When minimizing inequity in YLLs and when minimizing YLLs and inequity, the absolute inequity in YLLs is used.

Age-Group	0-19	20-49	50-59	60-69	70+
Base Case:					
White	3	9	67	180	182
Other	13	60	408	784	460
Minimizing Deaths: 91% total YLLs averted					
White	3 (0%)	8 (11%)	54 (19%)	75 (58%)	0 (100%)
Other	10 (23%)	49 (18%)	0 (100%)	0 (100%)	0 (100%)
Minimizing Inequity in Deaths: 73% total YLLs averted					
White	3 (0%)	7 (22%)	32 (52%)	135 (25%)	104 (43%)
Other	9 (31%)	7 (88%)	32 (92%)	138 (82%)	109 (76%)
Minimizing Both Deaths and Inequity: 80% total YLLs averted					
White	3 (0%)	8 (11%)	54 (19%)	133 (26%)	0 (100%)
Other	10 (23%)	28 (53%)	55 (87%)	137 (83%)	0 (100%)
Minimizing YLLs: 91% total YLLs averted					
White	3 (0%)	8 (11%)	51 (24%)	0 (100%)	66 (64%)
Other	10 (23%)	48 (20%)	0 (100%)	0 (100%)	0 (100%)
Minimizing Inequity in YLLs: 74% total YLLs averted					
White	2 (33%)	7 (22%)	8 (88%)	127 (29%)	135 (26%)
Other	9 (31%)	7 (88%)	8 (98%)	128 (84%)	135 (71%)
Minimizing Both YLLs and Inequity: 78% total YLLs averted					
White	3 (0%)	7 (22%)	52 (22%)	41 (77%)	126 (31%)
Other	10 (23%)	7 (88%)	52 (87%)	41 (95%)	126 (73%)

Table 4.8. Deaths per-group (% averted from base case) when minimizing measures of disease burden, measures of inequity, and combinations of measures with enough vaccine to vaccinate 30% of the total population. When minimizing inequity in deaths and when minimizing deaths and inequity, the relative inequity in deaths is used. When minimizing inequity in YLLs and when minimizing YLLs and inequity, the absolute inequity in YLLs is used.

Age-Group	0-19	20-49	50-59	60-69	70+
Base Case:					
White	0	3	12	58	220
Other	1	6	14	30	46
Minimizing Deaths: 97% total deaths averted					
White	0 (0%)	2 (33%)	5 (58%)	0 (100%)	0 (100%)
Other	0 (100%)	4 (33%)	0 (100%)	0 (100%)	0 (100%)
Minimizing Inequity in Deaths: 61% total deaths averted					
White	0 (0%)	2 (33%)	8 (33%)	12 (79%)	117 (47%)
Other	0 (100%)	1 (83%)	2 (86%)	1 (97%)	10 (78%)
Minimizing Both Deaths and Inequity: 94% total deaths averted					
White	0 (0%)	2 (33%)	8 (33%)	9 (84%)	0 (100%)
Other	0 (100%)	1 (83%)	2 (86%)	1 (97%)	0 (100%)
Minimizing YLLs: 97% total deaths averted					
White	0 (0%)	2 (33%)	5 (58%)	0 (100%)	0 (100%)
Other	0 (100%)	4 (33%)	0 (100%)	0 (100%)	0 (100%)
Minimizing Inequity in YLLs: 60% total deaths averted					
White	0 (0%)	1 (67%)	0 (100%)	14 (76%)	128 (42%)
Other	0 (100%)	0 (100%)	0 (100%)	2 (93%)	11 (76%)
Minimizing Both YLLs and Inequity: 84% total deaths averted					
White	0 (0%)	2 (33%)	8 (33%)	0 (100%)	46 (79%)
Other	0 (100%)	1 (83%)	2 (86%)	0 (100%)	4 (91%)

Table 4.9. YLLs per-group (% averted from base case) when minimizing measures of disease burden, measures of inequity, and combinations of measures with enough vaccine to vaccinate 30% of the total population. When minimizing inequity in deaths and when minimizing deaths and inequity, the relative inequity in deaths is used. When minimizing inequity in YLLs and when minimizing YLLs and inequity, the absolute inequity in YLLs is used.

Age-Group	0-19	20-49	50-59	60-69	70+
Base Case:					
White	3	9	67	180	182
Other	13	60	408	784	460
Minimizing Deaths: 96% total YLLs averted					
White	2 (33%)	6 (33%)	26 (61%)	0 (100%)	0 (100%)
Other	9(31%)	41 (32%)	0 (100%)	0 (100%)	0 (100%)
Minimizing Inequity in Deaths: 82% total YLLs averted					
White	3 (0%)	7 (22%)	48 (28%)	37 (79%)	97 (47%)
Other	9 (31%)	7 (88%)	49 (88%)	38 (95%)	101 (78%)
Minimizing Both Deaths and Inequity: 92% total YLLs averted					
White	2 (33%)	7 (22%)	45 (33%)	28 (84%)	0 (100%)
Other	9 (31%)	15 (75%)	44 (89%)	28 (96%)	0 (100%)
Minimizing YLLs: 96% total YLLs averted					
White	2 (33%)	6 (33%)	26 (61%)	0 (100%)	0 (100%)
Other	9 (31%)	41 (32%)	0 (100%)	0 (100%)	0 (100%)
Minimizing Inequity in YLLs: 85% total YLLs averted					
White	2 (33%)	5 (44%)	0 (100%)	42 (77%)	106 (42%)
Other	8 (38%)	5 (92%)	0 (100%)	42 (95%)	106 (77%)
Minimizing Both YLLs and Inequity: 91% total YLLs averted					
White	2 (33%)	7 (22%)	45 (33%)	0 (100%)	38 (79%)
Other	9 (31%)	7 (88%)	45 (89%)	0 (100%)	38 (92%)

Chapter 5

Conclusions

As the rate at which diseases emerge or re-emerge continues to increase [56–60], the way policymakers respond to novel outbreaks and work to prevent the spread of infectious diseases will become increasingly important. The use of optimization in determining the best policies or resource distributions is, and will continue to be, an important tool in making policy decisions. In this dissertation, I used optimization techniques to determine the best reduced-mixing strategies to limit the spread of *S. aureus* on dairy farms and to determine which COVID-19 vaccination strategies are best suited to achieving better health or equity outcomes.

In the first two chapters of this dissertation, I studied the use of biosecurity measures that reduced mixing to prevent the spread of *S. aureus* on dairy farms. In the first chapter, I formulated an optimal-control problem for maximizing economic output during an infectious-disease outbreak following SIS disease-dynamics. In this chapter, I was able to solve the optimal-control problem analytically as well as numerically. I found that the optimal solution used bang-bang controls, meaning that the population was either at its highest or lowest level of mixing at any time. Moreover, the optimal solution involved at most one switch from the lowest mixing level to the highest. If no switch occurred, the population was always at the highest mixing-level. The time of the switch from low activity to high activity, and whether

a switch occurred, was dependent on the model parameters. For example, if the ratio of the revenue and cost parameters was small, the reduce-mixing period was longer, and if the ratio of the revenue and cost parameters was increased, no switch would occur. The values of the transmission coefficient and the per-capita recovery rate also had significant effects on the switching time. Therefore, these results indicated that it would be beneficial to improve treatment options in order to reduce the need for strict contact-reducing strategies.

In the second chapter, I extended the bovine-mastitis problem by using an objective functional that takes the severity of the disease into account as cows with subclinical cases of bovine mastitis are still able to produce saleable milk. Although I was unable to find closed-form solutions to this new problem, I was able to analyze analytical solutions and solve this problem numerically. There were three possible cases for the solution: the no-switch case, the one-switch case, and the two-switch case. In the no-switch case, biosecurity measures are minimally used for all time. In the one-switch case, biosecurity measures are maximally used at the beginning of the time frame, and a switch to the minimal use of biosecurity measures occurs before the end of the time frame. In the two-switch case, biosecurity measures are minimally used at the beginning and end of the time frame but are maximally used for a significant amount of time in between. For controlling the transmission of *S. aureus*, I found that a one-switch solution, with a switch occurring after about 260 days, was optimal.

When analyzing the numerical solutions, I found that multiple candidate-solutions may satisfy the first-order necessary conditions of Pontryagin's maximum principle. Two candidate-solutions were local maxima, but corresponded to very different mitigation-strategies. Each of these strategies could be optimal, depending on small differences in parameter values, and often had similar economic payoffs. The results on multiple-candidate solutions are especially important as they indicate the need to take more factors into consideration when making decisions on mitigation strategies. In livestock populations, factors like ease of implementation and animal welfare are needed to decide between very different solutions with

similar outputs.

Debates over disease mitigation-strategies are not limited to economics and cost effectiveness. Scientists, policymakers, and the general public also debate what the primary goal of disease mitigation-strategies should be and what groups should be prioritized when resources are limited. For example, when vaccines for COVID-19 were first available, supplies were limited and there was much debate over whether the older population at the highest risk for severe disease, needed to be prioritized [203, 204] or if BIPOC communities, facing the most disparities and working more often in essential occupations, should be prioritized [205–208].

In the third chapter of this dissertation, I explored the trade-off between equity in disease outcomes between racial groups and overall disease burden for vaccine allocation strategies that are optimized to reduce inequity, disease burden, or both. The goal of this chapter was to provide a race-conscious framework to quantify and minimize inequity that can be used for future pandemics and other public health interventions. To do this, I used an age-and-race-stratified mathematical model of SARS-CoV-2 transmission fitted to age-and-race-stratified data from 2020 in Oregon and analyzed counterfactual vaccination strategies in early 2021. When resources were very limited, such as when there only enough resources to vaccinate 10% of the population, there was a trade-off between minimizing disease burden and minimizing inequity. Although both strategies improved both mortality and inequity from the random base case, older age groups were prioritized when minimizing mortality and younger, BIPOC populations were prioritized when minimizing inequity. When minimizing combinations of disease burden and inequity measures, disease burden and inequity were similarly improved. Compared to minimizing disease burden or inequity alone, however, the results from the combination measure had a smaller improvement in either disease burden or inequity. With enough resources to vaccinate 20% or 30% of the population, the trade-off between equity and disease burden decreases, and vaccine allocation strategies minimizing combinations of measures did as well in each measure as when minimizing individual measures.

The work in this dissertation emphasized that the factors that are most important in

decision making varies depending on the severity of a disease as well as if a disease is in human, livestock, or plant populations. Moreover, when using optimization to inform decision making about the control of infectious diseases, it is important to take into consideration any issues specific to that population whether it be inequity in human population or economic concerns in the agricultural industry. I plan to bring these considerations, especially equity considerations, into my future work in infectious-disease modeling.

Bibliography

[1] BH van den Borne, HU Graber, V Voelk, C Sartori, A Steiner, MC Haerdi-Landerer, and M Bodmer. A longitudinal study on transmission of Staphylococcus aureus *genotype B in Swiss communal dairy herds*. *Preventive Veterinary Medicine*, 136:65–68, 2017. doi: 10.1016/j.prevetmed.2016.11.008.

[2] JW Barlow, LJ White, RN Zadoks, and YH Schukken. A mathematical model demonstrating indirect and overall effects of lactation therapy targeting subclinical mastitis in dairy herds. *Preventive Veterinary Medicine*, 90:31–42, 2009. doi: 10.1016/j.prevetmed.2009.03.016.

[3] E Stafford and M Kot. Optimal reduced-mixing for an SIS infectious-disease model. *Journal of Biological Dynamics*, 16:746–765, 2022. doi: 10.1080/17513758.2022.2148764.

[4] T Beck. Dairy financial performance: How did 2020 compare to previous years? *Penn State Extension*, 2022. `https://extension.psu.edu/dairy-financial-performance-how-did-2021-compare-to-previous-years`.

[5] M Cobirka, V Tancin, and P Slama. Epidemiology and classification of mastitis. *Animals*, 10:2212, 2020. doi: 10.3390/ani10122212.

[6] R Abebe, H Hatiya, M Abera, B Megersa, and K Asmare. Bovine mastitis: Prevalence, risk factors and isolation of *Staphylococcus aureus* in dairy herds at Hawassa milk shed, South Ethiopia. *BMC Veterinary Research*, 12:270, 2016. doi: 10.1186/s12917-016-0905-3.

[7] J Piret and G Boivin. Pandemics throughout history. *Frontiers in Microbiology*, 11:631736, 2021. doi: 10.3389/fmicb.2020.631736.

[8] KA Glatter and P Finkelman. History of the plague: An ancient pandemic for the age of COVID-19. *The American Journal of Medicine*, 134:176–181, 2021. doi: 10.1016/j.amjmed.2020.08.019.

[9] World Health Organization. WHO coronavirus (COVID-19) dashboard, 2023. `https://covid19.who.int/`.

[10] PS Ojiambo, J Yuen, F van den Bosch, and LV Madden. Epidemiology: Past, present, and future impacts on understanding disease dynamics and improving plant disease management – a summary of focus issue articles. *Phytopathology*, 107:1092–1094, 2017. doi: 10.1094/PHYTO-07-17-0248-FI.

[11] WG Powderly. How infection shaped history: Lessons from the Irish famine. *Transactions of the American Clinical and Climatological Association*, 130:127–135, 2019.

[12] TJD Knight-Jones and J Rushton. The economic impacts of foot and mouth disease: What are they, how big are they and where do they occur? *Preventive Veterinary Medicine*, 112:161–173, 2013. doi: 10.1016/j.prevetmed.2013.07.013.

[13] LK Dixon, H Sun, and H Roberts. African swine fever. *Antiviral Research*, 165:34–41, 2019. doi: 10.1016/j.antiviral.2019.02.018.

[14] J Cohen. Bird shots. *Science*, 380:24–27, 2023. doi: 10.1126/science.adi1004.

[15] F Brauer. Mathematical epidemiology: Past, present, and future. *Infectious Disease Modeling*, 2: 113–127, 2017. doi: 10.1016/j.idm.2017.02.001.

[16] D Bernoulli. Réflexions sur les avantages de l'inoculation. *Mercure de Paris*, 173, 1760.

[17] D Bernoulli. Essai d'une nouvelle analyse de la mortalité causeé par la petite vérole. *Mémoires de mathématique et de physique, presentés à l'Académie royale des sciences, par divers sçavans & lûs dans ses assemblées*, 1766.

[18] TH Tulchinsky. John Snow, cholera, the broad street pump; waterborne diseases then and now. *Case Studies in Public Health*, pages 77–99, 2018. doi: 10.1016/B978-0-12-804571-8.00017-2.

[19] J Snow. *The Mode of Communication of Cholera*. 2nd ed Churchill; London, 1855.

[20] WO Kermack and AG McKendrick. A contribution to the mathematical theory of epidemics. *Proceedings of the Royal Society A*, 115:700–721, 1927. doi: 10.1098/rspa.1927.0118.

[21] RC Reiner, TA Perkins, CM Barker, T Niu, LF Chaves, AM Ellis, DB George, A Le Menach, JR Pulliam, D Bisanzio, and et al. A systematic review of mathematical models of mosquito-borne pathogen transmission: 1970–2010. *Journal of The Royal Society Interface*, 10:20120921, 2013. doi: 10.1098/rsif.2012.0921.

[22] NTJ Bailey. *The Mathematical Theory of Epidemics*. Charles Griffin and Co., Ltd., London, 1957.

[23] NF Britton. *Essential Mathematical Biology*. Springer, London, 2003. doi: 10.1007/978-1-4471-0049-2.

[24] S Ahmetolan, AH Bilge, A Demirci, and AP Dobie. A Susceptible-Infectious (SI) model with two infective stages and an endemic equilibrium. *Mathematics and Computers in Simulation*, 194:19–35, 2022. doi: 10.1016/j.matcom.2021.11.003.

[25] F Brauer. A model for an SI disease in an age-structured population. *Discrete and Continuous Dynamical Systems - Series B*, 2:257–264, 2002. doi: 10.3934/dcdsb.2002.2.257.

[26] MB Barongo, K Ståhl, B Bett, RP Bishop, EM Fèvre, T Aliro, E Okoth, C Masembe, D Knobel, A Ssematimba, and et al. Estimating the basic reproductive number (R0) for African swine fever virus (ASFV) transmission between pig herds in Uganda. *PLOS One*, 10, 2015. doi: 10.1371/journal.pone.0125842.

[27] F Brauer, C Castillo-Chavez, and Z Feng. *Mathematical Models in Epidemiology*. Springer, New York, 2019. doi: 10.1007/978-1-4939-9828-9.

[28] HW Hethcote. Three basic epidemiological models. In *Applied Mathematical Ecology*, pages 119–144. Springer, Berlin, Heidelberg, 1989. doi: 10.1007/978-3-642-61317-3_5.

[29] K Hempel and DJD Earn. A century of transitions in New York City's measles dynamics. *Journal of The Royal Society Interface*, 12:20150024, 2015. doi: 10.1098/rsif.2015.0024.

[30] PG Coen, AG Luckins, HC Davison, and MEJ Woolhouse. Trypanosoma evansi *in Indonesian buffaloes: evaluation of simple models of natural immunity to infection. Epidemiology and Infection*, 126: 111–118, 2001. `https://www.jstor.org/stable/3864773`.

[31] MJ Keeling and P Rohani. *Modeling Infectious Diseases in Humans and Animals*. Princeton University Press, Princeton, 2008. doi: 10.2307/j.ctvcm4gk0.

[32] S Lenhart and JT Workman. *Optimal Control Applied to Biological Models*. Chapman and Hall/CRC, Boca Raton, 2007. doi: 10.1201/9781420011418.

[33] LS Pontryagin, VG Boltyanskii, RV Gamkrelidze, and EF Mishchenko. *The Mathematical Theory of Optimal Processes*. John Wiley & Sons, New York, 1962. doi: 10.1002/zamm.19630431023.

[34] W Hackbusch. A numerical method for solving parabolic equations with opposite orientations. *Computing*, 20:229–240, 1978. doi: 10.1007/BF02251947.

[35] M McAsey, L Mou, and W Han. Convergence of the forward-backward sweep method in optimal control. *Computational Optimization and Applications*, 53:207–226, 2012. doi: 10.1007/s10589-011-9454-7.

[36] JA Sharp, K Burrage, and MJ Simpson. Implementation and acceleration of optimal control for systems biology. *Journal of the Royal Society Interface*, 18:20210241, 2021. doi: 10.1098/rsif.2021.0241.

[37] BC Fabien. dsoa: The implementation of a dynamic system optimization algorithm. *Optimal Control Applications and Methods*, 31:231–247, 2010. doi: 10.1002/oca.898.

[38] O Sharomi and T Malik. Optimal control in epidemiology. *Annals of Operations Research*, 251:55–71, 2017. doi: 10.1007/s10479-015-1834-4.

[39] ML Brandeau. Allocating resources to control infectious diseases. In *Operations Research and Health Care*, chapter 17, pages 443–464. Springer, Boston, MA, 2005. doi: 10.1007/1-4020-8066-2_17.

[40] CJ Murray, DB Evans, A Acharya, and RM Baltussen. Development of WHO guidelines on generalized cost-effectiveness analysis. *Health Economics*, 9:235–251, 2000. doi: 10.1002/(SICI)1099-1050(200004)9:3⟨235::AID-HEC502⟩3.0.CO;2-O.

[41] EH Bussell, CE Dangerfield, CA Gilligan, and NJ Cunniffe. Applying optimal control theory to complex epidemiological models to inform real-world disease management. *Philosophical Transactions of the Royal Society B*, 374:20180284, 2019. doi: 10.1098/rstb.2018.0284.

[42] H Gaff and E Schaefer. Optimal control applied to vaccination and treatment strategies for various epidemiological models. *Mathematical Biosciences and Engineering*, 6:469–492, 2009. doi: 10.3934/mbe.2009.6.469.

[43] WJM Probert, K Shea, CJ Fonnesbeck, MC Runge, TE Carpenter, S Dürr, MG Garner, N Harvey, MA Stevenson, CT Webb, M Werkman, MJ Tildesley, and MJ Ferrari. Decision-making for foot-and-mouth disease control: Objectives matter. *Epidemics*, 15:10–19, 2016. doi: 10.1016/j.epidem.2015.11.002.

[44] S Sharma and GP Samanta. Analysis of a chlamydia epidemic model. *Journal of Biological Systems*, 22:713–744, 2014. doi: 10.1142/S0218339014500296.

[45] S Sharma, A Mondal, AK Pal, and GP Samanta. Stability analysis and optimal control of avian influenza virus a with time delays. *International Journal of Dynamics and Control*, 6:1351–1366, 2018. doi: 10.1007/s40435-017-0379-6.

[46] O Sharomi and T Malik. Optimal control in epidemiology. *Annals of Operations Research*, 251:55–71, 2017. doi: 10.1007/s10479-015-1834-4.

[47] K Wickwire. Mathematical models for the control of pests and infectious diseases: a survey. *Theoretical Population Biology*, 11:182–238, 1977. doi: 10.1016/0040-5809(77)90025-9.

[48] L Miralles-Pechuán, F Jiménez, H Ponce, and L Martínez-Villaseñor. A methodology based on deep q-learning/genetic algorithms for optimizing COVID-19 pandemic government actions. In *Proceedings of the 29th ACM International Conference on Information & Knowledge Management*, CIKM '20, page 1135–1144, New York, NY, USA, 2020. Association for Computing Machinery. doi: 10.1145/3340531.3412179.

[49] TF Zhao, WN Chen, AWC Liew, T Gu, XK Wu, and J Zhang. A binary particle swarm optimizer with priority planning and hierarchical learning for networked epidemic control. *IEEE Transactions on Systems, Man, and Cybernetics: Systems*, 51:5090–5104, 2021. doi: 10.1109/TSMC.2019.2945055.

[50] GS Zaric and ML Brandeau. Resource allocation for epidemic control over short time horizons. *Mathematical Biosciences*, 171:33–58, 2001.

[51] S Flessa. Where efficiency saves lives: A linear programme for the optimal allocation of health care resources in developing countries. *Health Care Management Science*, 3:249–267, 2000. doi: 10.1023/A:1019053710258.

[52] S Flessa. Priorities and allocation of health care resources in developing countries: A case-study from the Mtwara region, Tanzania. *European Journal of Operational Research*, 150:67–80, 2003. doi: 10.1016/S0377-2217(02)00786-5.

[53] Ö Coşgun and İE Büyüktahtakın. Stochastic dynamic resource allocation for HIV prevention and treatment: An approximate dynamic programming approach. *Computers & Industrial Engineering*, 118:423–439, 2018. doi: 10.1016/j.cie.2018.01.018.

[54] M Koyuncu and R Erol. Optimal resource allocation model to mitigate the impact of pandemic influenza: A case study for Turkey. *Journal of Medical Systems*, 34:61–70, 2010. doi: 10.1007/s10916-008-9216-y.

[55] E Stafford, D Dimitrov, R Ceballos, G Campelia, and L Matrajt. Retrospective analysis of equity-based optimization for COVID-19 vaccine allocation. *PNAS Nexus*, 2:pgad283, 2023. doi: 10.1093/pnasnexus/pgad283.

[56] FM Tomley and MW Shirley. Livestock infectious diseases and zoonoses. *Philosophical Transactions of the Royal Society B*, 364:2637–2642, 2009. doi: 10.1098/rstb.2009.0133.

[57] KE Jones, NG Patel, MA Levy, A Storeygard, D Balk, JL Gittleman, and P Daszak. Global trends in emerging infectious diseases. *Nature*, 451:990–993, 2008. doi: 10.1038/nature06536.

[58] P Corredor-Moreno and DGO Saunders. Expecting the unexpected: factors influencing the emergence of fungal and oomycete plant pathogens. *New Phytologist*, 225:118–125, 2020. doi: 10.1111/nph.16007.

[59] JB Ristaino, PK Anderson, DP Bebber, KA Brauman, NJ Cunniffe, NV Fedoroff, C Finegold, KA Garrett, CA Gilligan, CM Jones, MD Martin, GK MacDonald, P Neenan, A Records, DG Schmale, L Tateosian, and Q Wei. The persistent threat of emerging plant disease pandemics to global food security. *Proceedings of the National Academy of Sciences*, 118:e2022239118, 2021. doi: 10.1073/pnas.2022239118.

[60] KF Smith, M Goldberg, S Rosenthal, L Carlson, J Chen, C Chen, and S Ramachandran. Global rise in human infectious disease outbreaks. *Journal of the Royal Society Interface*, 11:20140950, 2014. doi: 10.1098/rsif.2014.0950.

[61] J Bedford, J Farrar, C Ihekweazu, G Kang, M Koopmans, and J Nkengasong. A new twenty-first century science for effective epidemic response. *Nature*, 575:130–136, 2019. doi: 10.1038/s41586-019-1717-y.

[62] RA Weiss and AJ McMichael. Social and environmental risk factors in the emergence of infectious diseases. *Nature Medicine*, 10:S70–6, 2004. doi: 10.1038/nm1150.

[63] RE Baker, AS Mahmud, IF Miller, M Rajeev, F Rasambainarivo, BL Rice, S Takahashi, AJ Tatem, CE Wagner, LF Wang, A Wesolowski, and CJE Metcalf. Infectious disease in an era of global change. *Nature Reviews Microbiology*, 2021. doi: 10.1038/s41579-021-00639-z.

[64] K Schneider, W van der Werf, M Cendoya, M Mourits, JA Navas-Cortés, A Vicent, and AO Lansink. Impact of *Xylella fastidiosa* subspecies *pauca* in European olives. *Proceedings of the National Academy of Sciences*, 117:9250–9259, 2020. doi: 10.1073/pnas.1912206117.

[65] S Zhang, JS Griffiths, G Marchand, MA Bernards, and A Wang. Tomato brown rugose fruit virus: An emerging and rapidly spreading plant RNA virus that threatens tomato production worldwide. *Molecular Plant Pathology*, 23:1262–1277, 2022. doi: 10.1111/mpp.13229.

[66] JD Porter and KP McAdam. The re-emergence of tuberculosis. *Annual Review of Public Health*, 15, 1994. doi: 10.1146/annurev.pu.15.050194.001511.

[67] TC Pierson and MS Diamond. The emergence of Zika virus and its new clinical syndromes. *Nature*, 560:573–581, 2018. doi: 10.1038/s41586-018-0446-y.

[68] VG da Costa, ML Moreli, and MV Saivish. The emergence of SARS, MERS and novel SARS-2 coronaviruses in the 21st century. *Archives of Virology*, 165:1517–1526, 2020. doi: 10.1007/s00705-020-04628-0.

[69] G Neumann, T Noda, and Y Kawaoka. Emergence and pandemic potential of swine-origin H1N1 influenza virus. *Nature*, 459:931–939, 2009. doi: 10.1038/nature08157.

[70] S Kalra, D Kelkar, SC Galwankar, TJ Papadimos, SP Stawicki, B Arquilla, BA Hoey, RP Sharpe, D Sabol, and JA Jahre. The emergence of ebola as a global health security threat: from 'lessons learned' to coordinated multilateral containment efforts. *Journal of Global Infectious Diseases*, 6:164–177, 2014. doi: 10.4103/0974-777X.145247.

[71] PJ Sánchez-Cordón, M Montoya, AL Reis, and LK Dixon. African swine fever: A re-emerging viral disease threatening the global pig industry. *The Veterinary Journal*, 233:41–48, 2018. doi: 10.1016/j.tvjl.2017.12.025.

[72] P Beutels, N Jia, QY Zhou, R Smith, WC Cao, and SJ de Vlas. The economic impact of SARS in Beijing, China. *Tropical Medicine & International Health*, 14:85–91, 2009. doi: 10.1111/j.1365-3156.2008.02210.x.

[73] C Klap, N Luria, E Smith, E Bakelman, E Belausov, O Laskar, O Lachman, A Gal-On, and A Dombrovsky. The potential risk of plant-virus disease initiation by infected tomatoes. *Plants*, 9:623, 2020. doi: 10.3390/plants9050623.

[74] NG Becker. *Modeling to Inform Infectious Disease Control*. Chapman and Hall/CRC, Boca Raton, 2015. doi: 10.1201/b18377.

[75] S Saha, GP Samanta, and JJ Nieto. Epidemic model of COVID-19 outbreak by inducing behavioural response in population. *Nonlinear Dynamics*, 102:455–487, 2020. doi: 10.1007/s11071-020-05896-w.

[76] S Saha, GP Samanta, and JJ Nieto. Impact of optimal vaccination and social distancing on COVID-19 pandemic. *Mathematics and Computers in Simulation*, 200:285–314, 2022. doi: 10.1016/j.matcom.2022.04.025.

[77] RAC Jones. Using epidemiological information to develop effective integrated virus disease management strategies. *Virus Research*, 100:5–30, 2004. doi: 10.1016/j.virusres.2003.12.011.

[78] CRR Hooks and A Fereres. Protecting crops from non-persistently aphid-transmitted viruses: A review on the use of barrier plants as a management tool. *Virus Research*, 120:1–16, 2006. doi: 10.1016/j.virusres.2006.02.006.

[79] NJ Cunniffe, FF Laranjeira, FM Neri, RE DeSimone, and CA Gilligan. Cost-effective control of plant disease when epidemiological knowledge is incomplete: modelling Bahia bark scaling of citrus. *PLOS Computational Biology*, 10:e1003753, 2014. doi: 10.1371/journal.pcbi.1003753.

[80] R Mazzucco, U Dieckmann, and JAJ Metz. Epidemiological, evolutionary, and economic determinants of eradication tails. *Journal of Theoretical Biology*, 405:58–65, 2016. doi: 10.1016/j.jtbi.2016.03.019.

[81] SE Heath. The impact of epizootics on livelihoods. *Journal of Applied Animal Welfare Science*, 11: 98–111, 2008. doi: 10.1080/10888700801946048.

[82] J Rushton, PK Thornton, and MJ Otte. Methods of economic impact assessment. *Revue scientifique et technique*, 18:315–342, 1999. doi: 10.20506/rst.18.2.1172.

[83] T Halasa, K Huijps, O Østerås, and H Hogeveen. Economic effects of bovine mastitis and mastitis management: A review. *Veterinary Quarterly*, 29:18–31, 2007. doi: 10.1080/01652176.2007.9695224.

[84] AD James and J Rushton. The economics of foot and mouth disease. *Revue scientifique et technique*, 21:637–644, 2002. doi: 10.20506/rst.21.3.1356.

[85] EP Fenichel, C Castillo-Chavez, MG Ceddia, G Chowell, PAG Parra, GJ Hickling, G Holloway, R Horan, B Morin, C Perrings, M Springborn, L Velazquez, and C Villalobos. Adaptive human behavior in epidemiological models. *Proceedings of the National Academy of Sciences*, 108:6306–6311, 2011. doi: 10.1073/pnas.1011250108.

[86] PA Bliman and M Duprez. How best can finite-time social distancing reduce epidemic final size? *Journal of Theoretical Biology*, 511:110557, 2021. doi: 10.1016/j.jtbi.2020.110557.

[87] E Shim. Optimal strategies of social distancing and vaccination against seasonal influenza. *Mathematical Biosciences and Engineering*, 10:1615–1634, 2013. doi: 10.3934/mbe.2013.10.1615.

[88] F Lin, K Muthuraman, and M Lawley. An optimal control theory approach to non-pharmaceutical interventions. *BMC Infectious Diseases*, 10:32, 2010. doi: 10.1186/1471-2334-10-32.

[89] J González-Guzmán. An epidemiological model for direct and indirect transmission of typhoid fever. *Mathematical Biosciences*, 96:33–46, 1989. doi: 10.1016/0025-5564(89)90081-3.

[90] M Gambhir, MG Basáñez, MJ Burton, AW Solomon, RL Bailey, MJ Holland, IM Blake, CA Donnelly, I Jabr, DC Mabey, and NC Grassly. The development of an age-structured model for trachoma transmission dynamics, pathogenesis and control. *PLOS Neglected Tropical Diseases*, 3:e462, 2009. doi: 10.1371/journal.pntd.0000462.

[91] C Castillo-Chavez, W Huang, and J Li. Competitive exclusion in gonorrhea models and other sexually transmitted diseases. *SIAM Journal on Applied Mathematics*, 56:494–508, 1996. doi: 10.1137/S003613999325419X.

[92] H Hethcote and J Yorke. Gonorrhea transmission dynamics and control. *Lecture Notes in Biomathematics*, 56:18–24, 1984. doi: 10.1007/978-3-662-07544-9.

[93] WO Kermack and AG McKendrick. A contribution to the mathematical theory of epidemics. *Proceedings of the Royal Society A*, 115:700–721, 1927. doi: 10.1098/rspa.1927.0118.

[94] SP Sethi. Optimal quarantine programmes for controlling an epidemic spread. *Journal of the Operational Research Society*, 29:265–268, 1978. doi: 10.2307/3009454.

[95] L Bolzoni, E Bonacini, C Soresina, and M Groppi. Time-optimal control strategies in SIR epidemic models. *Mathematical Biosciences*, 292:86–96, 2017. doi: 10.1016/j.mbs.2017.07.011.

[96] DJ Daley and J Gani. *Epidemic Modelling: An Introduction*. Cambridge University Press, Cambridge, 1999. doi: 10.1017/CBO9780511608834.

[97] WN Cheng and SG Han. Bovine mastitis: risk factors, therapeutic strategies, and alternative treatments - a review. *Asian-Australasian Journal of Animal Sciences*, 33:1699–1713, 2020. doi: 10.5713/ajas.20.0156.

[98] E Rollin, KC Dhuyvetter, and MW Overton. The cost of clinical mastitis in the first 30 days of lactation: An economic modeling tool. *Preventive Veterinary Medicine*, 122:257–264, 2015. doi: 10.1016/j.prevetmed.2015.11.006.

[99] S Pyörälä. Treatment of mastitis during lactation. *Irish Veterinary Journal*, 62:S40, 2009. doi: 10.1186/2046-0481-62-S4-S40.

[100] DJ Wilson, RN Gonzalez, and PM Sears. Segregation or use of separate milking units for cows infected with Staphylococcus aureus*: effects on prevalence of infection and bulk tank somatic cell count. Journal of Dairy Science*, 78:2083–2085, 1995. doi: 10.3168/jds.S0022-0302(95)76834-5.

[101] C Offen and S Ober-Blöbaum. Bifurcation preserving discretisations of optimal control problems. *IFAC-PapersOnLine*, 54:334–339, 2021. doi: 10.1016/j.ifacol.2021.11.099.

[102] SY Serovaiskii. *Counterexamples in Optimal Control Theory*. De Gruyter, Berlin, Boston, 2011.

[103] V Alfano and S Ercolano. The efficacy of lockdown against COVID-19: A cross-country panel analysis. *Applied Health Economics and Health Policy*, 18:509–517, 2020. doi: 10.1007/s40258-020-00596-3.

[104] AK Lugnér and MJ Postma. Mitigation of pandemic influenza: Review of cost–effectiveness studies. *Expert Review of Pharmacoeconomics & Outcomes Research*, 9:547–558, 2009. doi: 10.1586/erp.09.56.

[105] H Pasquini-Descomps, N Brender, and D Maradan. Value for money in H1N1 influenza: A systematic review of the cost-effectiveness of pandemic interventions. *Value in Health*, 20:819–827, 2017. doi: 10.1016/j.jval.2016.05.005.

[106] KM Smith, CC Machalaba, R Seifman, Y Feferholtz, and WB Karesh. Infectious disease and economics: The case for considering multi-sectoral impacts. *One Health*, 7:100080, 2019. doi: 10.1016/j.onehlt.2018.100080.

[107] PE Hulme. One biosecurity: A unified concept to integrate human, animal, plant, and environmental health. *Emerging Topics in Life Sciences*, 4:539–549, 2020. doi: 10.1042/etls20200067.

[108] D Lewis. What scientists have learnt from COVID lockdowns, 2022. `https://www.nature.com/articles/d41586-022-02823-4`.

[109] M Demir, IH Aslan, and S Lenhart. Analyzing the effect of restrictions on the COVID-19 outbreak for some US states. *Theoretical Ecology*, 16:117–129, 2023. doi: 10.1007/s12080-023-00557-1.

[110] M Buhman, G Dewell, and D Griffin. Biosecurity basics for cattle operations and good management practices (GMP) for controlling infectious diseases, 2007. `https://extensionpublications.unl.edu/assets/pdf/g1411.pdf`.

[111] SC Merrill, S Moegenburg, CJ Koliba, A Zia, L Trinity, E Clark, G Bucini, S Wiltshire, T Sellnow, D Sellnow, and et al. Willingness to comply with biosecurity in livestock facilities: Evidence from experimental simulations. *Frontiers in Veterinary Science*, 6:156, 2019. doi: 10.3389/fvets.2019.00156.

[112] C Ritter, J Jansen, S Roche, DF Kelton, CL Adams, K Orsel, RJ Erskine, G Benedictus, TJ Lam, and HW Barkema. Invited review: Determinants of farmers' adoption of management-based strategies for infectious disease prevention and control. *Journal of Dairy Science*, 100:3329–3347, 2017. doi: 10.3168/jds.2016-11977.

[113] V Renault, MF Humblet, P Pham, and C Saegerman. Biosecurity at cattle farms: Strengths, weaknesses, opportunities and threats. *Pathogens*, 10:1315, 2021. doi: 10.3390/pathogens10101315.

[114] S Moya, F Tirado, J Espluga, G Ciaravino, R Armengol, J Diéguez, E Yus, B Benavides, J Casal, and A Allepuz. Dairy farmers' decision-making to implement biosecurity measures: A study of psychosocial factors. *Transboundary and Emerging Diseases*, 67:698–710, 2019. doi: 10.1111/tbed.13387.

[115] RGM Olde Riekerink, HW Barkema, DT Scholl, DE Poole, and DF Kelton. Management practices associated with the bulk-milk prevalence of *Staphylococcus aureus* in Canadian dairy farms. *Preventive Veterinary Medicine*, 97:20–28, 2010. doi: 10.1016/j.prevetmed.2010.07.002.

[116] WN Cheng and SG Han. Bovine mastitis: Risk factors, therapeutic strategies, and alternative treatments — a review. *Asian-Australasian Journal of Animal Sciences*, 33:1699–1713, 2020. doi: 10.5713/ajas.20.0156.

[117] F Gomes and M Henriques. Control of bovine mastitis: Old and recent therapeutic approaches. *Current Microbiology*, 72:377–382, 2015. doi: 10.1007/s00284-015-0958-8.

[118] MZ Khan and A Khan. Basic facts of mastitis in dairy animals: A review. *Pakistan Veterinary Journal*, 26:204–208, 2006.

[119] J Romero, E Benavides, and C Meza. Assessing financial impacts of subclinical mastitis on Colombian dairy farms. *Frontiers in Veterinary Science*, 5:273, 2018. doi: 10.3389/fvets.2018.00273.

[120] ME Cousin, MC Härdi-Landerer, V Völk, and M Bodmer. Control of *Staphylococcus aureus* in dairy herds in a region with raw milk cheese production: Farmers' attitudes, knowledge, behaviour and belief in self-efficacy. *BMC Veterinary Research*, 14:46, 2018. doi: 10.1186/s12917-018-1352-0.

[121] Bovine Alliance on Management and Nutrition, 2001. `https://www.aphis.usda.gov/animal_health/nahms/dairy/downloads/bamn/BAMN01_BiosecurityDairies.pdf`.

[122] Z Deng, G Koop, H Hogeveen, EA Fischer, BH van den Borne, R van der Tol, and TJ Lam. Transmission dynamics of *Staphylococcus aureus* and *Streptococcus agalactiae* in a Dutch dairy herd using an automatic milking system. *Preventive Veterinary Medicine*, 192:105384, 2021. doi: 10.1016/j.prevetmed.2021.105384.

[123] C Offen and S Ober-Blöbaum. Bifurcation preserving discretisations of optimal control problems. *IFAC-PapersOnLine*, 54:3340339, 2021. doi: 10.1016/j.ifacol.2021.11.099.

[124] S Pyörälä. Treatment of mastitis during lactation. *Irish Veterinary Journal*, 62, 2009. doi: 10.1186/2046-0481-62-s4-s40.

[125] JM Swinkels, WD Kremer, CL Kruitwagen, and RN Zadoks. Effect of penethamate hydriodide treatment on bacteriological cure, somatic cell count and milk production of cows and quarters with chronic subclinical *Streptococcus uberis* or *Streptococcus dysgalactiae* infection. *Journal of Dairy Research*, 70:387–394, 2003. doi: 10.1017/s0022029903006460.

[126] N Steele and S McDougall. Effect of prolonged duration therapy of subclinical mastitis in lactating dairy cows using penethamate hydriodide. *New Zealand Veterinary Journal*, 62:38–46, 2013. doi: 10.1080/00480169.2013.830350.

[127] H Deluyker, S Van Oye, and J Boucher. Factors affecting cure and somatic cell count after pirlimycin treatment of subclinical mastitis in lactating cows. *Journal of Dairy Science*, 88:604–614, 2005. doi: 10.3168/jds.s0022-0302(05)72724-7.

[128] S Nickerson and VE Ryman. Antibiotic therapy in mastitis control for lactating and dry cows, 2019. https://extension.uga.edu/publications/detail.html?number=B1516\&title=antibiotic-therapy-in-mastitis-control-for-lactating-and-dry-cows.

[129] E Alfonseca-Silva, JC Cruz-Villa, L Gutiérrez, and H Sumano. Successful treatment of recurrent subclinical mastitis in cows caused by enrofloxacin resistant bacteria by means of the sequential intramammary infusion of enrofloxacin HCL-2H_2O and ceftiofur HCL: A clinical trial. *Journal of Veterinary Science*, 22:e78, 2021. doi: 10.4142/jvs.2021.22.e78.

[130] S McDougall, LM Clausen, HM Hussein, and CW Compton. Therapy of subclinical mastitis during lactation. *Antibiotics*, 11:209, 2022. doi: 10.3390/antibiotics11020209.

[131] SP Sethi. *Optimal Control Theory: Applications to Management Science and Economics*. Springer Nature, Cham, Switzerland, third edition, 2019.

[132] Oregon.gov. COVID-19 updates, 2022. https://www.oregon.gov/oha/covid19/pages/index.aspx.

[133] Centers for Disease Control and Prevention. Risk for COVID-19 infection, hospitalization, and death by race/ethnicity, 2022. https://www.cdc.gov/coronavirus/2019-ncov/covid-data/investigations-discovery/hospitalization-death-by-race-ethnicity.html.

[134] K Mackey, CK Ayers, KK Kondo, S Saha, SM Advani, S Young, H Spencer, M Rusek, J Anderson, S Veazie, M Smith, and D Kansagara. Racial and ethnic disparities in COVID-19-related infections, hospitalizations, and deaths : A systematic review. *Annals of Internal Medicine*, 174:362–373, 2021. doi: 10.7326/M20-6306.

[135] C Nau, K Bruxvoort, RA Navarro, SG Chevez, TA Hogan, KR Ironside, SM Ludwig, Q Ngo-Metzger, NR Mourra, DR Young, N Sangha, BP Turner, IX Li, A Padilla, A Chen, V Hong, V Yau, and S Tartof. COVID-19 inequities across multiple racial and ethnic groups: Results from an integrated health care organization. *Annals of Internal Medicine*, 174:1183–1186, 2021. doi: 10.7326/m20-8283.

[136] S Singu, A Acharya, K Challagundla, and SN Byrareddy. Impact of social determinants of health on the emerging COVID-19 pandemic in the United States. *Frontiers in Public Health*, 8:406, 2020. doi: 10.3389/fpubh.2020.00406.

[137] JK Stockman, BA Wood, and KM Anderson. Racial and ethnic differences in COVID-19 outcomes, stressors, fear, and prevention behaviors among US women: Web-based cross-sectional study. *Journal of Medical Internet Research*, 23:e26296, 2021. doi: 10.2196/26296.

[138] HB Gershengorn, S Patel, B Shukla, PR Warde, M Bhatia, D Parekh, and T Ferreira. Association of race and ethnicity with COVID-19 test positivity and hospitalization is mediated by socioeconomic factors. *Annals of the American Thoracic Society*, 18:1326–1334, 2021. doi: 10.1513/AnnalsATS.202011-1448OC.

[139] RB Hawkins, EJ Charles, and JH Mehaffey. Socio-economic status and COVID-19-related cases and fatalities. *Public Health*, 189:129–134, 2020. doi: 10.1016/j.puhe.2020.09.016.

[140] Q Lin, S Paykin, D Halpern, A Martinez-Cardoso, and M Kolak. Assessment of structural barriers and racial group disparities of COVID-19 mortality with spatial analysis. *JAMA Network Open*, 5: e220984, 2022. doi: 10.1001/jamanetworkopen.2022.0984.

[141] JL Nguyen, T Alfred, M Reimbaeva, D Malhotra, F Khan, D Swerdlow, and FJ Angulo. Population attributable fractions of underlying medical conditions for coronavirus disease 2019 (COVID-19) diagnosis and COVID-19 hospitalizations, ventilations, and deaths among adults in the United States. *Open Forum Infectious Diseases*, 9:ofac099, 2022. doi: 10.1093/ofid/ofac099.

[142] M Walls, JS Priem, CA Mayfield, A Sparling, A Aneralla, LM Krinner, and YJ Taylor. Disparities in level of care and outcomes among patients with COVID-19: Associations between race/ethnicity, social determinants of health and virtual hospitalization, inpatient hospitalization, intensive care, and mortality. *Journal of Racial and Ethnic Health Disparities*, 10:859–869, 2023. doi: 10.1007/s40615-022-01274-x.

[143] MT Bassett, JT Chen, and N Krieger. Variation in racial/ethnic disparities in COVID-19 mortality by age in the United States: A cross-sectional study. *PLOS Medicine*, 17:1–14, 2020. doi: 10.1371/journal.pmed.1003402.

[144] AK Dalsania, MJ Fastiggi, A Kahlam, R Shah, K Patel, S Shiau, S Rokicki, and M DallaPiazza. The relationship between social determinants of health and racial disparities in COVID-19 mortality. *Journal of Racial and Ethnic Health Disparities*, 9:288–295, 2021. doi: 10.1007/s40615-020-00952-y.

[145] M Abedin, A Wahab, FN Rahman, FR Omi, S Shareen, S Rakhshanda, L Islam, CA Mayaboti, UK Saha, F Faruque, LM Fletcher, and S Mashreky. Impact and variability of social determinants of health on the transmission and outcomes of COVID-19 across the world: a systematic review protocol. *BMJ Open*, 11:e053481, 2021. doi: 10.1136/bmjopen-2021-053481.

[146] AM Acosta, S Garg, H Pham, M Whitaker, O Anglin, A O'Halloran, J Milucky, K Patel, C Taylor, J Wortham, SJ Chai, PD Kirley, NB Alden, B Kawasaki, J Meek, K Yousey-Hindes, EJ Anderson, KP Openo, A Weigel, ML Monroe, P Ryan, L Reeg, A Kohrman, R Lynfield, E Bye, S Torres, Y Salazar-Sanchez, A Muse, G Barney, NM Bennett, S Bushey, L Billing, E Shiltz, M Sutton, N Abdullah, HK Talbot, W Schaffner, J Ortega, A Price, AM Fry, A Hall, L Kim, and FP Havers. Racial and ethnic disparities in rates of COVID-19-associated hospitalization, intensive care unit admission, and in-hospital death in the United States from March 2020 to February 2021. *JAMA Network Open*, 4: e2130479, 2021. doi: 10.1001/jamanetworkopen.2021.30479.

[147] HS Abdel Magid, JM Ferguson, R Van Cleve, AL Purnell, and TF Osborne. Differences in COVID-19 risk by race and county-level social determinants of health among veterans. *International Journal of Environmental Research and Public Health*, 18:13140, 2021. doi: 10.3390/ijerph182413140.

[148] ME Kimani, M Sarr, Y Cuffee, C Liu, and NS Webster. Associations of race/ethnicity and food insecurity with COVID-19 infection rates across US counties. *JAMA Network Open*, 4:e2112852, 2021. doi: 10.1001/jamanetworkopen.2021.12852.

[149] CT Rentsch, F Kidwai-Khan, JP Tate, LS Park, JTJ King, M Skanderson, RG Hauser, A Schultze, CI Jarvis, M Holodniy, Vr Lo Re, KM Akgün, K Crothers, TH Taddei, MS Freiberg, and AC Justice. Patterns of COVID-19 testing and mortality by race and ethnicity among United States veterans: A nationwide cohort study. *PLOS Medicine*, 17:e1003379, 2020. doi: 10.1371/journal.pmed.1003379.

[150] A Fawzy, TD Wu, K Wang, ML Robinson, J Farha, A Bradke, SH Golden, Y Xu, and BT Garibaldi. Racial and ethnic discrepancy in pulse oximetry and delayed identification of treatment eligibility among patients with COVID-19. *JAMA Internal Medicine*, 182:730–738, 2022. doi: 10.1001/jamainternmed.2022.1906.

[151] L Lopez, LH Hart, and MH Katz. Racial and ethnic health disparities related to COVID-19. *JAMA*, 325:719–720, 2021. doi: 10.1001/jama.2020.26443.

[152] A Khanijahani, S Iezadi, K Gholipour, S Azami-Aghdash, and D Naghibi. A systematic review of racial/ethnic and socioeconomic disparities in COVID-19. *International Journal for Equity in Health*, 20:248, 2021. doi: 10.1186/s12939-021-01582-4.

[153] MW Webb Hooper, AM Nápoles, and EJ Pérez-Stable. COVID-19 and racial/ethnic disparities. *JAMA*, 323:2466–2467, 2020. doi: 10.1001/jama.2020.8598.

[154] DBG Tai, A Shah, CA Doubeni, IG Sia, and ML Wieland. The disproportionate impact of COVID-19 on racial and ethnic minorities in the United States. *Clinical Infectious Diseases*, 72:703–706, 2021. doi: 10.1093/cid/ciaa815.

[155] C Madlock-Brown, K Wilkens, N Weiskopf, N Cesare, S Bhattacharyya, NO Riches, J Espinoza, D Dorr, K Goetz, J Phuong, A Sule, H Kharrazi, F Liu, C Lemon, and WG Adams. Clinical, social, and policy factors in COVID-19 cases and deaths: methodological considerations for feature selection and modeling in county-level analyses. *BMC Public Health*, 22:747, 2022. doi: 10.1186/s12889-022-13168-y.

[156] L Paremoer, S Nandi, H Serag, and F Baum. COVID-19 pandemic and the social determinants of health. *BMJ*, 372:n129, 2021. doi: 10.1136/bmj.n129.

[157] MG Findling, LS Casey, SA Fryberg, S Hafner, RJ Blendon, JM Benson, JM Sayde, and C Miller. Discrimination in the United States: Experiences of Native Americans. *Health Services Research*, 54: 1431–1441, 2019. doi: 10.1111/1475-6773.13224.

[158] National Academies of Sciences, Engineering, and Medicine. *Framework for Equitable Allocation of COVID-19 Vaccine*. The National Academies Press, Washington, DC, 2020. `https://nap.nationalacademies.org/catalog/25917/framework-for-equitable-allocation-of-covid-19-vaccine`. doi: 10.17226/25917.

[159] World Health Organization. WHO SAGE values framework for the allocation and prioritization of COVID-19 vaccination, 14 September 2020, 2020. https://apps.who.int/iris/bitstream/handle/10665/334299/WHO-2019-nCoV-SAGE_Framework-Allocation_and_prioritization-2020.1-eng.pdf?sequence=1.

[160] AA Malik, SM McFadden, J Elharake, and SB Omer. Determinants of COVID-19 vaccine acceptance in the US. *eClinicalMedicine*, 26:100495, 2020. doi: 10.1016/j.eclinm.2020.100495.

[161] J Louis-Jean, K Cenat, CV Njoku, J Angelo, and D Sanon. Coronavirus (COVID-19) and racial disparities: A perspective analysis. *Journal of Racial and Ethnic Health Disparities*, 7:1039–1045, 2020. doi: 10.1007/s40615-020-00879-4.

[162] I Hernandez, S Dickson, S Tang, N Gabriel, LA Berenbrok, and J Guo. Disparities in distribution of COVID-19 vaccines across US counties: A geographic information system-based cross-sectional study. *PLOS Medicine*, 19:e1004069, 2022. doi: 10.1371/journal.pmed.1004069.

[163] M Kuehn, J LaMori, JK DeMartino, M Mesa-Frias, J Doran, L Korrapati, R Bhojwani, P Lefebvre, and N Kirson. Assessing barriers to access and equity for COVID-19 vaccination in the US. *BMC Public Health*, 22:2263, 2022. doi: 10.1186/s12889-022-14636-1.

[164] A Vasan, M Foote, and T Long. Ensuring widespread and equitable access to treatments for COVID-19. *JAMA*, 328:705–706, 2022. doi: 10.1001/jama.2022.13554.

[165] K Moore. Racial disparities in New York State's vaccine distribution, 2022. https://www.naacpldf.org/naacp-publications/ldf-blog/racial-disparities-in-new-york-states-vaccine-distribution/.

[166] M Reitsma, J Goldhaber-Fiebert, and J Salomon. Quantifying and benchmarking disparities in COVID-19 vaccination rates by race and ethnicity. *JAMA Network Open*, 4:e2130343, 2021. doi: 10.1001/jamanetworkopen.2021.30343.

[167] A Takian, MM Kiani, and K Khanjankhani. COVID-19 and the need to prioritize health equity and social determinants of health. *International Journal of Public Health*, 65:521–523, 2020. doi: 10.1007/s00038-020-01398-z.

[168] B Duff-Brown. Stanford researchers document progress, missed opportunities in equitable COVID-19 vaccine uptake, 2021. https://fsi.stanford.edu/news/stanford-researchers-document-progress-missed-opportunities-equitable-covid-19-vaccine-uptake).

[169] L Matrajt, J Eaton, T Leung, and ER Brown. Vaccine optimization for COVID-19: Who to vaccinate first? *Science Advances*, 7:eabf1374, 2021. doi: 10.1126/sciadv.abf1374.

[170] L Matrajt, J Eaton, T Leung, D Dimitrov, JT Schiffer, DA Swan, and H Janes. Optimizing vaccine allocation for COVID-19 vaccines shows the potential role of single-dose vaccination. *Nature Communications*, 12:3449, 2021. doi: 10.1038/s41467-021-23761-1.

[171] N Gozzi, M Chinazzi, NE Dean, IM Longini, ME Halloran, N Perra, and A Vespignani. Estimating the impact of COVID-19 vaccine allocation inequities: A modeling study. *Nature Communications*, 14:3272, 2023. doi: 10.1038/s41467-023-39098-w.

[172] Z Hong, Y Li, Y Gong, and W Chen. A data-driven spatially-specific vaccine allocation framework for COVID-19. *Annals of Operations Research*, pages 1–24, 2022. doi: 10.1007/s10479-022-05037-z.

[173] E Aruffo, P Yuan, Y Tan, E Gatov, I Moyles, J Bélair, J Watmough, S Collier, J Arino, H Zhu, and et al. Mathematical modelling of vaccination rollout and NPIs lifting on COVID-19 transmission with VOC: A case study in Toronto, Canada. *BMC Public Health*, 22:1349, 2022. doi: 10.1186/s12889-022-13597-9.

[174] JC Lemaitre, D Pasetto, M Zanon, E Bertuzzo, L Mari, S Miccoli, R Casagrandi, M Gatto, and A Rinaldo. Optimal control of the spatial allocation of COVID-19 vaccines: Italy as a case study. *PLOS Computational Biology*, 18:e1010237, 2022. doi: 10.1371/journal.pcbi.1010237.

[175] X Chen, G Zhu, L Zhang, Y Fang, L Guo, and X Chen. Age-stratified COVID-19 spread analysis and vaccination: A multitype random network approach. *IEEE Transactions on Network Science and Engineering*, 8:1862–1872, 2021. doi: 10.1109/tnse.2021.3075222.

[176] JH Buckner, G Chowell, and MR Springborn. Dynamic prioritization of COVID-19 vaccines when social distancing is limited for essential workers. *Proceedings of the National Academy of Sciences*, 118:e2025786118, 2021. doi: 10.1073/pnas.2025786118.

[177] A del Munguía-López and JM Ponce-Ortega. Fair allocation of potential COVID-19 vaccines using an optimization-based strategy. *Process Integration and Optimization for Sustainability*, 5:3–12, 2020. doi: 10.21203/rs.3.rs-83772/v1.

[178] V Khodaee, V Kayvanfar, and A Haji. A humanitarian cold supply chain distribution model with equity consideration: The case of COVID-19 vaccine distribution in the European Union. *Decision Analytics Journal*, 4:100126, 2022. doi: 10.1016/j.dajour.2022.100126.

[179] L Chen, F Xu, Z Han, K Tang, P Hui, J Evans, and Y Li. Strategic COVID-19 vaccine distribution can simultaneously elevate social utility and equity. *Nature Human Behaviour*, 6:1503–1514, 2022. doi: 10.1038/s41562-022-01429-0.

[180] E Rumpler, JM Feldman, MT Bassett, and M Lipsitch. Fairness and efficiency considerations in COVID-19 vaccine allocation strategies: A case study comparing front-line workers and 65-74 year olds in the United States. *PLOS Global Public Health*, 3:e0001378, 2023. doi: 10.1371/journal.pgph.0001378.

[181] R Cookson, AJ Mirelman, S Griffin, M Asaria, B Dawkins, OF Norheim, S Verguet, and A J Culyer. Using cost-effectiveness analysis to address health equity concerns. *Value in Health*, 20:206–212, 2017. doi: 10.1016/j.jval.2016.11.027.

[182] CH Braddock. Racism and bioethics: The myth of color blindness. *The American Journal of Bioethics*, 21:28–32, 2020. doi: 10.1080/15265161.2020.1851812.

[183] DJ Lundon, N Mohamed, A Lantz, HH Goltz, BD Kelly, and AK Tewari. Social determinants predict outcomes in data from a multi-ethnic cohort of 20,899 patients investigated for COVID-19. *Frontiers in Public Health*, 8:571364, 2020. doi: 10.3389/fpubh.2020.571364.

[184] US Census Bureau. Population estimates categorical variables, 2021. https://www.census.gov/data/developers/data-sets/popest-popproj/popest/popest-vars.Vintage_2019.html.

[185] X Wang, RF Pasco, Z Du, M Petty, SJ Fox, AP Galvani, M Pignone, SC Johnston, and ML A. Impact of social distancing measures on coronavirus disease healthcare demand, Central Texas, USA. *Emerging Infectious Diseases*, 26:2361–2369, 2020. doi: 10.3201/eid2610.201702.

[186] N Ferguson, D Laydon, G Nedjati-Gilani, N Imai, K Ainslie, M Baguelin, S Bhatia, A Boonyasiri, ZM Cucunubá, G Cuomo-Dannenburg, A Dighe, I Dorigatti, H Fu, K Gaythorpe, W Green, A Hamlet, W Hinsley, L Okell, S van Elsland, and A Ghani. Report 9: Impact of non-pharmaceutical interventions (NPIs) to reduce COVID-19 mortality and healthcare demand. *Imperial College COVID-19 Response Team*, 2020. doi: 10.25561/77482.

[187] AM Dorélien, A Ramen, I Swanson, and R Hill. Analyzing the demographic, spatial, and temporal factors influencing social contact patterns in U.S and implications for infectious disease spread. *BMC Infectious Diseases*, 21:1009, 2021. doi: 10.1186/s12879-021-06610-w.

[188] B Rico, RM Kreider, and L Anderson. Examining change in the percent of married-couple households that are interracial and interethnic: 2000 to 2012-2016, 2018. https://www.census.gov/content/dam/Census/library/working-papers/2018/demo/SEHSD-WP2018-11.pdf.

[189] L Casura, R Lowe, J R, C Martinez, S Serpas, V Castellanos, and J Singelmann. Frontline workers in the U.S.: race, ethnicity, and gender, 2020. https://www.niussp.org/education-work-economy/frontline-workers-in-the-u-s-race-ethnicity/.

[190] K Prem, K van Zandvoort, P Klepac, RM Eggo, NG Davies, Centre for the Mathematical Modelling of Infectious Diseases COVID-19 Working Group, AR Cook, and M Jit. Projecting contact matrices in 177 geographical regions: An update and comparison with empirical data for the COVID-19 era. *PLOS Computational Biology*, 17:e1009098, 2021. doi: 10.1371/journal.pcbi.1009098.

[191] ME Halloran, CJ Struchiner, and IM Longini Jr. Study designs for evaluating different efficacy and effectiveness aspects of vaccines. *American Journal of Epidemiology*, 146:789–803, 1997. doi: 10.1093/oxfordjournals.aje.a009196.

[192] DA Swan, C Bracis, H Janes, M Moore, L Matrajt, DB Reeves, E Burns, D Donnell, MS Cohen, JT Schiffer, and D Dimitrov. COVID-19 vaccines that reduce symptoms but do not block infection need higher coverage and faster rollout to achieve population impact. *Scientific Reports*, 11:15531, 2021. doi: 10.1038/s41598-021-94719-y.

[193] Vaccines and related biological products advisory committee. FDA briefing document, Moderna COVID-19 vaccine, 2020. https://www.fda.gov/media/144434/download.

[194] FP Polack, SJ Thomas, N Kitchin, J Absalon, A Gurtman, S Lockhart, JL Perez, G Pérez Marc, ED Moreira, C Zerbini, and et al. Safety and efficacy of the BNT162B2 MRNA COVID-19 vaccine. *New England Journal of Medicine*, 383:2603–2615, 2020. doi: 10.1056/nejmoa2034577.

[195] Novavax Investor Relations. Novavax COVID-19 vaccine demonstrates 89.3% efficacy in UK phase 3 trial, 2021. https://ir.novavax.com/2021-01-28-Novavax-COVID-19-Vaccine-Demonstrates-89-3-Efficacy-in-UK-Phase-3-Trial.

[196] M Voysey, SA Clemens, SA Madhi, LY Weckx, PM Folegatti, PK Aley, B Angus, VL Baillie, SL Barnabas, QE Bhorat, and et al. Safety and efficacy of the ChAdOx1 nCoV-19 vaccine (AZD1222) against SARS-COV-2: An interim analysis of four randomised controlled trials in Brazil, South Africa, and the UK. *Lancet*, 397:99–111, 2021. doi: 10.1016/s0140-6736(20)32661-1.

[197] W Haenszel. A standardized rate for mortality defined in units of lost years of life. *American Journal of Public Health and the Nation's Health*, 40:17–26, 1950. doi: 10.2105/ajph.40.1.17.

[198] R Martinez, P Soliz, R Caixeta, and P Ordunez. Reflection on modern methods: years of life lost due to premature mortality – a versatile and comprehensive measure for monitoring non-communicable disease mortality. *International Journal of Epidemiology*, 48:1367–1376, 2019. doi: 10.1093/ije/dyy254.

[199] JN Pearcy and KG Keppel. A summary measure of health disparity. *Public Health Reports*, 117: 273–280, 2002. doi: 10.1016/s0033-3549(04)50161-9.

[200] A Khan, S Marks, D Katz, SB Morris, L Lambert, E Magee, S Bowman, and G Grant. Changes in tuberculosis disparities at a time of decreasing tuberculosis incidence in the United States, 1994-2016. *American Journal of Public Health*, 108:S321_S326, 2018. doi: 10.2105/ajph.2018.304606.

[201] MM Jonczyk, C Homsy, S Naber, and A Chatterjee. Examining a decade of racial disparity in partial mastectomy and oncoplastic surgery. *Journal of Surgical Oncology*, 127:1–9, 2022. doi: 10.1002/jso.27173.

[202] A Goodnough and J Hoffman. The elderly vs essential workers: Who should get the coronavirus vaccine first?, 2020. https://www.nytimes.com/2020/12/05/health/covid-vaccine-first.html?smid=em-share.

[203] S Moore, EM Hill, L Dyson, MJ Tildesley, and MJ Keeling. Modelling optimal vaccination strategy for SARS-COV-2 in the UK. *PLOS Computational Biology*, 17:e1008849, 2021. doi: 10.1371/journal.pcbi.1008849.

[204] J Tolbert, J Kates, and J Michaud. The COVID-19 vaccine priority line continues to change as states make further updates, 2021. https://www.kff.org/policy-watch/the-covid-19-vaccine-priority-line-continues-to-change-as-states-make-further-updates/.

[205] A Giubilini, J Savulescu, and D Wilkinson. COVID-19 vaccine: Vaccinate the young to protect the old? *Journal of Law and the Biosciences*, 7:lsaa050, 2020. doi: 10.1093/jlb/lsaa050.

[206] N Ndugga and S Artiga. How are states addressing racial equity in COVID-19 vaccine efforts?, 2021. https://www.kff.org/racial-equity-and-health-policy/issue-brief/how-are-states-addressing-racial-equity-in-covid-19-vaccine-efforts/.

[207] H Schmidt, L Gostin, and M Williams. Is it lawful and ethical to prioritize racial minorities for COVID-19 vaccines? *JAMA*, 324:2023–2024, 2020. doi: 10.1001/jama.2020.20571.

[208] Morehouse School of Medicine. The push for COVID vaccine priority in hard-hit black and Latino communities, 2020. https://www.msm.edu/RSSFeedArticles/2020/December/ vaccinepriorityinhigh-riskgroups.php.

[209] KC Lee, N Al-Ramahi, L Hahn, T Donnell, LJ Schonewolf, N Khan, C O'Malley, UG Khatri, E Pearlman, M Balachandran, DA Asch, WL Herndon, C Mallozzi, J Green-McKenzie, N Kasbekar, C Cullom, S Carney, RW Shaw, P Sullivan, P Okala, PJ Brennan, and E South. Operationalizing equity: A rapid-cycle innovation approach to covid-19 vaccination in black neighborhoods. *Catalyst non-issue content*, 2, 2021. doi: 10.1056/CAT.21.0094.

[210] J Zhang, M Litvinova, W Wang, Y Wang, X Deng, X Chen, M Li, W Zheng, L Yi, X Chen, and et al. Evolving epidemiology and transmission dynamics of coronavirus disease 2019 outside Hubei Province, China: A descriptive and modelling study. *Lancet Infectious Diseases*, 20:793–802, 2020. doi: 10.1016/s1473-3099(20)30230-9.

[211] SA Lauer, KH Grantz, Q Bi, FK Jones, Q Zheng, HR Meredith, AS Azman, NG Reich, and J Lessler. The incubation period of coronavirus disease 2019 (COVID-19) from publicly reported confirmed cases: Estimation and application. *Annals of Internal Medicine*, 172:577–582, 2020. doi: 10.7326/m20-0504.

[212] J Zhang, M Litvinova, Y Liang, Y Wang, W Wang, S Zhao, Q Wu, S Merler, C Viboud, A Vespignani, and et al. Changes in contact patterns shape the dynamics of the COVID-19 outbreak in China. *Science*, 368:1481–1486, 2020. doi: 10.1126/science.abb8001.

[213] WE Wei, Z Li, CJ Chiew, SE Yong, MP Toh, and VJ Lee. Presymptomatic transmission of SARS-COV-2 –Singapore, January 23-March 16, 2020. *Morbidity and Mortality Weekly Report*, 69:411–415, 2020. doi: 10.15585/mmwr.mm6914e1.

[214] Z Du, X Xu, Y Wu, L Wang, BJ Cowling, and LA Meyers. Serial interval of COVID-19 among publicly reported confirmed cases. *Emerging Infectious Diseases*, 26:1341–1343, 2020. doi: 10.3201/eid2606.200357.

[215] Q Bi, Y Wu, S Mei, C Ye, X Zou, Z Zhang, X Liu, L Wei, SA Truelove, T Zhang, and et al. Epidemiology and transmission of COVID-19 in 391 cases and 1286 of their close contacts in Shenzhen, China: A retrospective cohort study. *Lancet Infectious Diseases*, 20:911–919, 2020. doi: 10.1016/s1473-3099(20)30287-5.

[216] Centers for Disease Control and Prevention. COVID-19 pandemic planning scenarios, 2021. https://www.cdc.gov/coronavirus/2019-ncov/hcp/planning-scenarios.html.

[217] MK Slifka, WB Messer, and IJ Amanna. Analysis of COVID-19 transmission: Low risk of presymptomatic spread? *Archives of Pathology & Laboratory Medicine*, 144:1161–1162, 2020. doi: 10.5858/arpa.2020-0255-LE.

[218] JT Wu, K Leung, and GM Leung. Nowcasting and forecasting the potential domestic and international spread of the 2019-nCoV outbreak originating in Wuhan, China: A modelling study. *Lancet*, 395:689–697, 2020. doi: 10.1016/s0140-6736(20)30260-9.

[219] S Zhao, Q Lin, J Ran, SS Musa, G Yang, W Wang, Y Lou, D Gao, L Yang, D He, and et al. Preliminary estimation of the basic reproduction number of novel coronavirus (2019-nCoV) in China, from 2019 to 2020: A data-driven analysis in the early phase of the outbreak. *International Journal of Infectious Diseases*, 92:214–217, 2020. doi: 10.1016/j.ijid.2020.01.050.